NEUTRON-ACTIVATION OF MATERIAL MATRICES FOR PRODUCING THERAPEUTIC RADIONUCLIDES

Junghyun Kim

A dissertation submitted to the faculty at the University of North Carolina at Chapel Hill in partial fulfillment of the requirements for the degree of Doctor of Philosophy in the Eshelman School of Pharmacy (Division of Pharmacoengineering and Molecular Pharmaceutics)

Chapel Hill
2017

Approved By:

Michael Jay

Kristy Ainslie

Samuel Lai

Shawn Hingtgen

Matthew Parrott

ABSTRACT

Junghyun Kim: Neutron-Activation of Material Matrices for Producing Therapeutic Radionuclides
(Under the direction of Michael Jay)

The importance of developing better cancer therapeutics cannot be over-emphasized. Among several approaches for improving patient outcome and satisfaction, targeted drug delivery has gained a lot of attention as a solution to maximizing therapeutic efficacy and minimizing the off-target side effects. Although there have been tremendous improvements in delivering chemotherapeutics using nanocarriers for achieving targeted drug delivery, reports on the use of this strategy for delivering therapeutic radionuclides are scarce. Considering the fact that radiation therapy is a standard of care for about half of all cancer patients, there is much evidence that more advancements are needed in the field of targeted delivery of therapeutic radionuclides. In this dissertation, with the goal of delivering targeted radiation to cancer, a neutron-activation approach was exploited for producing therapeutic radionuclides with minimum handling of highly radioactive substances. Various material matrices were explored for this strategy.

In Chapter 1, three different types of radiation therapy – external beam radiation therapy, internal radiation therapy and systemic radiation therapy – along with neutron-activatable radionuclides and the rationale for proper isotope selection – were discussed. Additionally, carbon nanomaterials which have drawn great interest in numerous research fields for decades were thoroughly reviewed with a focus on biomedical applications in order to introduce the versatility of these materials.

Among carbon-based matrices, graphene oxide nanoplatelets (GONs) and mesoporous carbon nanoparticles (MCNs) were chosen and examined for their application to systemic radiation therapy. In Chapter 2, GONs that were designed so that they would not leach neutron-activated radionuclides in normal tissues but would selectively release their radioactive cargo in the tumor microenvironment are described. MCNs possessing a more uniform size and shape were investigated as a carrier for the stable isotope ^{165}Ho are presented in Chapter 3. To achieve complete prevention of holmium leaching, the synthesis of holmium oxide in the pores of MCNs was employed, and this resulted in the MCNs maintaining their structural integrity with almost no holmium leaching after a prolonged neutron irradiation time (10 h).

As an extension of this neutron-activation technology using radioactive needles that mimicked the microneedle technology adopted in transdermal drug delivery was developed for internal radiation therapy is described in Chapter 4. The ultimate goal of this work was to deliver high doses of targeted radiation directly into solid tumors by insertion of the radioactive needles. As a means to replace current radiation applicators used in the treatment of some solid tumors, custom-sized titanium and molybdenum needles were prepared as base materials. Neutron-activatable radionuclides (holmium and rhenium) were coated on the surface of these needles by pulsed laser deposition and chemical vapor deposition. The stability of the coatings under physiological-mimicking conditions as well as after neutron irradiation was extensively evaluated.

In summary, carbon-based nanocarriers and solid needles containing or coated with neutron-activatable elements were demonstrated to be very suitable for use in radiation therapy. Irradiation of these matrices in a neutron flux produced therapeutic amounts of radiation without affecting their physical integrity.

I dedicate this work to my family, friends and mentors.

ACKNOWLEDGMENTS

First and foremost, I would like to express my deepest gratitude to my advisor, Dr. Michael Jay, for his tremendous support throughout this dissertation. He has been not only my academic mentor, but he has also been a great role model for my personal growth. His work ethic, a passion and an attitude to the science, maintaining a good balance between work and family have truly inspired me to carry for the rest of my life. In serving a number of important administrative positions for the division and the Eshelman School of Pharmacy, Dr. Jay never forgot to find a time to meet with me for discussing my projects and giving guidance and encouragements, which must not be easy for him. Even before joining the UNC, his presence in the division was a very important factor for me to select this program in pursuing my degree, and if I can go back to the time of coming to the UNC, I would never hesitate to join his lab.

I am very fortunate to have many great mentors in the dissertation committee. I appreciate Dr. Kristy Ainslie for being the chair of my dissertation committee and sharing her great insights throughout this work. I would like to thank Dr. Samuel Lai that he has been the mentor for me from the first day in the UNC. During the rotation in his lab, I learned the most of nanoparticle-related concepts and techniques, which I was able to apply them in this dissertation. While serving as a teaching assistant in his Basic Pharmaceutics class, I was also taught principles of pharmaceutics as well as class management from him. Additionally, I am very grateful to Dr. Shawn Hingtgen for his guidance in planning animal models and invaluable discussions about targeting strategies as a future direction of the MCN project. And, I want to express my appreciation to Dr. Matthew Parrot. I would not be able to develop the neutron-activatable radiation needle project without his suggestion and encouragement.

I would also like to acknowledge past and present Jay-Mumper lab members. Drs. Mumper, Sadgrove, Benhabbour, Yang, Zhang, Liu, Sueda, Peng, Huckle, Marson, Bae, Fu, Glatt and Lee have provided excellent advices and influenced me to grow as a better scientist throughout my time in the UNC. Furthermore, I greatly appreciate Ms. Carla Coste Sánchez, Dr. John Prybylski and Ms. Erin Maxwell. They have always willing to help me with any matter from science discussions to graphical illustrations. I have genuinely enjoyed my journey in the graduate school by spending the time with all of Jay-Mumper lab members. Besides, I want to thank all the DPMP students and staffs, who have been greatly supportive for past five years.

Last but not least, I cannot thank enough to Dr. Gregory Amidon at the University of Michigan, who has welcomed me into the pharmaceutical science world and served as my lifetime mentor. It was a privilege for me to work in Dr. Amidon's lab as an undergraduate student and, thanks to his suggestion, I first thought of pursing further degree in science. It is hard to imagine myself without having met him at Michigan. I would like to show my continuous development to him throughout my scientific career.

TABLE OF CONTENTS

LIST OF TABLES

LIST OF FIGURES

LIST OF ABBREVIATIONS

Ac	actinium
AFM	atomic force microscopy
ANOVA	analysis of variance
At	astatine
BET	Brunauer-Emmett-Teller
Bi	bismuth
CCK-8	cell counting kit-8
CNSI	Carbon Nanoparticles Suspension Injection
CNTs	carbon nanotubes
Cu	copper
CVD	chemical vapor deposition
DLS	dynamic light scattering
DOTA	1,4,7,10-tetraazacyclododecane-1,4,7,10-tetraacetic acid
DOX	doxorubicin
DSPE-PEG	1,2-distearoyl-*sn*-glycero-3-phospho-ethanolamine-N-[methoxy (polyethylene glycol)-3000]
DTPA	diethylenetriaminepentaacetic acid
EBRT	external beam radiation therapy
EDC	1-ethyl-3-(-3-dimethylaminopropyl) carbodiimide hydrochloride
EDS	energy-dispersive X-ray spectroscopy
EPR	enhanced permeability and retention
FA	folic acid
f-CNTs	functionalized carbon nanotubes

FDA	Food and Drug Administration
FTIR	Fourier transform infrared spectroscopy
Ga	gallium
GBCAs	gadolinium-based contrast agents
Gd	gadolinium
GFP	green fluorescent protein
GONs	graphene oxide nanoplatelets
GQDs	graphene quantum dots
GRAS	generally recognized as safe
HCC	hepatocellular carcinoma
HDR	high-dose-rate brachytherapy
Ho	holmium
I	iodine
ICG	indoyanine green
ICP-MS	inductively coupled plasma mass spectrometry
ICRU	International Commission of Radiation Units
IMRT	intensity-modulated radiation therapy
In	indium
Ir	iridium
LDR	low-dose-rate brachytherapy
Lu	lutetium
MAS	magic angle spinning
MCNs	mesoporous carbon nanoparticles
mIBG	metaiodobenzylguanidine
Mo	molybdenum

MRI	magnetic resonance imaging
MSNs	mesoporous silica nanoparticles
MWNTs	multi-wall nanotubes
NAA	neutron-activation analysis
NHS	N-hydroxysuccinimide
NICS	nucleus-independent chemical shift
NIR	near-infrared
NMR	nuclear magnetic resonance
NOTA	1,4,7-triazacyclononane-1,4,7-triacetic acid
Pd	palladium
PBS	phosphate buffered saline
PDI	polydispersity index
pDNA	plasmid DNA
PDT	photodynamic therapy
PEG	polyethylene glycol
PEI	polyethylenimine
PET	positron emission tomography
PLD	pulsed laser deposition
PS	photosensitizer
PTT	photothermal therapy
PTX	paclitaxel
PXRD	powder X-ray powder diffraction
Ra	radium
RAI	radioactive iodine
RBM	radical breathing mode

Re	rhenium
RGD	Arg-Gly-Asp
rGO	reduced graphene oxide
rGONs	reduced graphene oxide nanoplatelets
ROS	reactive oxygen species
SEM	scanning electron microscopy
siRNA	small interfering RNA
SPECT	single photon emission computed tomography
SWNTs	single-wall nanotubes
Tc	technetium
TGA	thermogravimetric analysis
Ti	titanium
WI	wet impregnation
XPS	X-ray photoelectron spectroscopy
XRD	X-ray powder diffraction
Y	yttrium

CHAPTER 1 INTRODUCTION

1.1 Radiation Therapy for Cancer

Radiation therapy is the method of destroying diseased cells with ionizing radiation, and it may be used for either treatment or palliative purposes [1]. With this therapy, cell death is induced primarily through either direct DNA strand breakage or indirect DNA damage caused by free radical generation [2]. Notably, cancer cells are more vulnerable to radiation than normal cells as they lack necessary mechanisms to recover from resulting damage in a timely manner [3]. Since the first cancer patient was treated with this therapy in 1896, there have been vast improvements in the field focusing on increasing radiation delivery to cancer cells while limiting damage to normal cells [4]. Recent advances have been achieved through the development of novel cancer imaging techniques. Image-guided radiation therapy, for example, has led to 50% decreased irradiation of normal tissue [1]. About 50% of cancer patients will receive radiation therapy alone, or in conjunction with surgery and/or chemotherapy, at some point during their treatment [3]. It is not only an effective and curative option but also favored from a cost perspective with reports indicating that radiation therapy accounts for only ~5% of the total cost of cancer care expenses. Currently, there are three different types of radiation therapy: external beam radiation therapy (EBRT), internal radiation therapy and systemic radiation therapy. These can be differentiated either by the location of the radiation source or the route of administration. Each type of radiation therapy will be discussed in the following sections.

1.1.1 External Beam Radiation Therapy (EBRT)

EBRT is the most prevalent type of radiation therapy [5]. As the name of EBRT suggests, this radiation therapy differs from other types in that the radiation source is outside of the body. High energy radiation in the form of X-rays, photons, protons or particles can be delivered to the tumor with this option [3]. Low-energy X-rays (kV range) and gamma rays were initial choices for EBRT but since the development of linear accelerators, their use has been mostly replaced by megavoltage X-rays [4].

Moreover, thanks to advancement in technology a number of new EBRT approaches have been introduced in the past few decades. Examples of these new options include: 3D conformal radiotherapy, intensity-modulated radiation therapy (IMRT), stereotactic radiotherapy, proton therapy and carbon ion therapy [4]. Among them, IMRT, has received a lot of attention in the field for its ability to deliver concentrated doses by adjusting radiation intensity with the assistance of computer-based inverse planning programs [6]. This method is currently used in many clinical settings for the treatment of head, neck, prostate and gynecological cancers [3].

The most pronounced side effect of EBRT is external skin damage, which may cause varying degrees of pain and discomfort for patients [7]. Unfortunately, this issue is inherently unavoidable owing to external placement of the radiation source. The problem is exacerbated by the delivery schedule which consists of with 20-30 fractions over 4-6 weeks because this dosing allows normal cells to recover from sub-lethal radiation damage [1, 8]. However, this frequent treatment schedule significantly lowers the patient compliance.

1.1.2 Internal Radiation Therapy

Internal radiation therapy is commonly known as brachytherapy (brachy meaning ‘short,’ in Greek) [9]. It is a compelling therapeutic option for selectively damaging cancer

cells by placing the radiation source, in the form of seeds, wires or pellets, within or adjacent to target tissues [10]. Since brachytherapy delivers the radiation dose inside of the body, it not only avoids the issue of skin damage but also delivers more radiation directly to target sites through a higher ratio of tumor to normal tissue dose, compared to EBRT [11, 12]. In the treatment of prostate cancer, for instance, the dose delivered by advanced EBRT (IMRT) is limited to ~80 Gy whereas the delivery more than 100 Gy can be achieved by utilizing brachytherapy [13].

Radionuclides such as ^{226}radium (Ra), ^{125}iodine (I), ^{103}palladium (Pa) and ^{192}iridium (Ir) have been favored for brachytherapy applications [4]. They can be used via: external applicators (for external cancer sites), interstitial implantation (for temporary or permanent insertion into tissue), or intracavitary therapy (predominantly for cervical cancer) [14]. According to the International Commission of Radiation Units (ICRU), brachytherapy is classified as either low-dose-rate brachytherapy (LDR; 0.4-2 Gy/h) or high-dose-rate brachytherapy (HDR; higher than 12 Gy/h) based on delivery type [15]. ^{125}I and ^{103}Pd are common choices for LDR, and ^{192}Ir is mostly used in HDR [16]. Depending on the size and location of cancer cells, the appropriate radionuclide, method of insertion, and dose may be selected to maximize patient outcomes.

There are a few distinct disadvantages to brachytherapy. Unlike EBRT, brachytherapy requires personnel handling (e.g., radiotherapist, nurses, radiation oncologists); these providers are unavoidably exposed to radiation at some point during the formulation preparation or treatment processes [9]. Additionally, this technique usually requires surgical insertion by skilled radiation oncologists [9, 17]. Lastly, only certain cancer sites can be treated due to anatomical limitations. Distant metastases, for instance, are not candidates for this type of radiation [18].

1.1.3 Systemic Radiation Therapy

Systemic radiation therapy is an approach to delivering radiotherapeutics via oral ingestion, catheter infusion, or intravenous administration [19]. Common principles of drug delivery are applicable to this therapy, and the proper choice of both delivery method and active ingredient, in this case the radionuclides, is crucial in achieving desirable efficacy. Unlike brachytherapy, systemic radiation allows for radiopharmaceutical delivery to metastatic sites as well as primary tumor sites [20, 21].

Radionuclide emitting α-particles (e.g., ^{225}actinium (Ac), ^{211}astatine (At), ^{213}bismuth (Bi)) and Auger electrons (e.g., ^{67}gallium (Ga), ^{123}I, ^{125}I) have been actively investigated for use in systemic radiation therapy. However, translation to the clinic has been slow. A common limitation of α-emitters is their short therapeutic half-life; Auger-emitters, unfortunately, can only travel over extremely short distance (< 150 nm) [19]. Thus, β-emitters (γ-photon emitters usually adopted in imaging application) have been the dominant choice for systemic radiation applications [20, 22]. Among several candidates, ^{131}I and ^{90}yttrium (Y) have been preferred for systemic radiation therapy formulations due to high availability, inexpensive cost, and relatively long half-life (192.5 h for ^{131}I and 64.1 h for ^{90}Y) [19].

As iodine is naturally taken up by the thyroid gland, radioactive iodine (RAI) has a long history of treating thyroid-related diseases. ^{131}I was first used to treat a patient with hyperthyroidism in 1941 and its first use in a thyroid cancer patient occurred in 1946 [20, 23]. A renowned example of RAI is ^{131}I-metaiodobenzylguanidine (^{131}I-mIBG). It is a compound with a structure very similar to norepinephrine that, when administered, accumulated in neural crest cells [24]. Accordingly, ^{131}I-mIBG has been actively investigated as a therapeutic agent for neuroendocrine cancers (e.g., pheochromocytoma, neuroblastoma) [22, 24]. In spite of the active application of RAI, the relatively high energy-carrying γ-photons of ^{131}I (364 keV) has

raised some safety concern as a γ-photon travels much further than β-particles and may induce off-target ablation [19, 25].

On the other hand, ^{90}Y is a pure β-emitter which does not have issues with γ-photon ablation and even delivers higher energy than ^{131}I (E_{max} of ^{90}Y: 2.28 Me cf. E_{max} of ^{131}I: 0.61 MeV) [26, 27]. The beneficial properties of yttrium have led to the development of several ^{90}Y-based formulations, a few of which have been introduced to the market. ^{90}Y-containing glass microsphere was approved by the U.S. Food and Drug Administration (FDA) under the brand name TheraSphere® for the treatment of hepatocellular carcinoma (HCC). Patients indicated for this drug are treated with the microparticles by catheter administration [27]. Furthermore, ^{90}Y has been conjugated to a monoclonal antibody (ibritumomab) and the resulting radioimmunotherapy agent, Zevalin®, was approved by FDA for the treatment of non-Hodgkin's lymphoma [28].

1.1.4 Neutron-Activatable Radionuclides

Neutron-activation is a process of generating radioactive substances by conferring neutrons to stable nuclei. The process can be incorporated into brachytherapy and systemic radiation therapy as well as utilized by nuclear medicine imaging applications [29]. When stable isotopes capture additional neutrons, they become heavier (excited) and decay by emitting particles (α or β) and/or γ-photons. The amount of radioactivity generated by neutron irradiation can be calculated by the following equation:

$$A = n * f * \sigma * (1 - e^{-\lambda T}) * e^{-\lambda T}$$

where *A* is radioactivity (Ci), *n* is the number of atom (multiplied by natural abundance factor), f is neutron flux density (neutrons cm^{-2} s), σ is neutron cross-section (cm^2), λ is decay constant ($ln2/t_{1/2}$, h^{-1}), and T is irradiation time (h).

Parameters

There are a number of factors involved in generating radioactivity by neutron-activation. Some parameters, such as natural abundance, neutron cross-section and half-life, are intrinsic proprieties of the radionuclides themselves and cannot be altered during the activation process. Thus, neutron-activatable radionuclides need to be wisely selected for appropriate therapy and imaging purposes. In addition to element selection, there are still two aspects that must be considered when manipulating this process: irradiation time and neutron flux. Considering that the neutron flux is often limited by type of nuclear reactor and its set-up, adjusting the neutron irradiation time is regarded as a more realistic option for controlling final radioactivity.

Candidates for Neutron-Activatable Radionuclides

To examine potential neutron-activatable radionuclides, a list of clinically translated or investigated radionuclides are presented in **Table 1.1**. An important factor in selecting a suitable candidate for this application is its natural abundance. In the case of samarium (Sm), 4 out of 7 isotopes can generate sufficient amounts of radioactivity following neutron-activation. Since they all have different half-lives and energy levels, the use of Sm for neutron-activatable formulation requires purification processes in order to avoid complicated dosimetry calculation. Thus, with respect to natural abundance, 100% natural abundant elements such as Y, Au, and Holmium (Ho) are more desirable than other elements that exist as other isotopes. As shown in the above equation, neutron cross-section – probability of reaction between neutron and nucleus – is directly proportional to the production of radioactivity [30]. For example, clinically translated Y has relatively low neutron cross-section (1.28 barn) which is 77-fold lower than Au and 46-fold lower than Ho. Based on this knowledge, Y cannot yield the same radioactivity that may be achieved by Au or Ho under the same irradiation conditions.

Half-life, another important factor in dose calculations, must also be taken into consideration for neutron-activation. Since elements that produce isotopes with longer half-lives are disadvantageous in generating a large amount of radioactivity, it is not surprising that in a simulation of neutron irradiation, Au could not produce more radioactivity than Ho despite its ~1.7-fold higher neutron cross-section (**Table 1.1**). Thus, Ho was selected as the optimal investigative agent for the current research.

1.2 Carbon Nanomaterials in Biomedical Applications

In the biomedical field, tremendous developments, innovations and improvements are continually emerging, and reports of new findings are being published nearly every day. For the past decade, many developments have been accompanied by significant advances in nanotechnology which, in turn, have created new opportunities for tackling many long-harbored challenges. For example, advances in nanotechnology have allowed for the development of nanoparticle-based drug delivery systems which offer distinct advantages over conventional therapeutics, including: better tumor accumulation through exploitation of passive and active targeting, more favorable pharmacokinetics, and controlled or sustained drug release [32]. In order to exploit the unique benefits of this type of formulation, various kinds of nanomaterials including lipids, polymers, viruses, and inorganic composites (e.g., gold, silica, iron oxide, quantum dot) have been explored as vehicles for cargo delivery [33-39]. Among them, carbon nanomaterials such as carbon nanotubes (CNTs), fullerenes and graphene oxide nanoplatelets (GONs) have been actively investigated substances. Research into fullerene and graphene, in particular, has yielded Nobel Prize Winning research in the fields of Chemistry (1996) and Physics (2010), respectively [40, 41].

Carbon nanomaterials have garnered interest in a number of areas including electronics, biosensors, energy storage, mechanical systems, and biomedical application [42]. Due to

variations in size and shape of these materials, each carbon nanocarrier possesses distinct characteristics, but all carbon nanomaterials share the unique properties of chemical inertness, mechanical strength, semi-conductive behavior, superior thermal conductivity, elasticity, large surface area and biocompatibility[42, 43]. A notable drawback of carbon nanomaterials, however, is their insolubility in aqueous solvents. To overcome this issue, surface functionalization strategies have been examined; these will be discussed in subsequent sections. While fullerenes have the longest history of carbon nanomaterial research , starting from their 1985 discovery, CNTs are arguably the most heavily investigated material among the carbon family [44]. In this regard, most carbon nanomaterial studies have been conducted using CNTs; the approach refined in these studies has subsequently been used in research utilizing fullerenes and GONs.

Three of the most extensively investigated carbon nanomaterials are CNTs, fullerenes, and GONs and can be applied for imaging and therapeutic purposes. Along with these agents, mesoporous carbon nanoparticles (MCNs) have arisen as a relatively new class of carbon nanomaterials that is reported to have an exceptionally large surface area (up to 3000 m^2 g^{-1}) in addition to tunable size and porosity [45, 46]. Since research in this area is still in its nascence, most available publications have focused on other applications (e.g., energy storage) and reports of utilizing MCNs for therapeutic applications are not yet common [47].

1.2.1 Background and Synthesis

Carbon Nanotubes

CNTs are hollow and cylindrical structures with a high aspect ratio and are formed from a rolled graphitic layer. Based on the number of graphene layers, CNTs are largely classified as single-wall nanotubes (SWNTs) or multi-wall nanotubes (MWNTs). The diameter of SWNTs is typically 1-2 nm while that of MWNTs is in the range of 2-25 nm. The length of

both SWNTs and MWNTs can range from hundreds of nanometers to a few micrometers [48]. CNTs are small but remarkably strong (in terms of high Young's modulus and high tensile strength), especially when considering their low density. For instance, the density-normalized modulus of CNTs is approximately 19- and 2.4-fold higher than that of steel or silicon carbide nanorods, respectively [49]. CNTs were initially synthesized by electronic-arc discharge method from graphite with the assistance of metal catalysts [50]. Other synthesis methods (e.g., laser ablation technique, chemical vapor deposition (CVD), electrolysis, heat treatment of polymer) were investigated to attain a higher yield, narrower size distribution and efficient scale-up [51, 52].

Fullerenes

Fullerenes, like graphite and diamonds, are a type of carbon allotrope. The first discovered fullerene was C_{60}, a spherical and hollow carbon cage measuring approximately 1 nm in size [44, 53]. Soon after this finding, various sizes of fullerenes were synthesized and further distinguished as lower fullerenes (< C_{60}; e.g., C_{28}, C_{36}) or higher fullerenes (> C_{60}; e.g., C_{80}, C_{94}) [54-56]. Though fullerenes were found to exist in nature, they have been detected in meteors and in space, they have been generally synthesized by the arc-discharge method – a process involving evaporating graphite electrodes and recondensing them in a helium atmosphere [57-60]. Based on the modification methods, this type of carbon allotrope can be further classified as endohedral fullerenes (loading other molecules inside of their structure) and exohedral fullerenes (attaching other molecules outside of carbon skeleton) [59].

Graphene Oxide Nanoplatelets

Graphite consists of several stacked layers and one single layer of this structure is called a graphene. Graphene was previously regarded to be a theoretical material until its isolation in

2004 by the mechanical exfoliation of graphite [59]. The first experimental separation of graphene was performed by the labor-intensive scotch tape method (repetitive peeling until a single layer is isolated) [61]. In 2006, chemical exfoliation was developed. The process involves oxidizing graphite in water and adding mechanical energy (sonication) [62]. The oxidized form of graphene is called graphene oxide (GO) and is the preferred form for biomedical application because of its ability to dispersion both aqueous and organic solvents. Conversely, GO loses its electrical conductivity during the oxidation process which raises a problem in its use for other applications. Fortunately, this conductivity can be recovered by chemical or thermal reduction processes which GO to reduced graphene oxide (RGO) [63]. Alternative methods have been proposed for graphene preparation (e.g., CVD, epitaxial growth from silicon carbide, un-zipping CNTs), yet the chemical approach is still preferred due to its low-cost, scalability, and relatively ease in processing [63, 64].

GO is a single-atom-thick 2-dimensional structure – thickness is typically measured to ~ 1 nm by atomic force microscopy (AFM) – but lateral dimensions are variable [65]. Synthesis of nano-sized graphene oxide, referred to as graphene oxide nanoplatelets (GONs), can be achieved using strong mechanical energy to break GONs down to a nano-scale. GONs have been extensively explored for a number of different biomedical applications [66].

Mesoporous Carbon Nanoparticles

Thanks to large surface area, porous materials are widely utilized as adsorbents for pollutant removal (e.g., heavy metals) [67]. Depending on the pore size, they are subdivided to microporous (< 2 nm), mesoporous (2-50 nm) or microporous (> 59 nm) [68]. Since mesoporous silica nanoparticles (MSNs) have emerged as a new class of drug carrier, the attention has shifted to similarly structured carbon materials: MCNs [37, 69]. MCNs possess advantages over other carbon nanomaterials, in terms of structural rigidity and low density, and

over MSNs, due to a larger surface area for cargo loading. Moreover, MCNs have been shown to have better biocompatibility profile compared to MSNs [70]. MCNs are typically synthesized by either the hard-template or soft-template method. The hard-template strategy uses MSNs as a template, which are removed by acid treatment (hydrofluoric acid) when porous carbon structure is formed [71]. In the case of the soft-template method, self-assembly polymers (e.g., Pluronic® F-127) are employed as a template, which can later be eliminated by thermal treatments that degrade the polymeric template but allow carbon nanoparticles to stay intact at high temperatures (700-900 °C) in the presence of inert gas [46]. The latter method is favorable owing to lower production costs (avoiding the use of expensive MSNs) and higher mechanical stability (preventing the use of corrosive and toxic hydrofluoric acid) [71].

1.2.2 Functionalization

Covalent Modification

In an attempt to improve carbon nanoparticle dispersibility in aqueous solvents, several different surface modification strategies have been reported. These strategies can be classified as either covalent or non-covalent modification methods. Covalent modification involves introducing functional moieties on existing nanomaterials. The most common strategy for covalent modification has been introducing carboxylic group (-COOH) by oxidation. Since very strong acids, such as hydrochloric acid, nitric acid and sulfuric acid, are typically used for this oxidation, excessive washing processes must be followed [72-75].

This acid treatment is actually a part of typical GONs synthesis to attach carboxylic acid, hydroxide, and epoxide on the GON surface, hence reactions of adding functional groups are not prerequisite for GONs [65]. Many other functional groups (e.g., amine, ester, thiol) can also be formed on the surface of these carbon nanomaterials via assorted chemical reactions [76-78]. Upon introduction of various functional groups, a number of different conjugation

strategies can be conducted, including a well-known amine coupling reaction through EDC [1-ethyl-3-(-3-dimethylaminopropyl) carbodiimide hydrochloride] and NHS [N-hydroxysuccinimide] [78, 79]. Through the agency of conjugation, several chemical or biological entities can be attached to carbon nanomaterials to act as dispersing agents [80-82].

Non-Covalent Modification

On the other hand, the non-covalent modification does not require functional group induction on the surface of carbon nanomaterials. Rather, this approach exploits hydrophobic-hydrophobic, van der Walls, and electrostatic interactions between carbon structures and adducts [56, 78, 83]. If the adduct carries aromatic groups in its chemical structure, stronger interaction – π-π stacking – can be formed with aromatic regions of carbon nanomaterials [50]. Amphiphilic surfactants and polymers, which can bind to hydrophobic carbon nanomaterials in order to confer dispersibility in aqueous solvents, have been popular choices as non-covalent modification agents; other biological molecules (e.g., proteins, nucleic acids, carbohydrates) have also been widely studied for this strategy [78, 83]. A number of studies detailing the attachment of non-covalent adducts have been conducted with CNTs and GONs, but research on fullerenes using this approach remains relatively scarce. Interestingly, fullerenes have been investigated as guest molecules for encapsulation within other carriers (e.g., cyclodextrins, micelles, liposomes), likely due to their small size (~1 nm) and therapeutic capabilities as both antivirals and antioxidants [77]. As few studies have investigated MCNs for biomedical application, it is difficult to find literature detailing experimental methods for this type of application. However, considering that MCNs are capable of moiety-loading via non-covalent interaction, future studies in this area can be expected [84, 85].

Covalent Modification vs. Non-Covalent Modification

There is no perfect strategy for surface modification. Each method has its benefits and its drawbacks. The main advantage to the covalent method is the ability to offer higher dispersion stability in organic or aqueous solvents due to the stronger covalent linkage between functional groups of carbon nanomaterials and the dispersing agents [42]. However, the structural rigidity of carbon nanomaterials is easily weakened and can be broken down during acid treatment or other functional group introduction processes [50]. Non-covalent modification has been favored as a means of a simple, quick, and non-destructive method of surface modification [86]. Regarding the lower dispersion stability of this method compared to covalent conjugation, Liu et al. have claimed that a carefully and rationally chosen amphiphilic moiety (e.g., phospholipid polyethylene glycol) could provide an excellent stability in the biological environment [87].

1.2.3 Cellular Uptake and Toxicity

Cellular Uptake

Among CNTs' many superior properties, its ability to easily cross cell membranes has made them an attractive carrier for therapeutic and imaging modality delivery application [80, 88]. Previous publications have suggested that functionalized CNTs (f-CNTs) are internalized in cells via both passive and endocytosis-independent methods by the aid of their needle-like structure; others have insisted that there were different cell uptake mechanisms heavily dependent on the size and functionalization strategies of CNTs [80, 88, 89]. These patterns were observed with other functionalized carbon nanomaterials as well [85, 90, 91]. Based on these findings, a variety of cargos (e.g., drug molecules, genes, vaccines, peptides, proteins) can be delivered to the intracellular target sites with the assistance of carbon nanocarriers [66, 82, 92].

Toxicity

Toxicity of carbon nanomaterials is another important subject. With respect to CNTs, their significant toxicity hampers their translation into the clinical setting [93]. A study conducted by Poland et al. found that CNTs induced asbestos-like pathogenicity stemming from the structural similarity with said toxin (i.e. needle-like fibrous shape) [94]. There have been countless debates regarding the toxicity of CNTs [95, 96]. Numerous publications have expressed concerns regarding the toxicity of CNTs, specifically with respect to unfunctionalized CNTs which can aggregate and induce necrosis, apoptosis and inflammation in both *in vitro* and *in vivo* models [89, 93]. Thus, well-dispersed CNTs with proper functionalization have been shown to successfully prevent signs of toxicity and have immensely enhanced their safety profile [89]. Since many synthetic methods utilize metal catalysts (e.g., iron, cobalt, nickel), toxicity assessments must be evaluated following the successful removal of the metal catalysis [51, 93]. Overall, the prevention of CNTs toxicity can be managed by a number of factors, including alterations in structure, size, aspect ratio, surface modification strategies and synthetic method [93, 97]

Early toxicity studies with fullerenes have identified concerns about oxidative stress [98, 99]. Later studies, however, determined that proper removal of organic solvent (tetrahydrofuran) and subsequent functionalization was able to prevent this issue [100, 101]. According to Sayes et al., surface modification of fullerenes rendered its lethal dose by up to 7 orders of magnitude [102]. As graphene has become a rising star among carbon nanomaterials over the past decade, subsequent toxicity assessments have found that results were no different compared to other members of the carbon family. Though pristine graphene has been shown to induce cytotoxicity through the generation of reactive oxygen species (ROS), GONs and rGO nanoplatelets (rGONs) exhibit enhanced biocompatibility [103]. Additional linking

biocompatible moieties such as polyethylene glycol (PEG) and dextran to GONs has been found to improve safety profiles [66]. Yang et al. investigated the long-term toxicity of PEGylated GONs and concluded that there was no observable toxicity even at high doses (20 mg/kg) over a 3 months follow-up period [104].

In the case of MCNs, there are a limited number publications available for evaluating the toxicity of these relatively new members of the carbon family. Despite the fact that pristine MCNs prepared by hard-template and soft-template methods did not present cytotoxicity up to 10 and 50 μg/mL, respectively, higher concentration clearly exhibited undesirable cytotoxic effect [46, 85]. To increase the dispersity of MCNs, Zhu et al. introduced carboxyl groups on the surface of MCNs and did not observe any cytotoxicity at testing concentrations (0.23 to 23 μg/mL) [74]. However, the concentration range tested in this study was lower than previous reports with pristine MCNs. Xu et al. functionalized MCNs with polyethylenimine (PEI) and folic acid (FA), and confirmed that this formulation does not exhibit toxicity within the range of 10-75 μg/mL [105]. This study did not disclose the percent composition of MCNs out of FA/PEI/MCNs; thus, it is difficult to conclude improved toxicity with this functionalization strategy. Based on toxicity examinations of previous carbon nanomaterials, a properly designed study with well-assorted functionalization of MCNs is anticipated to demonstrate superior biocompatibility than pristine MCNs.

1.2.4 Imaging

Fluorescence Imaging

Numerous researchers have been intrigued in optical properties of carbon nanomaterials. Exploiting the intrinsic characteristics of carbon structure for imaging applications is an advantageous method for long-term tracking, particularly when compared with fluorescence or radionuclide-labeling methods where trackers may be slowly detached or

completely decayed over time [106]. Since the biological system is substantially transparent and exhibits low autofluorescence in the near-infrared (NIR) region, strong NIR absorbance of CNTs from small band gaps allows them to be utilized in photoluminescence imaging, even without attaching a fluorophore to the carrier [87, 88]. A large band gap between excitation (550 – 850 nm) and emission (900 – 1600 nm) of CNTs is also beneficial because it can be easily distinguished from the background [87]. Using this imaging technique, Welsher et al. successfully visualized CNTs *in vivo* and employed them for intravital microscopy [107]. Low photoluminescence quantum efficiency of CNTs (less than 0.01) has been a limiting factor for this imaging option, but it has been suggested that this method could be enhanced by the appropriate surface coating methods or the addition of photoluminescence enhancers (e.g., gold nanoparticles, quantum dots) [42].

In addition to CNTs, GONs have been actively studied as a means for fluorescence imaging. When graphene or GO is generally smaller than 10 nm, they are referred to as graphene quantum dots (GQDs) and their intrinsic fluorescence can be visualized over a broad range (from ultraviolet to NIR) [108]. An interesting phenomenon is that large-sized pristine graphene is not an inherently fluorescent material but does emit fluorescence due to quantum confinement and edge effects following the induction of functional groups with size reduction [109]. Several merits – including the capability for color tuning and quantum yields up to 28% – are additional benefits when they are functionalized [64]. By using GQD's versatility in fluorescence imaging, Wu et al. showed that they can be displayed with different colors (blue, green and red) and be visualized *in vivo* [110].

Adequate quantum yields continued to be an issue with respect to fullerenes (less than 0.1%). To overcome this issue, Lin et al. attempted to break the structural symmetry of C_{60}. Results of this method suggested that the quantum yields were boosted 2-3-fold with this functionalization method [111, 112]. Nevertheless, this fluorescence imaging technique is not

preferred for fullerenes because of its low practicality (fluorescence emission in the visible region) [108]. While there are some publications concerning the incorporation of fluorescence molecules to MCNs, studies utilizing MCNs' intrinsic fluorescence have not been conducted yet [85, 113].

Raman Imaging

Raman spectral imaging is a relatively new technique which can offer useful information about the activity of carbon nanoparticles at the *in vitro*, *in vivo,* and even at the molecular-level [114]. The strong intrinsic resonance of Raman scattering at the graphitic-band (G-band; high frequency; 1500 – 1600 cm^{-1}) of carbon nanomaterials originates from the unique sp^2 chemical structure; this property allows them to be investigated as Raman imaging agents [87, 115]. Though GONs could be imaged with this technique *in vivo,* most investigations of Raman imaging applications were performed with CNTs [116, 117].

The radical breathing mode (RBM; low frequency; 100 – 300 cm^{-1}) has been observed only in CNTs. Along with G-band, this method is most effective in distinguishing CNTs from background spectra and is the most commonly adopted imaging method [118]. Attaching multicolor Raman contrast agents to CNTs confers a multiplexing capability, providing the possibility for imaging several biological incidents simultaneously *in vivo* [114]. As previously discussed, exploiting the intrinsic characteristics of CNTs in Raman imaging allows and extended visualization period compared to other modalities. Thus, using this technique, a study by Liu et al. was able to track the biodistribution and excretion of CNTs *in vivo* over a 3 month follow-up period [106]. Nonetheless, the general issue with Raman imaging is a severely low scattering cross section which is much smaller than that of fluorescence [115]. To overcome this problem, various strategies have been suggested to enhance Raman scattering, including the addition of nano-sized metal nanoparticles on CNTs. This method remains the preferred

solution for overcoming the limitations of Raman imaging [114]. For example, Kneipp et al. found that CNTs with silver colloidal clusters could augment Raman scattering up to 12 orders of magnitude [119].

Photoacoustic imaging

Photoacoustic imaging is a hybrid technique that incorporates optical and ultrasound imaging by applying the photoacoustic effect [120]. Photonic energy – usually generated by a short laser pulse – induces heating and acoustic (ultrasonic) emission in soft tissues by generating molecular vibrations in response to thermal expansion. These emissions can be detected by an ultrasound receiver and mapped into an image [121]. Due to higher spatial resolution and deeper tissue imaging capabilities compared to other optical imaging methods, this modality has been favored by researchers over the past decade [122]. Considering that scattering in deep tissue imaging can greatly lower spatial resolution, weaker ultrasound scattering with photoacoustic imaging, than optical scattering, is a valuable advantage [123]. In contrast to ultrasound imaging, photoacoustic imaging can also provide better specificity; it can even detect trace hemoglobin, lipids and other light-absorbing substances [120]. However, contrast agents are necessary for photoacoustic imaging. Carbon nanomaterials, such as CNTs, can be used as exogenous contrast agents for this application by virtue of their marked photoacoustic signal production from high optical density in the visible and NIR regions [108, 124].

As CNTs are easily modifiable for the attachment of targeting or signal-enhancing moieties, in addition to its intrinsic photoacoustic property, these materials have been identified as attractive agents for this imaging system [125]. De La Zerda et al. demonstrated that CNTs conjugated with cyclic Arg-Gly-Asp (RGD) peptides led to approximately 8-fold stronger photoacoustic signals in tumor imaging when compared to pristine CNTs [122]. The system

was even further enhanced by adding an indoyanine green (ICG) dye to the CNTs, resulting in ~300-fold better signal *in vivo* with sub-nanomolar sensitivities [126]. Other plasmonic nanoparticles (e.g., gold, silver) have also been frequently complexed with CNTs to boost photoacoustic signal and sensitivity because of their surface plasmon resonance effect [125]. Functionalized fullerenes, too, can be utilized with this imaging modality to offer high contrast images. Krishna et al. produced water-soluble fullerenes by the introduction of hydroxyl groups and used them for *in vivo* photoacoustic imaging [127]. Among graphene-based materials, rGONs are favored over GONs for photoacoustic images because of their intact pi-conjugated structure [108]. Sheng et al. showed that rGONs generated about 3-fold higher photoacoustic signals compared to GONs when employed for *in vivo* photoacoustic imaging [128].

Magnetic Resonance Imaging (MRI)

Though there have been tremendous improvements in the aforementioned optical imaging techniques, the most prominent limitation of these is their poor tissue penetration issue which limits their applicability to human subjects. Accordingly, conventional radiological imaging modalities are still preferred in terms of translation to practice. MRI is one of the most widely used techniques for non-invasive medical imaging in the current clinical setting. Like photoacoustic imaging, the use of contrast agents is necessary for this imaging method. To enhance the sensitivity of MRI, the majority of research has utilized either gadolinium (Gd)-based T_1 or iron oxide-based T_2 contrast agents; some of these studies have also integrated these agents with carbon nanomaterials [66, 77, 129].

Gd-based contrast agents (GBCAs) currently dominate the MRI contrast agent market due to their superior paramagnetic properties. Thus, most has approached MRI imaging by chelating Gd on CNTs [130, 131]. Sitharaman et al. incorporated Gd on CNTs and reported that they could achieve 40 to 90-fold larger reflexivity than currently approved MRI contrast

agents by allowing facile access for hydrogen of water to Gd [132]. This approach is certainly applicable to GONs. In fact, Gizzatov et al. coordinated Gd ions to carboxyl groups on GONs and reported much higher reflexivity values compared to the commercial product, Magnevist® [133]. On the other hand, the issue of nephrogenic toxicity is a highly studied complication of GBCAs which is caused by Gd-leaching from the chelating matrix [134]. To avoid this problem, others researchers selected iron oxide as an MRI contrast agent. Using iron oxide-based contrast agents, Ananta et al. showed that even negligible iron (Fe) content (less than 1 w/w%) on CNTs induced remarkably efficient T_2 relaxation [135]. Applying this idea to GONs, Ma et al. prepared iron oxide-loaded GONs and demonstrated successful *in vivo* MRI imaging [136].

The closed carbon cage structure of fullerenes allows Gd encapsulation instead of chelation at the surface of the carbon allotrope. When a metal ion is located inside the fullerene cage the complex is referred to as a 'metallofullerene,' a complex which has been actively researched for fullerene applications. It was conceived as an effective system of keeping potentially toxic metal ions within the rigid carbon cage, preventing unwanted release of Gd ions from Gd-related toxicity [100, 137]. Using Gd-encapsulated fullerenes, Mikawa et al. showed 20-fold enhanced proton relativity compared to the marketed agent (Magnevist®) [138]. Dorn's group later developed a method of encapsulating three metal atoms per fullerene by selecting larger fullerenes (C_{80}) for metal loading instead of the typical agents (C_{60}). Using this approach, they further improved relativity up to 40-fold compared to a commercial MRI contrast agent (gadodiamide) [139, 140].

Nuclear Medicine Imaging

In addition to radiolabeling, carbon nanomaterials have displayed their potential for nuclear medicine imaging applications such as single photon emission computed tomography

(SPECT) and positron emission tomography (PET). Prior to radionuclide attachment, chelators are usually conjugated to carbon nanomaterials in order to ensure binding between carbon structure and radionuclides. Commonly adopted chelators in nuclear medicine imaging 1,4,7,10-tetraazacyclododecane-1,4,7,10-tetraacetic acid (DOTA), 1,4,7-triazacyclononane-1,4,7-triacetic acid (NOTA) and diethylenetriaminepentaacetic acid (DTPA) [141, 142]. Imaging agents such as ^{86}Y and ^{64}copper (^{64}Cu) bound to CNTs via DOTA have successfully exhibited *in vivo* PET imaging [141, 143]. Wu et al. linked DTPA to CNTs via the covalent method and chelated the adduct with a frequently consumed radionuclide, ^{99m} technetium (^{99m}Tc) for SPECT imaging [144]. Exploiting the unique structural characteristics of CNTs, Hong et al. trapped radionuclides with metal halides (Na^{125}I) inside of CNTs and used them for *in vivo* SPECT imaging [145]. While radiolabeled peptides or proteins are capable of chelating only a few radionuclides per biomolecule, nanocarriers are able to carry a large number of chelators. For example, previous studies have successfully coupled 114 chelators of ^{111}indium (^{111}In) per CNT [48].

By an analogous system, Hong et al. conjugated NOTA on GONs for the chelation of two radionuclides, ^{64}Cu and ^{66}Ga, as a method for *in vivo* PET imaging to visualize tumor vasculature [146, 147]. Furthermore, Cornelissen et al. attached DTPA on GONs via π-π stacking and labeled ^{111}In for *in vivo* SPECT imaging [148]. While research by Li et al. attached a chelator outside of fullerenes for *in vivo* PET imaging (with ^{64}Cu labeling), it is anticipated that future endeavors will use metallofullerenes for repeat experiments [149]. Radionuclides such as ^{166}Ho, ^{177}lutetium (^{177}Lu) and ^{99m}Tc have previously been encapsulated inside of fullerenes, which could potentially be used for SPECT imaging [150-152]. Moreover, various radionuclide-based imaging agents – providing different half-lives and energy level – can be carefully selected for appropriate imaging purposes by loading or chelation with carbon nanomaterials.

1.2.5 Therapy

Photothermal Therapy (PTT)

Carbon nanomaterials have also been actively explored for therapeutic uses. For example, their high optical absorbance in the NIR region have allowed carbon nanomaterials to be applied for PTT. The process involves the local conversion of photon energy to thermal energy (over 40 °C) to destroy diseased cells [153]. This therapeutic option is particularly useful for cancer treatment as cancer cells are more vulnerable to hyperthermia by virtue of their decreased blood supply compared to normal cells [154]. Followed by NIR irradiation, several groups demonstrated the efficacy of CNT-based PTT in tumor-bearing mice models [155-157]. Robinson et al. described that CNT-based PTT was more effective than commonly used PTT agents (e.g., gold nanorods) in regards to achieving similar efficacy at lower doses and less laser power [158].

Yang et al. tried a similar experiment with GONs. They showed that GON-based PTT, intravenously administered, efficiently reduced tumor volume and greatly improved survival, likely due to the passive targeting effect [159]. The following study by Markovic et al. insisted that GONs could induce better PTT effect than CNTs owing to better dispersibility based on thermodynamic, optical and geometrical calculations [160]. Though fullerenes have not been heavily investigated for this therapeutic application, there are some studies that validate fullerene-based PTT. Krishna et al. demonstrated that some functionalization, such as polyhydroxy fullerenes or carboxy fullerenes, could induce photothermal effect with practical laser energy whereas pristine fullerenes and activated carbon could not [161]. In their follow -up study, they demonstrated the efficacy of fullerene-based PTT in a tumor-bearing mice model [127]. Likewise, graphitic-structured MCNs drew a photothermal effect from strong NIR light absorption and showed efficient photothermal conversion properties. With these

findings, Xu et al. asserted that MCNs were efficient and superior PTT agents in comparison to rGONs [105].

Photodynamic Therapy (PDT)

PDT is similar to PTT in the sense that it utilizes photon energy, but differs in its adoption of a photosensitizer (PS) (e.g., porphyrin, Chlorin e6) to produce an oxygen singlet or ROS, to trigger apoptosis of nearby cells [162]. Not only can carbon nanomaterials be used as a PS delivery platform, but also can also function as a PS themselves [108, 163]. For the purpose of CNT-based PDT, initial studies involved the delivery of photosensitizers [164, 165]. However, Wang et al. suggested the use of CNTs as a photosensitizer and showed that both covalently and non-covalently functionalized CNTs could generate the photodynamic effect with visual light [163]. Though GONs have not been reported as photosensitizers themselves, they have been frequently selected as PS delivery carriers. Rong et al. loaded photosensitizers (Photochlor®) by π-π stacking, and results showed tumor shrinkage and improved survival after PDT treatment with *in vivo* models [166].

Fullerenes are widely known as effective photosensitizers because they are more photostable and exhibit less photobleaching compared to many available PS [167]. In addition, they are capable of producing both free radicals and ROS, while some PS can produce only one or the other. Therefore, they are the most actively investigated carbon nanomaterials for this therapeutic strategy. Tabata et al. attached PEG to fullerenes, to enhance dispersibility, and injected the formulation intravenously into tumor-bearing mice [168]. Results showed that fullerene-based PDTs successfully suppress tumor growth and that this effect is superior to a commonly used PS, Photofrin®. A marked drawback of exploiting fullerenes in PDT is their lower range of optical absorption in the visible region, which significantly limits *in vivo* application owing to the issue of tissue penetration [167]. To extend their absorption spectra

into the red/NIR region, attaching another PS (e.g., Chlorin e6) and optical clearing agents on fullerenes have been proposed as possible options [169-171].

Drug Delivery

As briefly introduced above, carbon nanomaterials hold great promise for drug delivery applications based on their ability to cross cell membrane, their improved pharmacokinetics and biodistribution, the ease of surface modification, good biocompatibility, large loading capacity and tunable drug release [77, 172, 173]. Doxorubicin (DOX), as a popular example, can be strongly associated with CNTs via π-π stacking. According to Liu et al., DOX loading to CNTs can be achieved up to 400 w/w% capacity compared to only 8-10 w/w% Dox loading capacity with conventional liposomes. Furthermore, release profile of the CNT-DOX complex can be tuned by altering the pH [108, 174]. By taking an advantage of the CNT-based delivery system, other cancer chemotherapeutics have been loaded to CNTs by either covalent or non-covalent method; these endeavors have exhibited promising efficacy [89]. For example, Liu et al. conjugated water-insoluble paclitaxel (PTX) to the surface of CNTs by a cleavable linker. Cargo was released at the target site and results showed better efficacy in breast cancer-bearing mice compared to clinically approved Taxol® [175]. Due to the structural similarity with CNTs, similar approaches have been explored with GONs [89, 176]. In such a way, diverse small molecules (e.g., antimicrobials, anti-inflammatory drugs, boron neutron capture agent) as well as large molecules (e.g., peptides, proteins) can be delivered with both CNTs and GONs [80, 172, 177, 178].

While there are some publications describing the use of fullerene-based drug delivery systems, investigation in this area is less prevalent compared to other carbon nanocarriers [179]. The small size of fullerenes (~ 1nm) is a major hindrance for this application, as nanocarriers smaller than ~ 5 nm are quickly cleared by the kidney [77, 180]. To overcome this

obstacle, some research groups prepared fullerene aggregates which were approximately 50-200 nm in size in order to avoid renal clearance and take advantage of the enhanced permeability and retention (EPR) effect [181, 182]. With this method, Shi et al. conjugated polymers (PEI) and chemotherapeutics (docetaxel) to form a monodispersed and approximately 140 nm-sized fullerene aggregates and utilized this efficacious platform for treating cancer in a mouse model [181].

For drug delivery purpose, MCNs are usually compared with MSNs as a classification of porous materials, instead of other carbon matrices. In addition to the aforementioned advantage (better biocompatibility), MCNs are preferred over MSNs because of their higher surface area and, resulting in larger drug loading capacity [183]. Based on lessons learned from CNTs and GONs, Zhu et al. loaded DOX on MCNs using π-π interactions and showed a pH-dependent release profile, endocytosis and beneficial tumor-killing effect with *in vitro* experiments [74]. Gu et al. selected another chemotherapeutic (camptothecin) for MCN-based drug delivery system, and confirmed that carbon matrices offered a 1.7-fold increased loading capacity over MSNs [183]. Exploiting the high NIR absorbance of MCNs, other studies demonstrated a controlled release of drug by heat generation and explored applications of chemo-photothermal therapy [105, 113]. Wan et al. loaded PTX on PEI-functionalized MCNs and attached targeting ligands (folic acid) for active tumor targeting. Results showed superior efficacy compared to *in vivo* control groups [184].

Gene Delivery

Gene therapy provides a promising avenue for the treatment of diverse cancer types as well as genetic disorders that have no other therapeutic options. Poor pharmacokinetic profile and easy degradation by nucleases are common limiting factors for current gene therapies (e.g., small interfering RNA (siRNA), plasmid DNA (pDNA), antisense oligonucleotides).

Alternative delivery systems have been explored to overcome these issues [185]. In spite of lower transfection efficiency compared to viral vectors, non-viral vectors – including carbon nanomaterials – can possess lower immunogenicity while contributing potential for higher payload loading and scale-up [186-188]. Positive charges must generally be induced on carbon nanomaterials by functionalization so that they can bind to negatively charged DNA or RNA through electrostatic interactions. Though the first study of CNT-based gene delivery systems was able to enhance gene expression up to 10 times more than pDNA alone, researchers used beta-galactosidase as a proof-of-concept [189]. Another study conducted by Liu et al. showed that siRNA was successfully delivered with CNTs to transfected human T and primary cells, which has been a challenging task for non-viral vectors [190]. Later, McCarroll et al. and many others demonstrated the potency of CNT-based gene delivery system at an *in vivo* level [191, 192].

Since early studies of carbon nanomaterial-based gene therapy were investigated with CNTs, experiments have been repeated, and further improved upon, with GONs. Due to the inherent negative charge of unmodified GONs, both charge masking and introducing positive charge are imperative for condensing genetic cargos. PEI is a cationic polymer which has been extensively used in gene therapy by virtue of its high transfection efficiency, but the toxicity of the polymer itself has limited its applicability [108]. Feng et al. conjugated PEI to load genes (pDNA and siRNA) and PEG to enhance biocompatibility on GONs; findings showed outstanding transfection efficiency while reducing cytotoxicity of the polymer [193]. Thus, a large portion of GON-based gene therapy has exploited the GONs-PEI platform.

With regard to numerous gene delivery publications utilizing other carbon nanomaterials, fullerene-based gene therapy so far has received little attention. Besides the aforementioned issue of small size, fullerenes also carry a large price tag. In the past decade, the price has been lowered; it is thought to be a more accessible option in the near future [194].

Nevertheless, a study by Nakamura et al. pioneered the application of tetracationic fullerenes to induce strong association with double-stranded pDNA [195]. The group successfully transfected green fluorescent protein (GFP) to mammalian cells for the first time with fullerenes; this efficiency was comparable to the commercial agent (lipofection). Ten years later, the same group slightly modified the formulation and demonstrated the feasibility with an *in vivo* model. This was the first *in vivo* study for fullerene-based gene delivery systems [196].

1.3 REFERENCES

[1] T. Sridhar, R.P. Symonds, Principles of chemotherapy and radiotherapy, Obstetrics, Gynaecology & Reproductive Medicine 19(3) (2009) 61-67.

[2] M. Koukourakis, Radiation damage and radioprotectants: new concepts in the era of molecular medicine, The British journal of radiology (2014).

[3] R. Baskar, K.A. Lee, R. Yeo, K.-W. Yeoh, Cancer and radiation therapy: current advances and future directions, Int J Med Sci 9(3) (2012) 193-199.

[4] J. Thariat, J.-M. Hannoun-Levi, A.S. Myint, T. Vuong, J.-P. Gérard, Past, present, and future of radiotherapy for the benefit of patients, Nature reviews Clinical oncology 10(1) (2013) 52-60.

[5] X.G. Xu, B. Bednarz, H. Paganetti, A review of dosimetry studies on external-beam radiation treatment with respect to second cancer induction, Physics in medicine and biology 53(13) (2008) R193.

[6] E.J. Hall, Intensity-modulated radiation therapy, protons, and the risk of second cancers, International Journal of Radiation Oncology* Biology* Physics 65(1) (2006) 1-7.

[7] C.R. Baines, W. McGuiness, G.A. O'Rourke, An integrative review of skin assessment tools used to evaluate skin injury related to external beam radiation therapy, Journal of Clinical Nursing 26(7-8) (2017) 1137-1144.

[8] J.J. Kim, I.F. Tannock, Repopulation of cancer cells during therapy: an important cause of treatment failure, Nature Reviews Cancer 5(7) (2005) 516-525.

[9] C.A. Regueiro, Brachytherapy: basic concepts, current clinical indications and future perspectives, Clinical and Translational Oncology 4(9) (2002) 512-516.

[10] M.K. Bakht, M. Sadeghi, Internal radiotherapy techniques using radiolanthanide praseodymium-142: a review of production routes, brachytherapy, unsealed source therapy, Annals of nuclear medicine 25(8) (2011) 529.

[11] J.-J. Mazeron, J.-M. Ardiet, C. Haie-Méder, G. Kovács, P. Levendag, D. Peiffert, A. Polo, A. Rovirosa, V. Strnad, GEC-ESTRO recommendations for brachytherapy for head and neck squamous cell carcinomas, Radiotherapy and Oncology 91(2) (2009) 150-156.

[12] J.-M. Hannoun-Levi, M.-E. Chand-Fouche, C. Dejean, A. Courdi, Dose gradient impact on equivalent dose at 2 Gy for high dose rate interstitial brachytherapy, J Contemp Brachytherapy 4 (2012) 14-20.

[13] S. Langley, R. Laing, Prostate brachytherapy has come of age: a review of the technique and results, BJU international 89(3) (2002) 241-249.

[14] F.M. Khan, J.P. Gibbons, Khan's the physics of radiation therapy, Lippincott Williams & Wilkins2014.

[15] D. Chassagne, A. Dutreix, P. Almond, J.M.V. Burgers, M. Busch, C.A. Joslin, Report 38, Journal of the International Commission on Radiation Units and Measurements os20(1) (1985) NP-NP.

[16] C.R. King, LDR vs. HDR brachytherapy for localized prostate cancer: the view from radiobiological models, Brachytherapy 1(4) (2002) 219-226.

[17] L. Zografos, L. Bercher, L. Chamot, C. Gailloud, S. Raimondi, E. Egger, Cobalt-60 treatment of choroidal hemangiomas, American journal of ophthalmology 121(2) (1996) 190-199.

[18] W. Maier, K. Henne, A. Krebs, J. Schipper, Endoscopic ultrasound-guided brachytherapy of head and neck tumours. A new procedure for controlled application, The Journal of Laryngology & Otology 113(01) (1999) 41-48.

[19] L. Zhang, H. Chen, L. Wang, T. Liu, J. Yeh, G. Lu, L. Yang, H. Mao, Delivery of therapeutic radioisotopes using nanoparticle platforms: potential benefit in systemic radiation therapy, Nanotechnol Sci Appl 3 (2010) 159-170.

[20] D. Murray, A.J. McEwan, Radiobiology of systemic radiation therapy, Cancer biotherapy & radiopharmaceuticals 22(1) (2007) 1-23.

[21] O.M. Salazar, P. Rubin, B. Keller, C. Scarantino, Systeniic (half-body) radiation therapy: Response and toxicity, International Journal of Radiation Oncology* Biology* Physics 4(11-12) (1978) 937-950.

[22] I.R. McDougall, Systemic radiation therapy with unsealed radionuclides, Seminars in radiation oncology, Elsevier, 2000, pp. 94-102.

[23] M. Braga-Basaria, M.D. Ringel, Beyond radioiodine: a review of potential new therapeutic approaches for thyroid cancer, The Journal of Clinical Endocrinology & Metabolism 88(5) (2003) 1947-1960.

[24] M. Castellani, E. Seregni, M. Maccauro, C. Chiesa, G. Aliberti, E. Orunesu, E. Bombardieri, MIBG for diagnosis and therapy of medullay thyroid carcinoma: is there still a role?, The Quarterly Journal of Nuclear Medicine and Molecular Imaging 52(4) (2008) 430.

[25] M.F. Hawthorne, A. Maderna, Applications of radiolabeled boron clusters to the diagnosis and treatment of cancer, Chemical reviews 99(12) (1999) 3421-3434.

[26] B. Allen, N. Blagojevic, Alpha-and beta-emitting radiolanthanides in targeted cancer therapy: the potential role of terbium-149, Nuclear medicine communications 17(1) (1996) 40-47.

[27] R. Salem, R.J. Lewandowski, B. Atassi, S.C. Gordon, V.L. Gates, O. Barakat, Z. Sergie, C.-Y.O. Wong, K.G. Thurston, Treatment of unresectable hepatocellular carcinoma with use of 90 Y microspheres (TheraSphere): safety, tumor response, and survival, Journal of Vascular and Interventional Radiology 16(12) (2005) 1627-1639.

[28] G.A. Wiseman, C.A. White, R.B. Sparks, W.D. Erwin, D.A. Podoloff, D. Lamonica, N.L. Bartlett, J.A. Parker, W.L. Dunn, S.M. Spies, Biodistribution and dosimetry results from a phase III prospectively randomized controlled trial of Zevalin™ radioimmunotherapy for low-

grade, follicular, or transformed B-cell non-Hodgkin's lymphoma, Critical reviews in oncology/hematology 39(1) (2001) 181-194.

[29] D.T. Win, Neutron activation analysis (NAA), AU J Technol 8(1) (2004) 8-14.

[30] D.J. Hughes, Neutron cross sections, Elsevier2016.

[31] E.M. Baum, M.C. Ernesti, H.D. Knox, T.R. Miller, A.M. Wastson, Nuclides and Isotopes: Chart of the Nuclides, 17th ed., Knolls Atomic Power Laboratory2010.

[32] K. Cho, X. Wang, S. Nie, D.M. Shin, Therapeutic nanoparticles for drug delivery in cancer, Clinical cancer research 14(5) (2008) 1310-1316.

[33] D.C. Litzinger, L. Huang, Phosphatodylethanolamine liposomes: drug delivery, gene transfer and immunodiagnostic applications, Biochimica et Biophysica Acta (BBA)-Reviews on Biomembranes 1113(2) (1992) 201-227.

[34] Y. Bae, S. Fukushima, A. Harada, K. Kataoka, Design of environment-sensitive supramolecular assemblies for intracellular drug delivery: Polymeric micelles that are responsive to intracellular pH change, Angewandte Chemie 115(38) (2003) 4788-4791.

[35] H. Ma, S. Lin, Y.-H. Chiang, J. Li, S. Chen, Y. Tsao, X. Xiao, Intratumoral gene therapy of malignant brain tumor in a rat model with angiostatin delivered by adeno-associated viral (AAV) vector, Gene therapy 9(1) (2002) 2-11.

[36] Y. Cheng, A. C. Samia, J.D. Meyers, I. Panagopoulos, B. Fei, C. Burda, Highly efficient drug delivery with gold nanoparticle vectors for in vivo photodynamic therapy of cancer, Journal of the American Chemical Society 130(32) (2008) 10643-10647.

[37] I.I. Slowing, J.L. Vivero-Escoto, C.-W. Wu, V.S.-Y. Lin, Mesoporous silica nanoparticles as controlled release drug delivery and gene transfection carriers, Advanced drug delivery reviews 60(11) (2008) 1278-1288.

[38] B. Chertok, B.A. Moffat, A.E. David, F. Yu, C. Bergemann, B.D. Ross, V.C. Yang, Iron oxide nanoparticles as a drug delivery vehicle for MRI monitored magnetic targeting of brain tumors, Biomaterials 29(4) (2008) 487-496.

[39] P. Zrazhevskiy, M. Sena, X. Gao, Designing multifunctional quantum dots for bioimaging, detection, and drug delivery, Chemical Society Reviews 39(11) (2010) 4326-4354.

[40] R.E. Smalley, Discovering the fullerenes (Nobel lecture), Angewandte Chemie International Edition in English 36(15) (1997) 1594-1601.

[41] A.K. Geim, Random walk to graphene (Nobel Lecture), Angewandte Chemie International Edition 50(31) (2011) 6966-6985.

[42] V. Biju, Chemical modifications and bioconjugate reactions of nanomaterials for sensing, imaging, drug delivery and therapy, Chemical Society Reviews 43(3) (2014) 744-764.

[43] A. Jorio, E. Kauppinen, A. Hassanien, Carbon-nanotube metrology, Carbon Nanotubes, Springer2007, pp. 63-100.

[44] H.W. Kroto, J.R. Heath, S.C. O'Brien, R.F. Curl, R.E. Smalley, C 60: buckminsterfullerene, Nature 318(6042) (1985) 162-163.

[45] C. Liang, Z. Li, S. Dai, Mesoporous carbon materials: synthesis and modification, Angewandte Chemie International Edition 47(20) (2008) 3696-3717.

[46] Y. Fang, D. Gu, Y. Zou, Z. Wu, F. Li, R. Che, Y. Deng, B. Tu, D. Zhao, A Low-Concentration Hydrothermal Synthesis of Biocompatible Ordered Mesoporous Carbon Nanospheres with Tunable and Uniform Size, Angewandte Chemie International Edition 49(43) (2010) 7987-7991.

[47] J. Schuster, G. He, B. Mandlmeier, T. Yim, K.T. Lee, T. Bein, L.F. Nazar, Spherical ordered mesoporous carbon nanoparticles with high porosity for lithium–sulfur batteries, Angewandte Chemie 124(15) (2012) 3651-3655.

[48] R.M. Reilly, Carbon nanotubes: potential benefits and risks of nanotechnology in nuclear medicine, Journal of Nuclear Medicine 48(7) (2007) 1039-1042.

[49] R.H. Baughman, A.A. Zakhidov, W.A. De Heer, Carbon nanotubes--the route toward applications, science 297(5582) (2002) 787-792.

[50] A. Hirsch, Functionalization of single-walled carbon nanotubes, Angewandte Chemie International Edition 41(11) (2002) 1853-1859.

[51] R. Ding, G. Lu, Z. Yan, M. Wilson, Recent advances in the preparation and utilization of carbon nanotubes for hydrogen storage, Journal of nanoscience and nanotechnology 1(1) (2001) 7-29.

[52] K. Awasthi, A. Srivastava, O. Srivastava, Synthesis of carbon nanotubes, Journal of nanoscience and nanotechnology 5(10) (2005) 1616-1636.

[53] B.W. Smith, M. Monthioux, D.E. Luzzi, Encapsulated C60 in carbon nanotubes, Nature 396(6709) (1998) 323.

[54] T. Guo, M. Diener, Y. Chai, M. Alford, R. Haufler, S. McClure, T. Ohno, J. Weaver, G. Scuseria, R. Smalley, Uranium Stabilization of C~ 2~ 8: A Tetravalent Fullerene, Science 257(5077) (1992) 1661-1664.

[55] C. Piskoti, A. Zettl, H. Kuzmany, J. Fink, M. Mehring, S. Roth, The first stable lower fullerene: C 36, AIP Conference Proceedings, AIP, 1998, pp. 183-185.

[56] F. Diederich, R. Ettl, The Higher Fullerenes: Isolation and Characterization of C (76), C (84), C (90), C (94), and C (70) O, an Oxide of D (5h)-C (70), Science 252(5005) (1991) 548.

[57] S. Pizzarello, Y. Huang, L. Becker, R.J. Poreda, R.A. Nieman, G. Cooper, M. Williams, The organic content of the Tagish Lake meteorite, Science 293(5538) (2001) 2236-2239.

[58] J. Cami, J. Bernard-Salas, E. Peeters, S.E. Malek, Detection of C60 and C70 in a young planetary nebula, Science 329(5996) (2010) 1180-1182.

[59] A. Hirsch, The era of carbon allotropes, Nature materials 9(11) (2010) 868-871.

[60] W. Krätschmer, L.D. Lamb, K. Fostiropoulos, D.R. Huffman, Solid C60: a new form of carbon, Nature 347 (1990) 27.

[61] K.S. Novoselov, A.K. Geim, S.V. Morozov, D. Jiang, Y. Zhang, S.V. Dubonos, I.V. Grigorieva, A.A. Firsov, Electric field effect in atomically thin carbon films, science 306(5696) (2004) 666-669.

[62] S. Stankovich, R.D. Piner, X. Chen, N. Wu, S.T. Nguyen, R.S. Ruoff, Stable aqueous dispersions of graphitic nanoplatelets via the reduction of exfoliated graphite oxide in the presence of poly (sodium 4-styrenesulfonate), Journal of Materials Chemistry 16(2) (2006) 155-158.

[63] M.J. Allen, V.C. Tung, R.B. Kaner, Honeycomb carbon: a review of graphene, Chemical reviews 110(1) (2009) 132-145.

[64] S. Mohanty, S.K. Nayak, B. Kaith, S. Kalia, Polymer nanocomposites based on inorganic and organic nanomaterials, John Wiley & Sons2015.

[65] D.C. Marcano, D.V. Kosynkin, J.M. Berlin, A. Sinitskii, Z. Sun, A. Slesarev, L.B. Alemany, W. Lu, J.M. Tour, Improved synthesis of graphene oxide, ACS nano 4(8) (2010) 4806-4814.

[66] Y. Zhang, T.R. Nayak, H. Hong, W. Cai, Graphene: a versatile nanoplatform for biomedical applications, Nanoscale 4(13) (2012) 3833-3842.

[67] J.M. Dias, M.C. Alvim-Ferraz, M.F. Almeida, J. Rivera-Utrilla, M. Sánchez-Polo, Waste materials for activated carbon preparation and its use in aqueous-phase treatment: a review, Journal of Environmental Management 85(4) (2007) 833-846.

[68] K.S. Sing, Reporting physisorption data for gas/solid systems with special reference to the determination of surface area and porosity (Recommendations 1984), Pure and applied chemistry 57(4) (1985) 603-619.

[69] M. Vallet-Regí, F. Balas, D. Arcos, Mesoporous materials for drug delivery, Angewandte Chemie International Edition 46(40) (2007) 7548-7558.

[70] A. Yan, B.W. Lau, B.S. Weissman, I. Külaots, N.Y. Yang, A.B. Kane, R.H. Hurt, Biocompatible, hydrophilic, supramolecular carbon nanoparticles for cell delivery, Advanced Materials 18(18) (2006) 2373-2378.

[71] T.-Y. Ma, L. Liu, Z.-Y. Yuan, Direct synthesis of ordered mesoporous carbons, Chemical Society Reviews 42(9) (2013) 3977-4003.

[72] V. Datsyuk, M. Kalyva, K. Papagelis, J. Parthenios, D. Tasis, A. Siokou, I. Kallitsis, C. Galiotis, Chemical oxidation of multiwalled carbon nanotubes, Carbon 46(6) (2008) 833-840.

[73] W.S. Hummers Jr, R.E. Offeman, Preparation of graphitic oxide, Journal of the American Chemical Society 80(6) (1958) 1339-1339.

[74] J. Zhu, L. Liao, X. Bian, J. Kong, P. Yang, B. Liu, pH-Controlled Delivery of Doxorubicin to Cancer Cells, Based on Small Mesoporous Carbon Nanospheres, Small 8(17) (2012) 2715-2720.

[75] A. Hamwi, V. Marchand, Oxidized fullerene derivatives containing hydroxyl, nitro and fluorine groups, Fullerene Science and Technology 4(5) (1996) 835-851.

[76] P.-C. Ma, N.A. Siddiqui, G. Marom, J.-K. Kim, Dispersion and functionalization of carbon nanotubes for polymer-based nanocomposites: a review, Composites Part A: Applied Science and Manufacturing 41(10) (2010) 1345-1367.

[77] R. Bakry, R.M. Vallant, M. Najam-ul-Haq, M. Rainer, Z. Szabo, C.W. Huck, G.K. Bonn, Medicinal applications of fullerenes, International journal of nanomedicine 2(4) (2007) 639.

[78] V. Georgakilas, M. Otyepka, A.B. Bourlinos, V. Chandra, N. Kim, K.C. Kemp, P. Hobza, R. Zboril, K.S. Kim, Functionalization of graphene: covalent and non-covalent approaches, derivatives and applications, Chemical reviews 112(11) (2012) 6156-6214.

[79] E. Heister, V. Neves, C. Tîlmaciu, K. Lipert, V.S. Beltrán, H.M. Coley, S.R.P. Silva, J. McFadden, Triple functionalisation of single-walled carbon nanotubes with doxorubicin, a monoclonal antibody, and a fluorescent marker for targeted cancer therapy, Carbon 47(9) (2009) 2152-2160.

[80] A. Bianco, K. Kostarelos, M. Prato, Applications of carbon nanotubes in drug delivery, Current opinion in chemical biology 9(6) (2005) 674-679.

[81] Y. Wang, Z. Li, J. Wang, J. Li, Y. Lin, Graphene and graphene oxide: biofunctionalization and applications in biotechnology, Trends in biotechnology 29(5) (2011) 205-212.

[82] A. Montellano, T. Da Ros, A. Bianco, M. Prato, Fullerene C 60 as a multifunctional system for drug and gene delivery, Nanoscale 3(10) (2011) 4035-4041.

[83] Y. Xie, A. Soh, Investigation of non-covalent association of single-walled carbon nanotube with amylose by molecular dynamics simulation, Materials Letters 59(8) (2005) 971-975.

[84] L. Wan, J. Jiao, Y. Cui, J. Guo, N. Han, D. Di, D. Chang, P. Wang, T. Jiang, S. Wang, Hyaluronic acid modified mesoporous carbon nanoparticles for targeted drug delivery to CD44-overexpressing cancer cells, Nanotechnology 27(13) (2016) 135102.

[85] T.-W. Kim, P.-W. Chung, I.I. Slowing, M. Tsunoda, E.S. Yeung, V.S.-Y. Lin, Structurally ordered mesoporous carbon nanoparticles as transmembrane delivery vehicle in human cancer cells, Nano letters 8(11) (2008) 3724-3727.

[86] P.M. Ajayan, J.M. Tour, Materials science: nanotube composites, Nature 447(7148) (2007) 1066-1068.

[87] Z. Liu, S. Tabakman, K. Welsher, H. Dai, Carbon nanotubes in biology and medicine: in vitro and in vivo detection, imaging and drug delivery, Nano research 2(2) (2009) 85-120.

[88] W. Yang, P. Thordarson, J.J. Gooding, S.P. Ringer, F. Braet, Carbon nanotubes for biological and biomedical applications, Nanotechnology 18(41) (2007) 412001.

[89] Z. Liu, J.T. Robinson, S.M. Tabakman, K. Yang, H. Dai, Carbon materials for drug delivery & cancer therapy, Materials today 14(7) (2011) 316-323.

[90] S. Foley, C. Crowley, M. Smaihi, C. Bonfils, B.F. Erlanger, P. Seta, C. Larroque, Cellular localisation of a water-soluble fullerene derivative, Biochemical and biophysical research communications 294(1) (2002) 116-119.

[91] T. Lammel, P. Boisseaux, M.-L. Fernández-Cruz, J.M. Navas, Internalization and cytotoxicity of graphene oxide and carboxyl graphene nanoplatelets in the human hepatocellular carcinoma cell line Hep G2, Particle and fibre toxicology 10(1) (2013) 27.

[92] M. Prato, K. Kostarelos, A. Bianco, Functionalized carbon nanotubes in drug design and discovery, Accounts of chemical research 41(1) (2007) 60-68.

[93] M. Foldvari, M. Bagonluri, Carbon nanotubes as functional excipients for nanomedicines: II. Drug delivery and biocompatibility issues, Nanomedicine: Nanotechnology, Biology and Medicine 4(3) (2008) 183-200.

[94] C.A. Poland, R. Duffin, I. Kinloch, A. Maynard, W.A. Wallace, A. Seaton, V. Stone, S. Brown, W. MacNee, K. Donaldson, Carbon nanotubes introduced into the abdominal cavity of mice show asbestos-like pathogenicity in a pilot study, Nature nanotechnology 3(7) (2008) 423-428.

[95] L. Lacerda, A. Bianco, M. Prato, K. Kostarelos, Carbon nanotubes as nanomedicines: from toxicology to pharmacology, Advanced drug delivery reviews 58(14) (2006) 1460-1470.

[96] L. Meng, X. Zhang, Q. Lu, Z. Fei, P.J. Dyson, Single walled carbon nanotubes as drug delivery vehicles: targeting doxorubicin to tumors, Biomaterials 33(6) (2012) 1689-1698.

[97] M.F. De Volder, S.H. Tawfick, R.H. Baughman, A.J. Hart, Carbon nanotubes: present and future commercial applications, science 339(6119) (2013) 535-539.

[98] E. Oberdörster, Manufactured nanomaterials (fullerenes, C60) induce oxidative stress in the brain of juvenile largemouth bass, Environmental health perspectives (2004) 1058-1062.

[99] C.M. Sayes, A.M. Gobin, K.D. Ausman, J. Mendez, J.L. West, V.L. Colvin, Nano-C 60 cytotoxicity is due to lipid peroxidation, Biomaterials 26(36) (2005) 7587-7595.

[100] R. Partha, J.L. Conyers, Biomedical applications of functionalized fullerene-based nanomaterials, International journal of nanomedicine 4 (2009) 261.

[101] Z. Markovic, V. Trajkovic, Biomedical potential of the reactive oxygen species generation and quenching by fullerenes (C 60), Biomaterials 29(26) (2008) 3561-3573.

[102] C.M. Sayes, J.D. Fortner, W. Guo, D. Lyon, A.M. Boyd, K.D. Ausman, Y.J. Tao, B. Sitharaman, L.J. Wilson, J.B. Hughes, The differential cytotoxicity of water-soluble fullerenes, Nano letters 4(10) (2004) 1881-1888.

[103] V.C. Sanchez, A. Jachak, R.H. Hurt, A.B. Kane, Biological interactions of graphene-family nanomaterials–an interdisciplinary review, Chemical research in toxicology 25(1) (2012) 15.

[104] K. Yang, J. Wan, S. Zhang, Y. Zhang, S.-T. Lee, Z. Liu, In vivo pharmacokinetics, long-term biodistribution, and toxicology of PEGylated graphene in mice, ACS nano 5(1) (2010) 516-522.

[105] G. Xu, S. Liu, H. Niu, W. Lv, R.a. Wu, Functionalized mesoporous carbon nanoparticles for targeted chemo-photothermal therapy of cancer cells under near-infrared irradiation, RSC Advances 4(64) (2014) 33986-33997.

[106] Z. Liu, C. Davis, W. Cai, L. He, X. Chen, H. Dai, Circulation and long-term fate of functionalized, biocompatible single-walled carbon nanotubes in mice probed by Raman spectroscopy, Proceedings of the National Academy of Sciences 105(5) (2008) 1410-1415.

[107] K. Welsher, Z. Liu, S.P. Sherlock, J.T. Robinson, Z. Chen, D. Daranciang, H. Dai, A route to brightly fluorescent carbon nanotubes for near-infrared imaging in mice, Nature nanotechnology 4(11) (2009) 773-780.

[108] G. Hong, S. Diao, A.L. Antaris, H. Dai, Carbon nanomaterials for biological imaging and nanomedicinal therapy, Chemical reviews 115(19) (2015) 10816-10906.

[109] K. Nakada, M. Fujita, G. Dresselhaus, M.S. Dresselhaus, Edge state in graphene ribbons: Nanometer size effect and edge shape dependence, Physical Review B 54(24) (1996) 17954.

[110] X. Wu, F. Tian, W. Wang, J. Chen, M. Wu, J.X. Zhao, Fabrication of highly fluorescent graphene quantum dots using L-glutamic acid for in vitro/in vivo imaging and sensing, Journal of Materials Chemistry C 1(31) (2013) 4676-4684.

[111] S.-K. Lin, L.-L. Shiu, K.-M. Chien, T.-Y. Luh, T.-I. Lin, Fluorescence of Fullerene Derivatives at Room-Temperature, Journal of Physical Chemistry 99(1) (1995) 105-111.

[112] P. Anilkumar, F. Lu, L. Cao, P. G Luo, J.-H. Liu, S. Sahu, K. N Tackett II, Y. Wang, Y.-P. Sun, Fullerenes for applications in biology and medicine, Current medicinal chemistry 18(14) (2011) 2045-2059.

[113] L. Zhou, K. Dong, Z. Chen, J. Ren, X. Qu, Near-infrared absorbing mesoporous carbon nanoparticle as an intelligent drug carrier for dual-triggered synergistic cancer therapy, Carbon 82 (2015) 479-488.

[114] Y. Zhang, H. Hong, W. Cai, Imaging with Raman spectroscopy, Current pharmaceutical biotechnology 11(6) (2010) 654-661.

[115] A. Hartschuh, E.J. Sánchez, X.S. Xie, L. Novotny, High-resolution near-field Raman microscopy of single-walled carbon nanotubes, Physical Review Letters 90(9) (2003) 095503.

[116] J. Bartelmess, S. Quinn, S. Giordani, Carbon nanomaterials: multi-functional agents for biomedical fluorescence and Raman imaging, Chemical Society Reviews 44(14) (2015) 4672-4698.

[117] C.M. Girish, A. Sasidharan, G.S. Gowd, S. Nair, M. Koyakutty, Confocal Raman imaging study showing macrophage mediated biodegradation of graphene in vivo, Advanced healthcare materials 2(11) (2013) 1489-1500.

[118] M.E. Itkis, D.E. Perea, R. Jung, S. Niyogi, R.C. Haddon, Comparison of analytical techniques for purity evaluation of single-walled carbon nanotubes, Journal of the American Chemical Society 127(10) (2005) 3439-3448.

[119] K. Kneipp, H. Kneipp, P. Corio, S. Brown, K. Shafer, J. Motz, L. Perelman, E. Hanlon, A. Marucci, G. Dresselhaus, Surface-enhanced and normal Stokes and anti-Stokes Raman spectroscopy of single-walled carbon nanotubes, Physical review letters 84(15) (2000) 3470.

[120] P. Beard, Biomedical photoacoustic imaging, Interface focus (2011) rsfs20110028.

[121] A. Agarwal, S. Huang, M. O'donnell, K. Day, M. Day, N. Kotov, S. Ashkenazi, Targeted gold nanorod contrast agent for prostate cancer detection by photoacoustic imaging, Journal of applied physics 102(6) (2007) 064701.

[122] A. De La Zerda, C. Zavaleta, S. Keren, S. Vaithilingam, S. Bodapati, Z. Liu, J. Levi, B.R. Smith, T.-J. Ma, O. Oralkan, Carbon nanotubes as photoacoustic molecular imaging agents in living mice, Nature nanotechnology 3(9) (2008) 557-562.

[123] M. Xu, L.V. Wang, Photoacoustic imaging in biomedicine, Review of scientific instruments 77(4) (2006) 041101.

[124] M. Pramanik, K.H. Song, M. Swierczewska, D. Green, B. Sitharaman, L.V. Wang, In vivo carbon nanotube-enhanced non-invasive photoacoustic mapping of the sentinel lymph node, Physics in medicine and biology 54(11) (2009) 3291.

[125] G.P. Luke, D. Yeager, S.Y. Emelianov, Biomedical applications of photoacoustic imaging with exogenous contrast agents, Annals of biomedical engineering 40(2) (2012) 422-437.

[126] A.d.l. Zerda, Z. Liu, S. Bodapati, R. Teed, S. Vaithilingam, B.T. Khuri-Yakub, X. Chen, H. Dai, S.S. Gambhir, Ultrahigh sensitivity carbon nanotube agents for photoacoustic molecular imaging in living mice, Nano letters 10(6) (2010) 2168-2172.

[127] V. Krishna, A. Singh, P. Sharma, N. Iwakuma, Q. Wang, Q. Zhang, J. Knapik, H. Jiang, S.R. Grobmyer, B. Koopman, Polyhydroxy Fullerenes for Non-Invasive Cancer Imaging and Therapy, Small 6(20) (2010) 2236-2241.

[128] Z. Sheng, L. Song, J. Zheng, D. Hu, M. He, M. Zheng, G. Gao, P. Gong, P. Zhang, Y. Ma, Protein-assisted fabrication of nano-reduced graphene oxide for combined in vivo photoacoustic imaging and photothermal therapy, Biomaterials 34(21) (2013) 5236-5243.

[129] H.B. Na, I.C. Song, T. Hyeon, Inorganic nanoparticles for MRI contrast agents, Advanced materials 21(21) (2009) 2133-2148.

[130] P.H. Kuo, Gadolinium-containing MRI contrast agents: important variations on a theme for NSF, Journal of the American College of Radiology 5(1) (2008) 29-35.

[131] Y.-X.J. Wang, Superparamagnetic iron oxide based MRI contrast agents: current status of clinical application, Quantitative imaging in medicine and surgery 1(1) (2011) 35-40.

[132] B. Sitharaman, K.R. Kissell, K.B. Hartman, L.A. Tran, A. Baikalov, I. Rusakova, Y. Sun, H.A. Khant, S.J. Ludtke, W. Chiu, Superparamagnetic gadonanotubes are high-performance MRI contrast agents, Chemical Communications (31) (2005) 3915-3917.

[133] A. Gizzatov, V. Keshishian, A. Guven, A.M. Dimiev, F. Qu, R. Muthupillai, P. Decuzzi, R.G. Bryant, J.M. Tour, L.J. Wilson, Enhanced MRI relaxivity of aquated Gd 3+ ions by carboxyphenylated water-dispersed graphene nanoribbons, Nanoscale 6(6) (2014) 3059-3063.

[134] E.A. Neuwelt, B.E. Hamilton, C.G. Varallyay, W.R. Rooney, R.D. Edelman, P.M. Jacobs, S.G. Watnick, Ultrasmall superparamagnetic iron oxides (USPIOs): a future alternative magnetic resonance (MR) contrast agent for patients at risk for nephrogenic systemic fibrosis (NSF)?, Kidney international 75(5) (2009) 465-474.

[135] J.S. Ananta, M.L. Matson, A.M. Tang, T. Mandal, S. Lin, K. Wong, S.T. Wong, L.J. Wilson, Single-walled carbon nanotube materials as T 2-weighted MRI contrast agents, The Journal of Physical Chemistry C 113(45) (2009) 19369-19372.

[136] X. Ma, H. Tao, K. Yang, L. Feng, L. Cheng, X. Shi, Y. Li, L. Guo, Z. Liu, A functionalized graphene oxide-iron oxide nanocomposite for magnetically targeted drug delivery, photothermal therapy, and magnetic resonance imaging, Nano Research 5(3) (2012) 199-212.

[137] H.L. Fillmore, M.D. Shultz, S.C. Henderson, P. Cooper, W.C. Broaddus, Z.J. Chen, C.-Y. Shu, J. Zhang, J. Ge, H.C. Dorn, Conjugation of functionalized gadolinium metallofullerenes with IL-13 peptides for targeting and imaging glial tumors, Nanomedicine 6(3) (2011) 449-458.

[138] M. Mikawa, H. Kato, M. Okumura, M. Narazaki, Y. Kanazawa, N. Miwa, H. Shinohara, Paramagnetic water-soluble metallofullerenes having the highest relaxivity for MRI contrast agents, Bioconjugate chemistry 12(4) (2001) 510-514.

[139] S. Stevenson, G. Rice, T. Glass, K. Harich, F. Cromer, M. Jordan, J. Craft, E. Hadju, R. Bible, M. Olmstead, Small-bandgap endohedral metallofullerenes in high yield and purity, Nature 401(6748) (1999) 55-57.

[140] P.P. Fatouros, F.D. Corwin, Z.-J. Chen, W.C. Broaddus, J.L. Tatum, B. Kettenmann, Z. Ge, H.W. Gibson, J.L. Russ, A.P. Leonard, In Vitro and in Vivo Imaging Studies of a New Endohedral Metallofullerene Nanoparticle 1, Radiology 240(3) (2006) 756-764.

[141] M.R. McDevitt, D. Chattopadhyay, J.S. Jaggi, R.D. Finn, P.B. Zanzonico, C. Villa, D. Rey, J. Mendenhall, C.A. Batt, J.T. Njardarson, PET imaging of soluble yttrium-86-labeled carbon nanotubes in mice, Plos one 2(9) (2007) e907.

[142] R. Singh, D. Pantarotto, L. Lacerda, G. Pastorin, C. Klumpp, M. Prato, A. Bianco, K. Kostarelos, Tissue biodistribution and blood clearance rates of intravenously administered carbon nanotube radiotracers, Proceedings of the National Academy of Sciences of the United States of America 103(9) (2006) 3357-3362.

[143] Z. Liu, W. Cai, L. He, N. Nakayama, K. Chen, X. Sun, X. Chen, H. Dai, In vivo biodistribution and highly efficient tumour targeting of carbon nanotubes in mice, Nature nanotechnology 2(1) (2007) 47-52.

[144] W. Wu, R. Li, C.C.C.N.w.A.A.P.a.A.A. Bian, Z. Zhu, D. Ding, X. Li, Z. Jia, X. Jiang, Y. Hu, Covalently combining carbon nanotubes with anticancer agent: preparation and antitumor activity, ACS nano 3(9) (2009) 2740-2750.

[145] S.Y. Hong, G. Tobias, K.T. Al-Jamal, B. Ballesteros, H. Ali-Boucetta, S. Lozano-Perez, P.D. Nellist, R.B. Sim, C. Finucane, S.J. Mather, Filled and glycosylated carbon nanotubes for in vivo radioemitter localization and imaging, Nature materials 9(6) (2010) 485-490.

[146] H. Hong, K. Yang, Y. Zhang, J. Engle, L. Feng, C. Theuer, T. Barnhart, Z. Liu, W. Cai, In vivo targeting and imaging of tumor vasculature with radiolabeled, antibody-conjugated nano-graphene, Journal of Nuclear Medicine 53(supplement 1) (2012) 343-343.

[147] H. Hong, Y. Zhang, J.W. Engle, T.R. Nayak, C.P. Theuer, R.J. Nickles, T.E. Barnhart, W. Cai, In vivo targeting and positron emission tomography imaging of tumor vasculature with 66 Ga-labeled nano-graphene, Biomaterials 33(16) (2012) 4147-4156.

[148] B. Cornelissen, S. Able, V. Kersemans, P.A. Waghorn, S. Myhra, K. Jurkshat, A. Crossley, K.A. Vallis, Nanographene oxide-based radioimmunoconstructs for in vivo targeting and SPECT imaging of HER2-positive tumors, Biomaterials 34(4) (2013) 1146-1154.

[149] J. Li, W. Yang, R. Cui, D. Wang, Y. Chang, W. Gu, W. Yin, X. Bai, K. Chen, L. Xia, Metabolizer in vivo of fullerenes and metallofullerenes by positron emission tomography, Nanotechnology 27(15) (2016) 155101.

[150] L.R. Karam, M.G. Mitch, B.M. Coursey, Encapsulation of 99mTc within fullerenes: a novel radionuclidic carrier, Applied radiation and isotopes 48(6) (1997) 771-776.

[151] M.D. Shultz, J.C. Duchamp, J.D. Wilson, C.-Y. Shu, J. Ge, J. Zhang, H.W. Gibson, H.L. Fillmore, J.I. Hirsch, H.C. Dorn, Encapsulation of a Radiolabeled Cluster Inside a Fullerene Cage, 177LuxLu (3-x) N@ C80: An Interleukin-13 Conjugated Radiolabeled Metallofullerene Platform, Journal of the American Chemical Society 132(14) (2010) 4980.

[152] D.W. Cagle, S.J. Kennel, S. Mirzadeh, J.M. Alford, L.J. Wilson, In vivo studies of fullerene-based materials using endohedral metallofullerene radiotracers, Proceedings of the National Academy of Sciences 96(9) (1999) 5182-5187.

[153] X. Huang, P.K. Jain, I.H. El-Sayed, M.A. El-Sayed, Determination of the minimum temperature required for selective photothermal destruction of cancer cells with the use of immunotargeted gold nanoparticles, Photochemistry and photobiology 82(2) (2006) 412-417.

[154] X. Huang, P.K. Jain, I.H. El-Sayed, M.A. El-Sayed, Plasmonic photothermal therapy (PPTT) using gold nanoparticles, Lasers in medical science 23(3) (2008) 217.

[155] S. Ghosh, S. Dutta, E. Gomes, D. Carroll, R. D'Agostino Jr, J. Olson, M. Guthold, W.H. Gmeiner, Increased heating efficiency and selective thermal ablation of malignant tissue with DNA-encased multiwalled carbon nanotubes, ACS nano 3(9) (2009) 2667-2673.

[156] A. Burke, X. Ding, R. Singh, R.A. Kraft, N. Levi-Polyachenko, M.N. Rylander, C. Szot, C. Buchanan, J. Whitney, J. Fisher, Long-term survival following a single treatment of kidney tumors with multiwalled carbon nanotubes and near-infrared radiation, Proceedings of the National Academy of Sciences 106(31) (2009) 12897-12902.

[157] X. Liu, H. Tao, K. Yang, S. Zhang, S.-T. Lee, Z. Liu, Optimization of surface chemistry on single-walled carbon nanotubes for in vivo photothermal ablation of tumors, Biomaterials 32(1) (2011) 144-151.

[158] J.T. Robinson, K. Welsher, S.M. Tabakman, S.P. Sherlock, H. Wang, R. Luong, H. Dai, High performance in vivo near-IR (> 1 μm) imaging and photothermal cancer therapy with carbon nanotubes, Nano research 3(11) (2010) 779-793.

[159] K. Yang, S. Zhang, G. Zhang, X. Sun, S.-T. Lee, Z. Liu, Graphene in mice: ultrahigh in vivo tumor uptake and efficient photothermal therapy, Nano letters 10(9) (2010) 3318-3323.

[160] Z.M. Markovic, L.M. Harhaji-Trajkovic, B.M. Todorovic-Markovic, D.P. Kepić, K.M. Arsikin, S.P. Jovanović, A.C. Pantovic, M.D. Dramićanin, V.S. Trajkovic, In vitro comparison of the photothermal anticancer activity of graphene nanoparticles and carbon nanotubes, Biomaterials 32(4) (2011) 1121-1129.

[161] V. Krishna, N. Stevens, B. Koopman, B. Moudgil, Optical heating and rapid transformation of functionalized fullerenes, Nature nanotechnology 5(5) (2010) 330-334.

[162] B. Tian, C. Wang, S. Zhang, L. Feng, Z. Liu, Photothermally enhanced photodynamic therapy delivered by nano-graphene oxide, ACS nano 5(9) (2011) 7000-7009.

[163] L. Wang, J. Shi, R. Liu, Y. Liu, J. Zhang, X. Yu, J. Gao, C. Zhang, Z. Zhang, Photodynamic effect of functionalized single-walled carbon nanotubes: a potential sensitizer for photodynamic therapy, Nanoscale 6(9) (2014) 4642-4651.

[164] D.M. Guldi, H. Taieb, G.A. Rahman, N. Tagmatarchis, M. Prato, Novel Photoactive Single-Walled Carbon Nanotube–Porphyrin Polymer Wraps: Efficient and Long-Lived Intracomplex Charge Separation, Advanced Materials 17(7) (2005) 871-875.

[165] Z. Zhu, Z. Tang, J.A. Phillips, R. Yang, H. Wang, W. Tan, Regulation of singlet oxygen generation using single-walled carbon nanotubes, Journal of the American Chemical Society 130(33) (2008) 10856-10857.

[166] P. Rong, K. Yang, A. Srivastan, D.O. Kiesewetter, X. Yue, F. Wang, L. Nie, A. Bhirde, Z. Wang, Z. Liu, Photosensitizer loaded nano-graphene for multimodality imaging guided tumor photodynamic therapy, Theranostics 4(3) (2014) 229-39.

[167] S.K. Sharma, L.Y. Chiang, M.R. Hamblin, Photodynamic therapy with fullerenes in vivo: reality or a dream?, Nanomedicine 6(10) (2011) 1813-1825.

[168] Y. Tabata, Y. Murakami, Y. Ikada, Photodynamic Effect of Polyethylene Glycol–modified Fullerene on Tumor, Cancer Science 88(11) (1997) 1108-1116.

[169] C. Constantin, M. Neagu, R.-M. Ion, M. Gherghiceanu, C. Stavaru, Fullerene–porphyrin nanostructures in photodynamic therapy, Nanomedicine 5(2) (2010) 307-317.

[170] J. Jiang, M. Boese, P. Turner, R.K. Wang, Penetration kinetics of dimethyl sulphoxide and glycerol in dynamic optical clearing of porcine skin tissue in vitro studied by Fourier transform infrared spectroscopic imaging, Journal of biomedical optics 13(2) (2008) 021105-021105-7.

[171] T. Wharton, H. Gali, M.R. Hamblin, Photosensitizers for targeted photodynamic therapy, Google Patents, 2012.

[172] B.S. Wong, S.L. Yoong, A. Jagusiak, T. Panczyk, H.K. Ho, W.H. Ang, G. Pastorin, Carbon nanotubes for delivery of small molecule drugs, Advanced drug delivery reviews 65(15) (2013) 1964-2015.

[173] K. Yang, L. Feng, Z. Liu, Stimuli responsive drug delivery systems based on nano-graphene for cancer therapy, Advanced drug delivery reviews 105 (2016) 228-241.

[174] Z. Liu, X. Sun, N. Nakayama-Ratchford, H. Dai, Supramolecular chemistry on water-soluble carbon nanotubes for drug loading and delivery, ACS nano 1(1) (2007) 50-56.

[175] Z. Liu, K. Chen, C. Davis, S. Sherlock, Q. Cao, X. Chen, H. Dai, Drug delivery with carbon nanotubes for in vivo cancer treatment, Cancer research 68(16) (2008) 6652-6660.

[176] S. Goenka, V. Sant, S. Sant, Graphene-based nanomaterials for drug delivery and tissue engineering, Journal of Controlled Release 173 (2014) 75-88.

[177] Z. Yinghuai, A.T. Peng, K. Carpenter, J.A. Maguire, N.S. Hosmane, M. Takagaki, Substituted carborane-appended water-soluble single-wall carbon nanotubes: new approach to boron neutron capture therapy drug delivery, Journal of the American Chemical Society 127(27) (2005) 9875-9880.

[178] J. Liu, L. Cui, D. Losic, Graphene and graphene oxide as new nanocarriers for drug delivery applications, Acta biomaterialia 9(12) (2013) 9243-9257.

[179] T.Y. Zakharian, A. Seryshev, B. Sitharaman, B.E. Gilbert, V. Knight, L.J. Wilson, A Fullerene− paclitaxel chemotherapeutic: synthesis, characterization, and study of biological activity in tissue culture, Journal of the American Chemical Society 127(36) (2005) 12508-12509.

[180] H.S. Choi, W. Liu, F. Liu, K. Nasr, P. Misra, M.G. Bawendi, J.V. Frangioni, Design considerations for tumour-targeted nanoparticles, Nature nanotechnology 5(1) (2010) 42-47.

[181] J. Shi, H. Zhang, L. Wang, L. Li, H. Wang, Z. Wang, Z. Li, C. Chen, L. Hou, C. Zhang, PEI-derivatized fullerene drug delivery using folate as a homing device targeting to tumor, Biomaterials 34(1) (2013) 251-261.

[182] P. Chaudhuri, A. Paraskar, S. Soni, R.A. Mashelkar, S. Sengupta, Fullerenol− Cytotoxic Conjugates for Cancer Chemotherapy, Acs Nano 3(9) (2009) 2505-2514.

[183] J. Gu, S. Su, Y. Li, Q. He, J. Shi, Hydrophilic mesoporous carbon nanoparticles as carriers for sustained release of hydrophobic anti-cancer drugs, Chemical Communications 47(7) (2011) 2101-2103.

[184] L. Wan, Q. Zhao, P. Zhao, B. He, T. Jiang, Q. Zhang, S. Wang, Versatile hybrid polyethyleneimine–mesoporous carbon nanoparticles for targeted delivery, Carbon 79 (2014) 123-134.

[185] A. Bianco, Carbon nanotubes for the delivery of therapeutic molecules, Expert opinion on drug delivery 1(1) (2004) 57-65.

[186] S. Li, L. Huang, Gene therapy progress and prospects: non-viral gene therapy by systemic delivery, Gene therapy 13(18) (2006) 1313-1319.

[187] E. Nakamura, H. Isobe, Functionalized fullerenes in water. The first 10 years of their chemistry, biology, and nanoscience, Accounts of chemical research 36(11) (2003) 807-815.

[188] K. Yang, L. Feng, X. Shi, Z. Liu, Nano-graphene in biomedicine: theranostic applications, Chemical Society Reviews 42(2) (2013) 530-547.

[189] D. Pantarotto, R. Singh, D. McCarthy, M. Erhardt, J.P. Briand, M. Prato, K. Kostarelos, A. Bianco, Functionalized carbon nanotubes for plasmid DNA gene delivery, Angewandte Chemie 116(39) (2004) 5354-5358.

[190] Z. Liu, M. Winters, M. Holodniy, H. Dai, siRNA delivery into human T cells and primary cells with carbon-nanotube transporters, Angewandte Chemie International Edition 46(12) (2007) 2023-2027.

[191] J. McCarroll, H. Baigude, C.-S. Yang, T.M. Rana, Nanotubes functionalized with lipids and natural amino acid dendrimers: a new strategy to create nanomaterials for delivering systemic RNAi, Bioconjugate chemistry 21(1) (2009) 56-63.

[192] K. Bates, K. Kostarelos, Carbon nanotubes as vectors for gene therapy: past achievements, present challenges and future goals, Advanced drug delivery reviews 65(15) (2013) 2023-2033.

[193] L. Feng, X. Yang, X. Shi, X. Tan, R. Peng, J. Wang, Z. Liu, Polyethylene glycol and polyethylenimine dual-functionalized nano-graphene oxide for photothermally enhanced gene delivery, Small 9(11) (2013) 1989-1997.

[194] H. Murayama, S. Tomonoh, J.M. Alford, M.E. Karpuk, Fullerene production in tons and more: from science to industry, Fullerenes, Nanotubes and Carbon Nanostructures 12(1-2) (2005) 1-9.

[195] E. Nakamura, H. Isobe, N. Tomita, M. Sawamura, S. Jinno, H. Okayama, Functionalized fullerene as an artificial vector for transfection, Angewandte Chemie International Edition 39(23) (2000) 4254-4257.

[196] R. Maeda-Mamiya, E. Noiri, H. Isobe, W. Nakanishi, K. Okamoto, K. Doi, T. Sugaya, T. Izumi, T. Homma, E. Nakamura, In vivo gene delivery by cationic tetraamino fullerene, Proceedings of the National Academy of Sciences 107(12) (2010) 5339-5344.

Table 1.1 Candidates of neutron-activatable radionuclides. Radioactivity was calculated with irradiation of 1 g of natural abundance element for 1 h in a neutron flux of 5.5 x 10^{12} neutrons cm^{-2} s [31].

Element	Natural Abundance (%)	Neutron Cross-Section (barn)	Half-life (h)	Emax (MeV)	Radioactivity (mCi)
$^{89}Y/^{90}Y$	100	1.28	64.1	2.28 (β)	12.6
$^{144}Sm/^{145}Sm$	3.07	1.6	8160	0.06 (γ)	0.234
$^{150}Sm/^{151}Sm$	7.38	103	788400	0.076 (β)	0.003
$^{152}Sm/^{153}Sm$	26.75	210	46.3	0.69 (β), 0.1 (γ)	436.9
$^{154}Sm/^{155}Sm$	22.75	7	0.37	1.52 (β), 0.1 (γ)	860.6
$^{197}Au/^{198}Au$	100	98.7	640.7	0.96 (β)	434.4
$^{165}Ho/^{166}Ho$	100	59	26.8	1.86 (β) 0.08 (γ)	815.1

CHAPTER 2 NEUTRON-ACTIVATABLE CANCER THERAPY USING GRAPHENE OXIDE NANOANOPLATELETS[1]

2.1 Overview

Neutron-activation is a promising method of generating radiotherapeutics with minimal handling of radioactive materials by medical providers. Graphene oxide nanoplatelets (GONs) were examined as a carrier for neutron-activatable holmium for theranostic application. GONs have desirable characteristics as a theranostic agent such as a rigid structure, high metal loading capacity, low density, heat resistance, and the ability to withstand harsh environments associated with the neutron-activation process. Non-covalently PEGylated GONs (GONs-PEG) offered enhanced dispersibility and biocompatibility, and also exhibited increased holmium loading capacity nearly two-fold greater than unfunctionalized GONs. Holmium leaching was investigated *in vitro* over a wide pH range, including conditions that mimic the tumor microenvironment, following neutron irradiation. Cell-based cytotoxicity analysis of the GON-based formulations with non-radioactive holmium confirmed low cytotoxicity. These results demonstrate the potential of GONs as a carrier of neutron-activatable radiotherapeutic agents.

[1] Part of this chapter was submitted as an article to the Nulear Medicine and Biology as follows: J. Kim, M. Jay "Neutron-Activatable Radionuclide Cancer Therapy Using Graphene Oxide Nanoplatelets.", *Nuclear Medicine and Biology* (under revision).

2.2 Introduction

With the advent of the nano-revolution, carbon-based nanomaterials have gained much attention from various fields, and nanomedicine was not the exception [1]. Specifically, carbon nanotubes and fullerenes have been the initial subject of much attention owing mostly to their unique physical and chemical characteristics [2, 3]. Soon after the isolation of graphene by Geim and Novoselov in 2004, this material arguably became the 'hottest' carbon-based nanomaterial. Once called "the thinnest material in the universe and the strongest ever measured" [4], graphene has a myriad of attractive qualities: an extremely large surface area, chemical and mechanical strength, and superior thermal and electrical conductivity [5-7].

In the field of nanomedicine, graphene oxide nanoplatelets (GONs) are a preferred choice as a drug delivery system, because the hydrophobic nature of graphene makes it difficult to disperse in aqueous solvents [8]. Two specific findings dramatically increased the potential of GONs as a drug delivery carrier: that they are biocompatible with functionalization (e.g., with polyethylene glycol (PEG)), and they exhibit π–π stacking with aromatic-structured chemotherapeutics (e.g., doxorubicin) leading to exceptionally high loading capacity (400 w/w%) [9, 10]. In addition, high propensity for metal adsorption is an additional feature that makes them an attractiv carrier for therapeutic radionuclides. In one study, graphene oxide was reported to adsorb a 10-fold higher amount of copper ion compared to activated carbon, which has been a heavily investigated material for adsorbents by virtue of large surface area [11]. While there have been a number of published studies assessing the merits of GON-based delivery of small molecules (e.g., SN38, camptothecin analog, paclitaxel, cisplatin), as well as large molecules (e.g., vaccines, proteins, genes), publications detailing their utility for delivery of radionuclides are scarce [12-17].

The conventional methods of preparing radiotherapeutics begin with a radioactive isotope which is then conjugated or loaded onto a carrier (e.g. liposomes, polymeric micelles, peptides, or proteins) [18-21]. This method requires the researcher to deal with highly radioactive materials from the very start of the formulation preparation process. Neutron activation – a process by which stable isotopes are converted into radioactive isotopes through the capture of an additional neutron – is a promising approach to minimize the direct handling of radioactivity. Moreover, this strategy is able to offer the additional benefits of minimal use of excipients being able to control the amount of radioactivity produced by varying the neutron flux or irradiation time. In spite of these advantages, the neutron-activation process has not been widely utilized for the production of radiotherapeutics. This is because a significant amount of heat is generated during the neutron-activation process which may result in the degradation of conventional nanocarriers [22]. To overcome this, Di Pasqua et al. previously explored the application of mesoporous silica nanoparticles (MSNs) as neutron-activatable radionuclide carriers. These carriers were found to be able to withstand the harsh environment required for neutron-activation [23]. However, the relatively high density of the formulation has limited their utility to intraperitoneal administration.

In the current study, GONs were investigated as a lower density and more durable alternative to MSNs for neutron activation and delivery of radionuclides. Among the possible neutron-activatable radionuclide candidates, holmium (Ho) was selected for the current study. Ho possesses desirable characteristics for the proposed application, including its high natural abundance (^{165}Ho can only be activated to ^{166}Ho) and its large neutron capture cross-section (64 barns, cf. 1.3 barns of ^{89}Yttrium where 1 barn = 10^{-24} cm^2) [24-26]. Once stable Ho is activated, ^{166}Ho decays by emission of high energy β^- particles (E_{max}= 1.84 MeV, 8.7 mm maximum tissue penetration) and low energy γ-photons (81 keV, 6.7% photon yield) which allow for its theranostic application via SPECT/CT imaging (**Fig. 2.1**) [27, 28]. Also, its

relatively short half-life (26.8 h) reduces the concern of radioactive retention in the human body for extended periods of time. In this chapter, GONs were investigated as a carbon-based carrier for radiotherapeutics that could be loaded in a shorter period of time as well as to achieve better tumor penetration. The successful development of GONs as a neutron-activatable Ho matrix is projected to be utilized for radionuclide therapy which can potentially target multiple targets.

2.3 Materials and Methods

2.3.1 Chemicals

Graphite flakes, hydrogen peroxide (30%, USP testing grade) and holmium (III) acetate monohydrate (99.99%) were acquired from Sigma-Aldrich (St. Louis, MO). Sulfuric acid (ACS grade), sodium nitrate (analytical grade), sodium hydroxide (ACS grade), nitric acid (trace metal grade) and potassium permanganate (reagent grade) were obtained from Fisher Chemical (Fair Lawn, NJ). 1,2-distearoyl-*sn*-glycero-3-phospho-ethanolamine-N-[methoxy (polyethylene glycol)-3000] (DSPE-PEG) was purchased from Avanti Polar Lipids Inc. (Alabaster, Alabama).

2.3.2 Synthesis of GONs

GONs were synthesized based on a modification of the graphite flake oxidation and ultra-sonication method established by Tour et al. [29]. Briefly, graphite flakes were sieved through a U.S. standard testing sieve (300 μm). A 9:1 mixture of H_2SO_4 and H_3PO_4 (400 mL) in addition to 18 g of $KMnO_4$ were added to 3 g of sieved graphite flakes and stirred for 12 h at 50 °C. When the reaction had cooled to room temperature (taking on a purple color), 400

mL of Milli-Q water and 3 mL of 30% H_2O_2 were added. The mixture was sieved again (300 µm) and filtered through the polyester fiber. The resultant yellowish filtrate was centrifuged at 2400 x g for 2 h. The filtrate was washed with Milli-Q water, 30% HCl and ethanol (2 times) to remove unreacted precursors, and the washed product was vacuum-dried overnight at room temperature. Graphene oxide was further exfoliated and reduced to nano-size GONs by 2 h of sonication with probe sonicator (Fisher Scientific Model 505 Sonic Dismembrator; power: 500 watts, operating frequency: 20 kHz and amplitude: 25%). For additional purification, GONs were centrifuged at 1800 x g for 5 minutes and the supernatant was dialyzed for 3 days before their use (MWCO: 12 KDa).

2.3.3 Non-covalent PEGylation on GONs

In order to enhance colloidal stability and biocompatibility, GONs were PEGylated by a non-covalent method. Since DSPE-PEG was stored in chloroform, the solvent was evaporated and DSPE-PEG was re-suspended in Milli-Q water. Ten mL of GONs (0.5 mg/mL), suspended in Milli-Q water, were mixed with 5 mL of DSPE-PEG (2.5 mg/mL) and sonicated for 10 minutes. The unreacted precursor was removed by centrifugal filtration (3 times, MWCO: 50 KDa).

2.3.4 Physicochemical characterization of GONs

Fourier transform infrared spectroscopy (FTIR; Thermo Nicolet 380) was used to detect representative functional groups of graphite and GONs. The conversion of graphite to GONs was confirmed by X-ray powder diffraction (XRD; Rigaku Multiflex X-ray diffractometer with Cu Kα radiation (λ= 1.5418 Å)). The polydispersity index (PDI) and zeta potential of the GONs were measured using a Malvern Zetasizer Nano ZS. The morphology and thickness of GONs

were observed by atomic force microscopy (AFM; Asylum Research MFP3D Atomic Force Microscope), and size distribution was calculated from AFM images by ImageJ.

2.3.5 Holmium loading on GONs

Holmium acetate ($Ho(Ac)_3$) was added to either GONs or non-covalently PEGylated GONs (GONs-PEG). Three different loading methods – simple vertexing, short sonication (1-5 minutes), and stirring for 24 h – were compared. To ensure complete loading of Ho on the GON preparations, subsequent experiments were conducted using the short sonication method (5 minutes). To estimate the maximum loading of Ho on the GON preparations, varying amounts of Ho were mixed with the GONs and unbound Ho was removed by centrifugal filtration (MWCO: 50 KDa). The experiment was conducted with ^{166}Ho and the amount was quantified by a γ-counter (PerkinElmer 2470 Wizard γ-counter). The Ho loading capacity was also verified by inductively coupled plasma mass spectrometry (ICP-MS; Agilent 7500cx with Agilent 1260 Infinity Bioinert LC).

2.3.6 Holmium desorption from GONs in various pH

^{166}Ho-GONs or ^{166}Ho-GONs-PEG (0.5 mg of GONs/mL) were added to a range of pH solutions which were adjusted by sodium hydroxide and nitric acid titration. Solutions were stirred for 24 h at 100 rpm and then leached ^{166}Ho was separated by centrifugal filtration (MWCO: 100 KDa). ^{166}Ho was quantified using a γ-counter.

2.3.7 *In vitro* leaching study

Two hundred µL of ^{166}Ho-GONs or ^{166}Ho-GONs-PEG (0.5 mg of GONs/mL) were placed in a dialysis cup (Slide-A-Lyzer MINI dialysis®, 3500 MWCO) which was subsequently dialyzed against 20 mL of phosphate buffered saline (PBS) at 37 °C and shaken at 100 rpm (Thermo MAXQ 4450). A sample of the dialysate was drawn at pre-determined time points (1, 3, 6, 12, 24, 36 and 48 h) and the leached amount of ^{166}Ho was quantified with a γ-counter.

2.3.8 Stability of neutron-activated Ho-GONs-PEG

Freeze-dried ^{165}Ho-loaded GONs-PEG were irradiated for 1 h in the PULSTAR Reactor Facility at The North Carolina State University (reactor power = 1 MW; thermal neutron flux = 5.5 x 10^{12} neutrons cm^{-2} s), and the leached ^{166}Ho was separated by centrifugal filtration (MWCO: 50 KDa) and quantified by γ-counter. The exact amount of Ho in the Ho-GONs-PEG was determined by neutron-activation analysis (NAA). An ORTEC 42% high purity germanium detector system with a Canberra AFT research amplifier, multi-port II analog-to-digital converter and Genie 2000 MCA spectroscopy software was utilized to quantify the amount of ^{166}Ho produced by neutron-activation, which was adopted for back-calculating the amount of ^{165} Ho in the formulation.

2.3.9 *In vitro* cytotoxicity evaluation

Three non-radioactive GON-based formulations (GONs, ^{165}Ho-GONs and ^{165}Ho-GONs-PEG) were tested in a human ovarian cancer cell line (A2780) to assess the cytotoxicity of the formulation components. The ovarian cancer cells were cultured in RPMI-1640 medium with 10% FBS and 1% penicillin-streptomycin in 5% CO_2 at 37 °C. When cells became

confluent, they were seeded in a 96-well plate (5000 cells/well) and incubated for 24 h. Each well was treated with a pre-determined amount of formulation and cultured for 24 h or 48 h. After removing the formulations and washing with sterile PBS, the media (100 µL/well) and cell counting kit-8 (CCK-8) reagents (10 µL/well, Dojindo Laboratories) were added. Cells were further incubated for 4 h and the absorbance at 450 nm was measured with a plate reader (SpectraMax M5).

2.4 Results

2.4.1 Characterization of GONs

To confirm the successful oxidation of graphite, representative functional groups of GONs were analyzed by FTIR (**Fig. 2.2**a). The O-H stretching band of the GONs was observed between 3000 cm^{-1} and 3500 cm^{-1}. The C=O stretching region of carboxylic groups and the C-O-C stretching band of the epoxide groups were seen at 1725 cm^{-1} and 1052 cm^{-1}, respectively. A change of XRD pattern from graphite to GONs also supported the successful synthesis (**Fig. 2.2**b). To exploit passive targeting via the enhanced permeation and retention (EPR) effect, GONs were reduced to nano-size by sonication and they were shown to have an irregular shape with a wide size distribution (136.7 ± 85.2 nm) (**Fig. 2.3**a,c) [30]. The approximate 1.2 nm height of GONs suggested that they were successfully separated from stacked graphite to a single-layered graphene structure, which matches previous reports (**Fig. 2.3**e) [29]. The PDI and surface charge measurement by zetasizer exhibited monodispersity (0.230 ± 0.006) and a net negative charge (-49.8 ± 3.9 mV), primarily from the carboxylate groups of GONs.

2.4.2 Surface modification of GONs

To obtain a narrow size distribution, solutions were centrifuged to eliminate large-sized GONs, and resulting supernatant portion was used in the PEGylation process. GONs-PEG were shown to have narrower size distribution (62.1 ± 14.0 nm) (**Fig. 2.2**b,d). The non-covalent attachment of PEG resulted in an increased cross-section height to ~14 nm and a slight improvement in the PDI (0.185 ± 0.003) (**Fig 2.3**f).

2.4.3 Holmium loading on GONs

Three methods were evaluated for loading GONs with $Ho(Ac)_3$; and no significant difference in loading capacity and efficiency were observed. As shown in **Fig. 2.4**, GONs was able to maintain their dispersibility until the weight ratio of GONs:$Ho(Ac)_3$ reached 1:0.1, at which point above this holmium ratio, the suspensions were observed to aggregate. Based on ICP-MS analysis, the maximum loading capacity of holmium on GONs that could maintain dispersibility was determined to be 4.38 w/w %. When PEGylated, GONs maintained their dispersibility even at GONs:$Ho(Ac)_3$ ratios of 1:0.2. The maximum holmium loading on GONs-PEG was evaluated by NAA and determined to be 8.38 w/w %.

2.4.4 Holmium sorption on GONs

The binding of holmium on GONs was evaluated within pH range of 1 to 14. The sorption profiles of GONs and GONs-PEG were not significantly different based on two-way ANOVA analysis. Almost all of the Ho was bound to GONs and GONs-PEG (> 98%) between pH 4-14 (**Fig. 2.5**). However, as oxygen-containing functional groups of GONs were

protonated in acidic pH, sorption of Ho decreased as the pH. Only ~16% of holmium was bound to GONs and GONs-PEG at pH 1.

2.4.5 *In vitro* leaching assessment

As expected, there was almost no Ho leaching observed at physiological pH (7.4) until 12 h after incubation (**Fig. 2.6**). After 48 h, only 10% of Ho leaching was observed. Unlike GONs, GONs-PEG did not show any Ho leaching at pH 7.4 even after long incubation times. Under slightly acidic conditions (pH 5.5), GONs and GONs-PEG exhibited sustained-release profiles that were not significantly different.

2.4.6 Stability of neutron-activated GONs

The critical parameter to be assessed for carriers of neutron-activated radiotherapeutics is the leaching of radioactivity following neutron irradiation which may result in degradation of GONs in the relatively harsh reactor environment during the irradiation process. As the ultimate goal is to deliver therapeutic radionuclides to target tissues (e.g., tumors), a minimal amount of leaching of the radionuclide (^{166}Ho in this application) is desirable to prevent off-target accumulation of the released radionuclide. The non-radioactive Ho-loaded GONs and Ho-loaded GONs-PEG were irradiated in a neutron flux for 1 h and washed 3 times with Milli-Q water. Only very small amounts (<0.1% of the total radioactivity) of ^{166}Ho could be detected in the washings which indicated that leaching of radioactive holmium from these irradiated particles was minimal.

2.4.7 *In vitro* cytotoxicity evaluation

The viability of a human ovarian cancer cell line (A2780) following exposure to various concentrations of GONs, Ho-loaded GONs (^{165}Ho-GONs), and Ho-loaded GONs-PEG (^{165}Ho-GONs-PEG) was assessed. GONs did not induce any cytotoxicity at concentrations up to 10 µg/mL when incubated for 24 h or 48 h, and the addition of Ho and PEG did not add increase the toxicity of the carriers (**Fig. 2.7**).

2.5 Discussion

In this study, GONs were explored as a neutron-activatable radionuclide carrier. The successful synthesis of GONs was confirmed by FTIR, XRD and AFM. For a GON-based formulation, surface modification was necessary for passive tumor-targeting effects [31]. Previous studies have demonstrated that GONs undergo irreversible aggregation without proper capping agents [32-34]. The PEG moiety is generally recognized as safe (GRAS) by the U.S. Food and Drug Administration (FDA) and is frequently employed for enhancing both biocompatilibity and dispersibility of nano-carriers in biological systems [35]. Covalent and non-covalent PEGylation strategies were evaluated with the latter ultimately being selected based on ease of the method and the short reaction time (10 minutes of sonication) to exploit the strong association between the phospholipid portion of DSPE-PEG and the aromatic moieties of GONs.

Among the different forms of holmium, $Ho(Ac)_3$ was selected for incorporation into GONs. $Ho(Ac)_3$ is a preferred load versus $Ho(Cl)_3$, as the acetate form does not contain readily activatable nuclei, while radioisotopes of Cl can form upon neutron irradiation of $Ho(Cl)_3$. Other investigators report the use of cargo loading methods that require incubations for an extended period of time [36-38]. Since GONs are known to possess a large surface area, it was

assumed that the Ho loading process would proceed more rapidly with GONs compared to other nanocarriers. There was no significant difference between the three loading methods in terms of loading capacity or efficiency in GONs:$Ho(Ac)_3$ ratios tested. These results suggest that Ho associated quickly with GONs. Holmium binding on GONs is facilitated mostly through electrostatic interaction with the negatively-charged oxygen-containing functional groups on GONs; electrostatic repulsion results in a stable dispersion between resulting layers [39]. As these negatively charged groups are masked by Ho binding, products started to show aggregation at GONs:$Ho(Ac)_3$ ratios above 1:0.1. Since PEGylation was able to offer additional dispersibility even after the charge masking, Ho-GONs-PEG did not aggregate with higher Ho ratios, and Ho loading capacity increased from 4.38 (w/w) % to 8.38 (w/w) %.

Ho sorption was investigated over a wide pH range. Some elements such as U(IV), Sr(II), Tc(VII) and Np(V) have weaker and more pH-dependent association with graphene oxides compared to others [40]. Since GONs were not covalently PEGylated in this study, the functional groups of GONs were still intact following PEGylation. Hence, there was no significant difference in Ho sorption between GONs and GONs-PEG. The result of this sorption experiment showed a similar pH-dependent pattern – Ho sorption was nearly complete at pH $\geq$4, and significant leaching was seen in acidic conditions - in comparison to other heavy metals (Th(IV), Pu(IV), Am(III), Eu(III)) [40].

Although the sorption experiment demonstrated a strong binding affinity between Ho and GONs, this complex was further evaluated in conditions that mimic the tumor microenvironment. While the pH of human body fluid is well-regulated by homeostasis to be maintained at pH 7.4, the pH of the tumor microenvironment is slightly acidic (pH 5.5 to 7.0) due to glycolytic metabolism, hypoxia, and deficient blood perfusion [41, 42]. Although Ho was shown to bind to GONs quantitatively at pH >4 in the sorption study, holmium was observed to be slowly released from the GONs in the leaching study when the pH of the

medium was 5.5 due to a change in equilibrium resulting from the larger volume of dialysate in the leaching study. The faster release rate at pH 5.5 compared to pH 7.4 was likely due to protonation effects at the lower pH. Considering that Ho did not leach from the GONs-PEG at pH 7.4 after a long incubation time, DSPE-PEGylation was considered as a means to offer an additional barrier to holmium loss, but this effect was diminished in acidic conditions (pH 5.5).

One well-known limitation of nanocarrier-based drug delivery system is tumor penetration. A considerable portion of administered nanoparticles remains near blood vessels instead of penetrating into deep tumor region which often causes a sub-therapeutic effect. Cabral et al. showed that smaller nanoparticles (30 nm) were able to penetrate tumor tissue more efficiently than larger nanoparticles (50-100 nm); Wong et al. reported that 10 nm nanoparticles in the tumor microenvironment were capable of reaching deeper tumor sites than 100 nm nanoparticles [43, 44]. Based on these reports, the sustained holmium desorption in a mildly acidic environment may confer improved deep tumor penetration *in vivo*. Lastly, the safe toxicity profile of GON-based formulations (with non-radioactive holmium) verified that the tumor killing effect would exclusively result from the high energy of β^- particles emitted by ^{166}Ho and not by the toxicity of GONs themselves.

Overall, non-radioactive Ho-loaded GONs-PEG did not show any GONs-related cytotoxicity at concentrations up to 10 µg/mL for 48 h. After 1 h of neutron irradiation which produced radioactive holmium, no leaching of ^{166}Ho was observed when the ^{166}Ho-GONs-PEG were incubated at pH 7.4 for extended periods of time. The results suggest that Ho-loaded nanocarriers will stay intact not only during preparation, but also in the circulation *in vivo* after intravenous administration until they arrive at their target site.

2.6 Conclusion

Graphene oxide nanoplatelets (GONs) were evaluated as a neutron-activatable holmium carrier for theranostic application. GONs were synthesized from graphite and subsequently characterized. Through non-covalent PEGylation, their dispersibility and biocompatibility were improved, and the Ho-loading capacity increased nearly two-fold (w/w %). Leaching of radioactive holmium following neutron irradiation of Ho-GONs-PEG was minimal for 48 h which is almost two half-lives of the radionuclide. The safety of this formulation was supported by *in vitro* cytotoxicity assays in a human ovarian cancer cell line. As a platform technology, the neutron activation approach using GONS as the carrier is applicable for several therapeutic radionuclides such as ^{90}Y, ^{153}Sm, ^{177}Lu, ^{188}Re and ^{198}Au. GONs can also be used as a matrix for other therapeutic radionuclides by virtue of their ability to avidly adsorb a variety of metals. The adsorption of high-specific activity radioactive metals like ^{89}Sr and ^{90}Y to GONs would add an extra handling step, but would avoid the logistical issues of the neutron activation approach such as the availability of a high flux neutron source (e.g., a nuclear reactor). Further experimentation would be required to determine if GONs could be used as carriers for radiotherapeutic anions like [^{32}P]-phosphate or [^{131}I]-iodide. If the stability of chemotherapeutics entrapped within Ho-GONs-PEG can be confirmed following neutron irradiation, a combination therapy approach (chemoradiotherapy) is anticipated to enhance tumor killing and improve clinical outcomes.

2.7 REFERENCES

[1] Wonglimpiyarat J. The nano-revolution of Schumpeter's Kondratieff cycle. Technovation 2005;25:1349-54.

[2] Z. Liu, J.T. Robinson, S.M. Tabakman, K. Yang, H. Dai, Carbon materials for drug delivery & cancer therapy, Materials today 14(7) (2011) 316-323.

[3] V. Biju, Chemical modifications and bioconjugate reactions of nanomaterials for sensing, imaging, drug delivery and therapy, Chemical Society Reviews 43(3) (2014) 744-764.

[4] A.K. Geim, Graphene: status and prospects, science 324(5934) (2009) 1530-1534.

[5] K.S. Novoselov, A.K. Geim, S.V. Morozov, D. Jiang, Y. Zhang, S.V. Dubonos, I.V. Grigorieva, A.A. Firsov, Electric field effect in atomically thin carbon films, science 306(5696) (2004) 666-669.

[6] Y. Zhu, S. Murali, W. Cai, X. Li, J.W. Suk, J.R. Potts, R.S. Ruoff, Graphene and graphene oxide: synthesis, properties, and applications, Advanced materials 22(35) (2010) 3906-3924.

[7] J. Liu, L. Cui, D. Losic, Graphene and graphene oxide as new nanocarriers for drug delivery applications, Acta biomaterialia 9(12) (2013) 9243-9257.

[8] D. Li, M.B. Mueller, S. Gilje, R.B. Kaner, G.G. Wallace, Processable aqueous dispersions of graphene nanosheets, Nature nanotechnology 3(2) (2008) 101-105.

[9] X. Sun, Z. Liu, K. Welsher, J.T. Robinson, A. Goodwin, S. Zaric, H. Dai, Nano-graphene oxide for cellular imaging and drug delivery, Nano research 1(3) (2008) 203-212.

[10] L. Zhang, J. Xia, Q. Zhao, L. Liu, Z. Zhang, Functional graphene oxide as a nanocarrier for controlled loading and targeted delivery of mixed anticancer drugs, Small 6(4) (2010) 537-544.

[11] S.-T. Yang, Y. Chang, H. Wang, G. Liu, S. Chen, Y. Wang, Y. Liu, A. Cao, Folding/aggregation of graphene oxide and its application in Cu 2+ removal, Journal of colloid and interface science 351(1) (2010) 122-127.

[12] Z. Liu, J.T. Robinson, X. Sun, H. Dai, PEGylated nanographene oxide for delivery of water-insoluble cancer drugs, Journal of the American Chemical Society 130(33) (2008) 10876-10877.

[13] N. Arya, A. Arora, K. Vasu, A. Sood, D.S. Katti, Combination of single walled carbon nanotubes/graphene oxide with paclitaxel: a reactive oxygen species mediated synergism for treatment of lung cancer, Nanoscale 5(7) (2013) 2818-2829.

[14] L. Tian, X. Pei, Y. Zeng, R. He, Z. Li, J. Wang, Q. Wan, X. Li, Functionalized nanoscale graphene oxide for high efficient drug delivery of cisplatin, Journal of Nanoparticle Research 16(11) (2014) 1-14.

[15] L. Xu, J. Xiang, Y. Liu, J. Xu, Y. Luo, L. Feng, Z. Liu, R. Peng, Functionalized graphene oxide serves as a novel vaccine nano-adjuvant for robust stimulation of cellular immunity, Nanoscale 8(6) (2016) 3785-3795.

[16] H. Shen, M. Liu, H. He, L. Zhang, J. Huang, Y. Chong, J. Dai, Z. Zhang, PEGylated graphene oxide-mediated protein delivery for cell function regulation, ACS applied materials & interfaces 4(11) (2012) 6317-6323.

[17] B. Chen, M. Liu, L. Zhang, J. Huang, J. Yao, Z. Zhang, Polyethylenimine-functionalized graphene oxide as an efficient gene delivery vector, Journal of Materials Chemistry 21(21) (2011) 7736-7741.

[18] A.B. Satterlee, H. Yuan, L. Huang, A radio-theranostic nanoparticle with high specific drug loading for cancer therapy and imaging, Journal of Controlled Release 217 (2015) 170-182.

[19] M.E. Werner, S. Karve, R. Sukumar, N.D. Cummings, J.A. Copp, R.C. Chen, T. Zhang, A.Z. Wang, Folate-targeted nanoparticle delivery of chemo-and radiotherapeutics for the treatment of ovarian cancer peritoneal metastasis, Biomaterials 32(33) (2011) 8548-8554.

[20] H. Zhang, J. Chen, C. Waldherr, K. Hinni, B. Waser, J.C. Reubi, H.R. Maecke, Synthesis and evaluation of bombesin derivatives on the basis of pan-bombesin peptides labeled with indium-111, lutetium-177, and yttrium-90 for targeting bombesin receptor-expressing tumors, Cancer research 64(18) (2004) 6707-6715.

[21] T.E. Witzig, L.I. Gordon, F. Cabanillas, M.S. Czuczman, C. Emmanouilides, R. Joyce, B.L. Pohlman, N.L. Bartlett, G.A. Wiseman, N. Padre, Randomized controlled trial of yttrium-90–labeled ibritumomab tiuxetan radioimmunotherapy versus rituximab immunotherapy for patients with relapsed or refractory low-grade, follicular, or transformed B-cell non-Hodgkin's lymphoma, Journal of clinical oncology 20(10) (2002) 2453-2463.

[22] J. Nijsen, B. Zonnenberg, J. Woittiez, D. Rook, I. Swildens-van Woudenberg, P. Van Rijk, A. Van het Schip, Holmium-166 poly lactic acid microspheres applicable for intra-arterial radionuclide therapy of hepatic malignancies: effects of preparation and neutron activation techniques, European journal of nuclear medicine 26(7) (1999) 699-704.

[23] A.J. Di Pasqua, H. Yuan, Y. Chung, J.-K. Kim, J.E. Huckle, C. Li, M. Sadgrove, T.H. Tran, M. Jay, X. Lu, Neutron-activatable holmium-containing mesoporous silica nanoparticles as a potential radionuclide therapeutic agent for ovarian cancer, Journal of Nuclear Medicine 54(1) (2013) 111-116.

[24] R.J. Mumper, B. Mills, U.Y. Ryo, M. Jay, Polymeric microspheres for radionuclide synovectomy containing neutron-activated holmium-166, Journal of nuclear medicine: official publication, Society of Nuclear Medicine 33(3) (1992) 398-402.

[25] W.W. Meinke, R.E. Anderson, Activation Analysis of Several Rare Earth Elements, Analytical Chemistry 26(5) (1954) 907-909.

[26] J. Nijsen, A.v.h. Schip, W. Hennink, D. Rook, P. Van Rijk, J. Klerk, Advances in nuclear oncology: microspheres for internal radionuclide therapy of liver tumours, Current medicinal chemistry 9(1) (2002) 73-82.

[27] L. Johnson, J. Yanch, S. Shortkroff, C. Barnes, A. Spitzere, C. Sledge, Beta-particle dosimetry in radiation synovectomy, European journal of nuclear medicine 22(9) (1995) 977-988.

[28] R.J. Mumper, U.Y. Ryo, M. Jay, Neutron-activated holmium-166-poly (L-lactic acid) microspheres: a potential agent for the internal radiation therapy of hepatic tumors, J Nucl Med 32(11) (1991) 2139-2143.

[29] D.C. Marcano, D.V. Kosynkin, J.M. Berlin, A. Sinitskii, Z. Sun, A. Slesarev, L.B. Alemany, W. Lu, J.M. Tour, Improved synthesis of graphene oxide, ACS nano 4(8) (2010) 4806-4814.

[30] K. Maruyama, Intracellular targeting delivery of liposomal drugs to solid tumors based on EPR effects, Advanced drug delivery reviews 63(3) (2011) 161-169.

[31] F. Danhier, O. Feron, V. Préat, To exploit the tumor microenvironment: passive and active tumor targeting of nanocarriers for anti-cancer drug delivery, Journal of Controlled Release 148(2) (2010) 135-146.

[32] Q. Liu, J. Shi, J. Sun, T. Wang, L. Zeng, G. Jiang, Graphene and Graphene Oxide Sheets Supported on Silica as Versatile and High-Performance Adsorbents for Solid-Phase Extraction, Angewandte Chemie 123(26) (2011) 6035-6039.

[33] Y. Lin, J. Jin, M. Song, Preparation and characterisation of covalent polymer functionalized graphene oxide, Journal of Materials Chemistry 21(10) (2011) 3455-3461.

[34] B.J. Hong, O.C. Compton, Z. An, I. Eryazici, S.T. Nguyen, Successful stabilization of graphene oxide in electrolyte solutions: enhancement of biofunctionalization and cellular uptake, ACS nano 6(1) (2011) 63-73.

[35] T. Yu, Y.-Y. Wang, M. Yang, C. Schneider, W. Zhong, S. Pulicare, W.-J. Choi, O. Mert, J. Fu, S.K. Lai, Biodegradable mucus-penetrating nanoparticles composed of diblock copolymers of polyethylene glycol and poly (lactic-co-glycolic acid), Drug delivery and translational research 2(2) (2012) 124-128.

[36] A.M. Chen, M. Zhang, D. Wei, D. Stueber, O. Taratula, T. Minko, H. He, Co-delivery of doxorubicin and Bcl-2 siRNA by mesoporous silica nanoparticles enhances the efficacy of chemotherapy in multidrug-resistant cancer cells, Small 5(23) (2009) 2673-2677.

[37] F. Wang, Y.-C. Wang, S. Dou, M.-H. Xiong, T.-M. Sun, J. Wang, Doxorubicin-tethered responsive gold nanoparticles facilitate intracellular drug delivery for overcoming multidrug resistance in cancer cells, ACS nano 5(5) (2011) 3679-3692.

[38] Z. Luo, Y. Hu, K. Cai, X. Ding, Q. Zhang, M. Li, X. Ma, B. Zhang, Y. Zeng, P. Li, Intracellular redox-activated anticancer drug delivery by functionalized hollow mesoporous silica nanoreservoirs with tumor specificity, Biomaterials 35(27) (2014) 7951-7962.

[39] B. Konkena, S. Vasudevan, Understanding aqueous dispersibility of graphene oxide and reduced graphene oxide through p K a measurements, The journal of physical chemistry letters 3(7) (2012) 867-872.

[40] A.Y. Romanchuk, A.S. Slesarev, S.N. Kalmykov, D.V. Kosynkin, J.M. Tour, Graphene oxide for effective radionuclide removal, Physical Chemistry Chemical Physics 15(7) (2013) 2321-2327.

[41] W. Aoi, Y. Marunaka, Importance of pH homeostasis in metabolic health and diseases: Crucial role of membrane proton transport, BioMed research international 2014 (2014).

[42] C.R. Justus, L. Dong, L.V. Yang, Acidic tumor microenvironment and pH-sensing G protein-coupled receptors, Frontiers in physiology 4 (2013) 354.

[43] H. Cabral, Y. Matsumoto, K. Mizuno, Q. Chen, M. Murakami, M. Kimura, Y. Terada, M. Kano, K. Miyazono, M. Uesaka, Accumulation of sub-100 nm polymeric micelles in poorly permeable tumours depends on size, Nature nanotechnology 6(12) (2011) 815-823.

[44] C. Wong, T. Stylianopoulos, J. Cui, J. Martin, V.P. Chauhan, W. Jiang, Z. Popović, R.K. Jain, M.G. Bawendi, D. Fukumura, Multistage nanoparticle delivery system for deep penetration into tumor tissue, Proceedings of the National Academy of Sciences 108(6) (2011) 2426-2431.

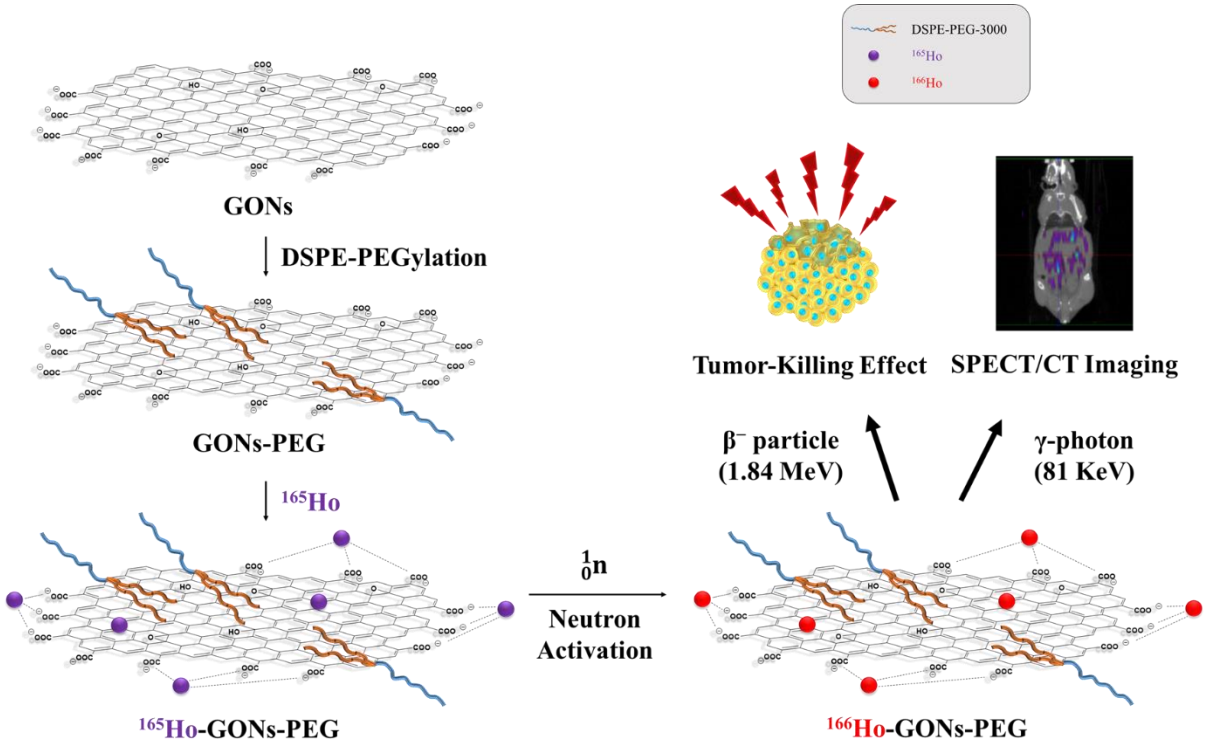

Figure 2.1 Schematic representation of neutron-activatable GON-based therapy

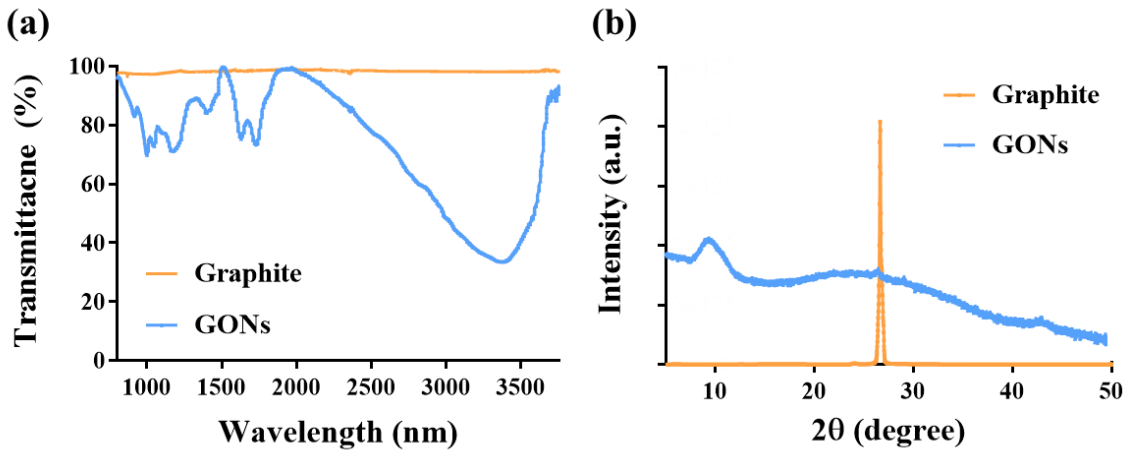

Figure 2.2 Synthesis of GONs confirmed by (a) FTIR and (b) XRD.

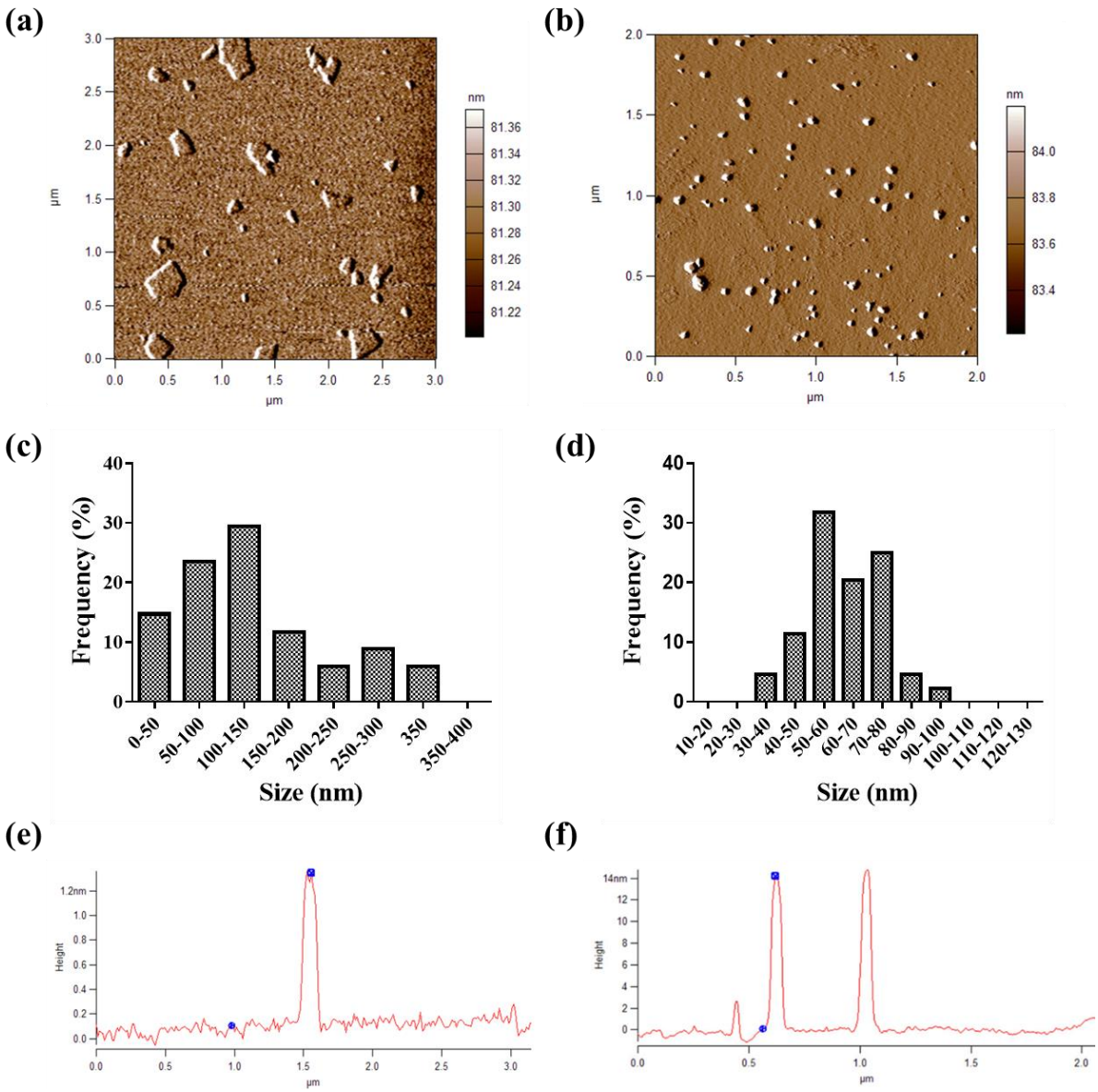

Figure 2.3 Characterization of GONs and GONs-PEG by AFM. AFM images of (a) GONs and (b) GONs-PEG. Size distribution of (c) GONs and (d) GONs-PEG as estimated by ImageJ. Cross-section analysis of (e) GONs and (f) GONs-PEG by AFM.

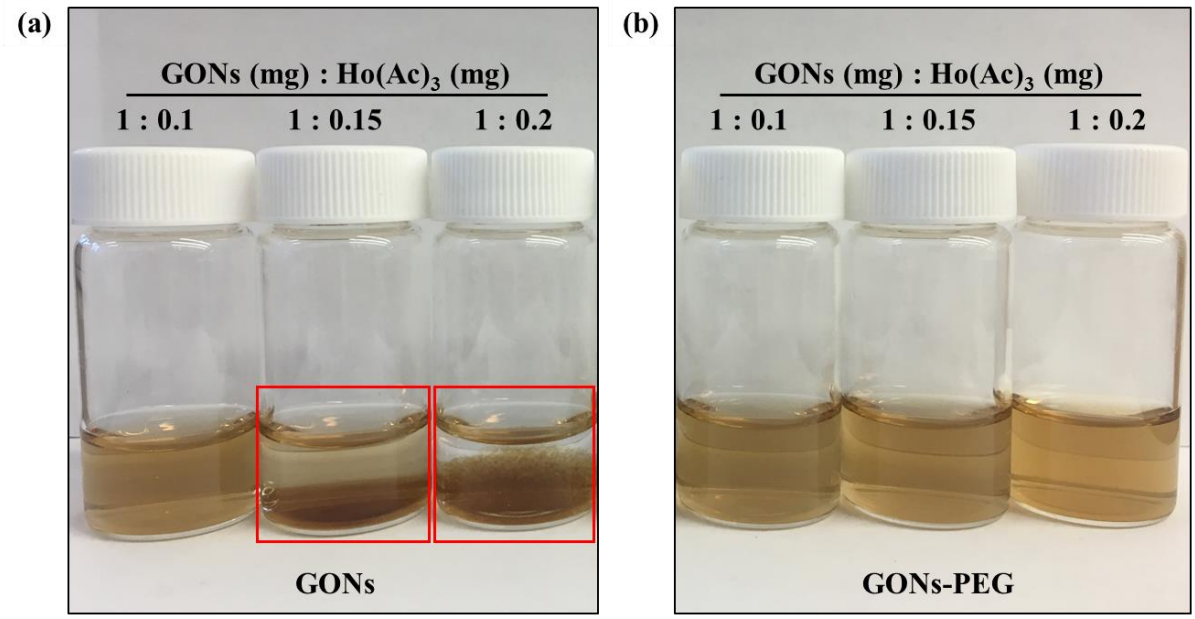

Figure 2.4 Evaluation holmium loading on (a) GONs and (b) GONs-PEG (red box indicates the aggregation of the formulation).

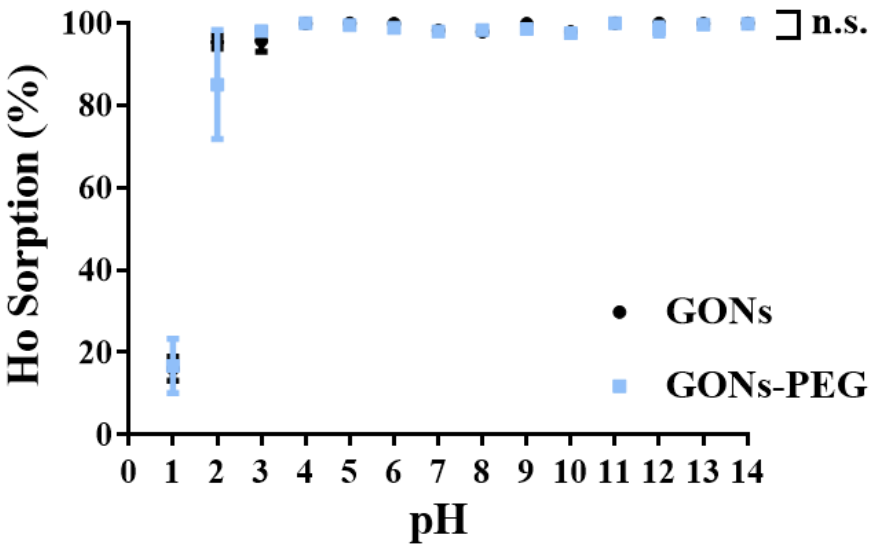

Figure 2.5 Holmium sorption on GONs and GONs-PEG in a wide range of pH. Groups were compared by two-way ANOVA (α= 0.05).

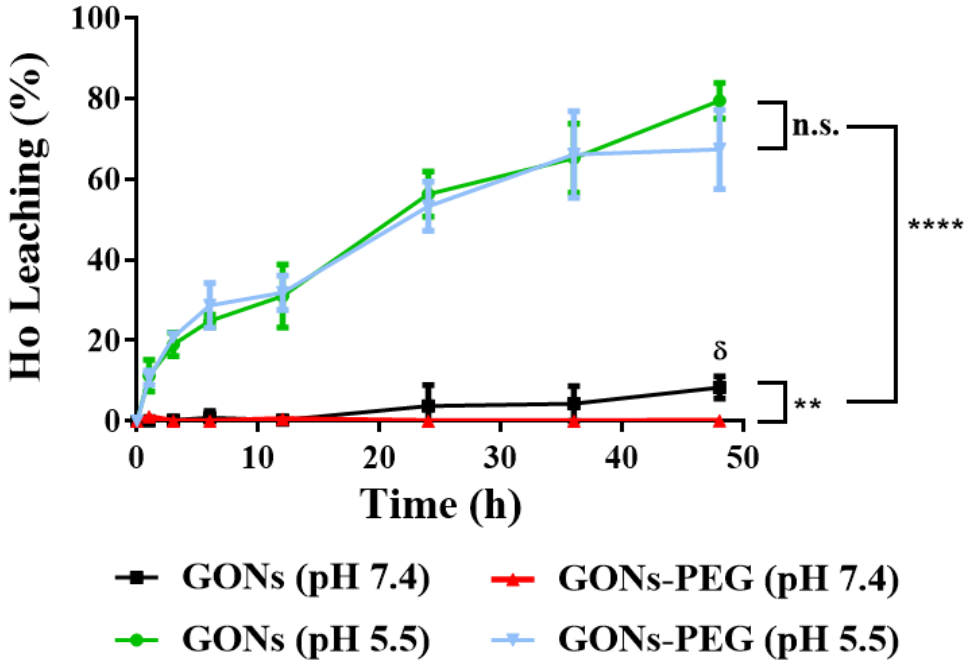

Figure 2.6 *In vitro* holmium leaching profile between GONs and GONs-PEG at pH 4.5 and 7.4. Groups were compared by two-way ANOVA (** for p< 0.01 and **** for p< 0.0001). Each time point of same pH groups was analyzed by Bonferroni's multiple comparisons test (δ for adjusted p<0.05 from GONs-PEG (pH 7.4)).

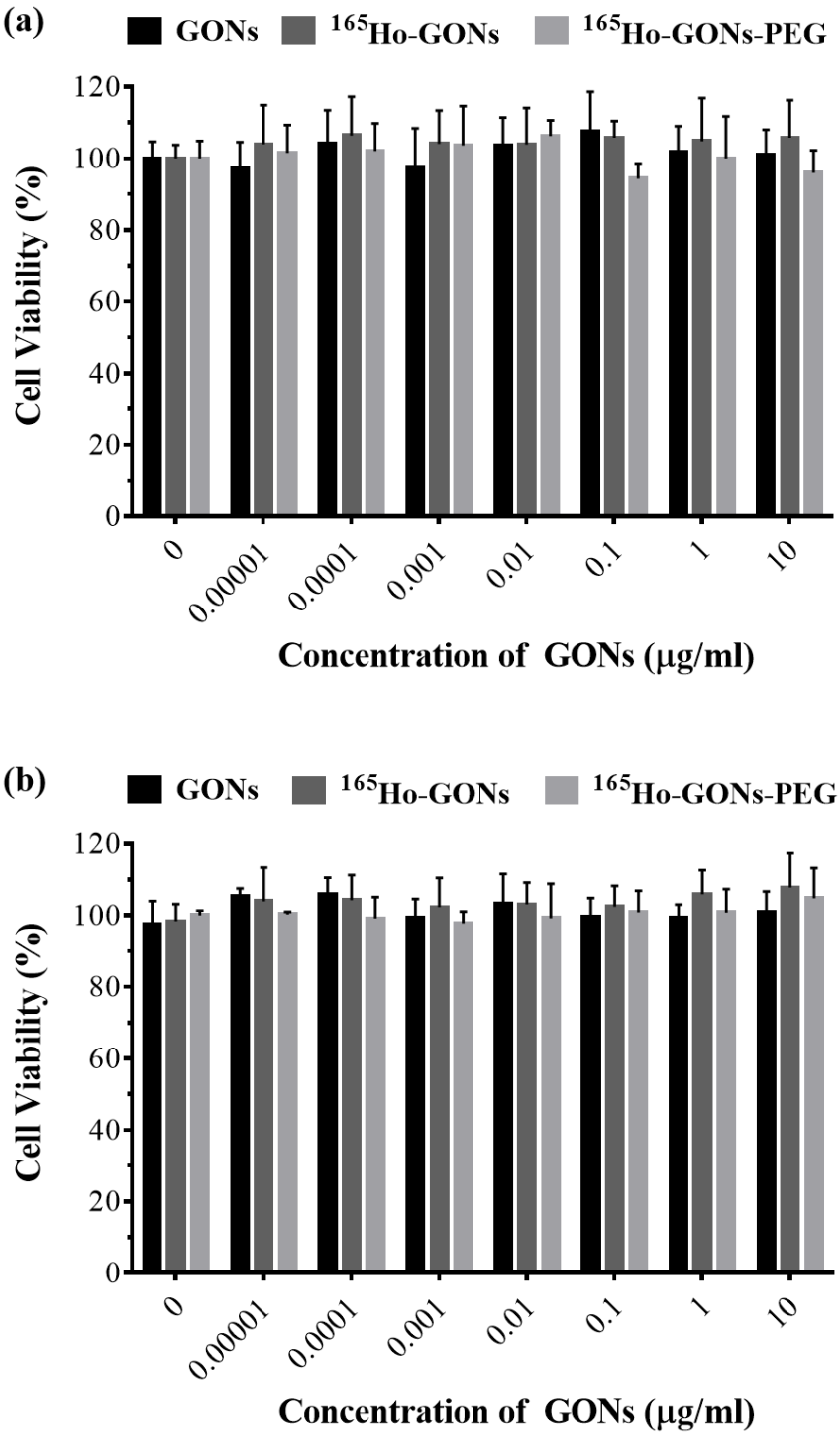

Figure 2.7 Viability of A2780 cells following 24 h (a) and 48 h (b) incubation of GONs and non-radioactive holmium-containing GONs and GONs-PEG.

CHAPTER 3 *IN-SITU* FORMATION OF HOLMIUM OXIDE IN PORES OF MESOPOROUS CARBON NANOPARTICLES AS SUBSTRATES FOR NEUTRON-ACTIVATABLE RADIOTHERAPEUTICS[2]

3.1 Overview

Radionuclide therapy with nano-sized carriers is a very promising approach to treat various types of cancer. The preparation of radioactive nanocarriers can be achieved with minimum handling using a neutron-activation approach. However, the nanocarrier material must possess certain characteristics such as low density, heat-resistance, high metal adsorption, easy surface modification and low toxicity in order to be useful. Mesoporous Carbon Nanoparticles (MCNs) in which holmium oxide is formed in their pores by a wet-impregnation process were investigated as a suitable material for this application. Holmium (^{165}Ho) has a natural abundance of 100% and possesses a large cross-section for capturing thermal neutrons. After irradiation of Ho-containing MCNs in a neutron flux, ^{166}Ho, which emits therapeutic high energy beta particles as well as diagnostic low energy gamma photons that can be imaged externally, is produced. The wet impregnation process (16 w/w% Ho loading) is shown to completely prevent the leaching of radioactive holmium from the MCNs without compromising their structural integrity. *In vitro* studies showed that the MCNs containing non-radioactive holmium do not exhibit toxicity and the same formulation with radioactive

[2] Part of this chapter previously appeared as an article in the Carbon. The original citation is as follows: J. Kim, J.-X. Luo, Y. Wu, X. Lu, M. Jay "*In-Situ* formation of holmium oxide in pores of Mesoporous Carbon Nanoparticles as substrates for neutron-activatable radiotherapeutics.", *Carbon* 117 (2017) 92-99.

holmium (^{166}Ho) demonstrated a tumoricidal effect. Post-irradiation PEGylation of the MCN surfaces endows dispersibility and biocompatibility.

3.2 Introduction

A variety of materials has been used in the design of nanocarriers for delivery of therapeutic agents to target organs and tissues. These agents include drugs, vaccines and radionuclides that emit particulate (α or β^-) radiation. For the latter application, creating nanocarrier materials containing large amounts of therapeutic radionuclides can be hazardous to the personnel involved in this process. This can be avoided by incorporating a carefully selected stable nucleus into the nanocarriers and subsequently exposing them to a high flux density of thermal neutrons such as is found in a nuclear reactor. If the stable nuclei have a sufficiently large thermal neutron capture cross-section, they can be activated to therapeutic (i.e., tumor cell killing) radioactive nuclei. This neutron-activation approach allows the stable isotope-containing nanocarriers to be produced without constraints related to handling hazardous radioactive materials or short isotopic half-lives. The nanocarriers can be subjected to neutron irradiation just prior to the time of administration to patients, thus limiting the handling of radioactive materials by personnel. For such an application, the nanocarrier materials must be able to entrap significant amounts of the stable isotope, withstand the harsh conditions in the core of a nuclear reactor, retain the radioactive isotope produced following neutron irradiation to prevent accumulation of the radionuclide in non-target tissues due to leaching, be of relatively low density for facile administration by the intravenous route, and be non-toxic.

Mesoporous Carbon Nanoparticles (MCNs) have been widely studied for use in a variety of applications including as fuel cells, supercapacitors, gas storage devices and as

catalysts, but only rarely for drug delivery applications. This is in contrast to other carbon-based materials such as carbon nanotubes, fullerenes, graphene oxide nanoplatelets and carbon nanodiamonds, all of which have been used as drug delivery vehicles [1-4]. Zhu et al. explored the possibility of using MCNs for chemo-therapeutic drug delivery by exploiting the hydrophobic nature, large surface area, easy surface modification and low toxicity profile of MCNs [5]. A product known as Carbon Nanoparticles Suspension Injection (CNSI®), which contain particles 150 nm in diameter, has been tested in human clinical trials and was approved as a lymph node tracer by the China Food and Drug Administration [6]. Interestingly, these carbon nanoparticles did not induce major toxicities or allergic reactions [7]. Here we report on the investigation of MCNs as a carrier of stable isotopes for subsequent conversion to radioactive isotopes following neutron irradiation. This neutron-activation approach allows the preparation of therapeutic radionuclides in carriers that can be targeted to tumors (requiring large amounts of radioactivity) with minimum handling by the operator. Among the potential candidates of stable neutron-activatable elements, holmium (^{165}Ho) was chosen due to its high natural abundance (100%) and its large thermal neutron capture cross-section (64 barns where 1 barn = 10^{-24} cm^2) for activation to ^{166}Ho. This radioactive isotope of holmium decays by the emission of high energy β^- particles (E_{max}= 1.84 MeV) and γ-photons (81 keV, 6.7% photon yield) with a relatively short half-life (26.9 h). These properties make ^{166}Ho suitable as a 'theranostic' agent whereby the β^- particles provide their tumor-killing radiotherapeutic function while the emitted γ-photons allows the biodistribution of ^{166}Ho-labeled MCNs to be assessed noninvasively by SPECT/CT imaging (**Fig. 3.1**) [8, 9]. Indeed, a ^{166}Ho/chitosan complex was formulated as a local tumor ablative agent in which their safety and efficacy were confirmed in a Phase IIb clinical study [10]. This formulation was approved under the brand name of Milican® in 2001 by the Korea Food and Drug Administration [11]. While this formulation demonstrated potential as a radiotherapeutic agent, it was produced by the

cumbersome process of incorporating ^{166}Ho into the formulation and not by neutron-activation of a ^{165}Ho/chitosan complex.

When considering materials as suitable carriers of neutron-activatable elements, one must take into account the loading capacity of the carriers for these elements as well as their stability following irradiation in a nuclear reactor where the neutron flux density is great enough to yield therapeutically-sufficient amounts of the activated radionuclide. Holmium encapsulated polymeric microspheres comprised of poly (L-lactic acid) have been used as carriers of neutron-activatable elements, and one such composition is currently in clinical trials for treating liver cancer [8, 12]. In spite of successful translation to the clinic, the biggest drawback of this formulation is degradation of the polymer by heat generated during the neutron-activation process. This can lead to premature leaching of the activated radionuclide which can result in radioactivity accumulating in non-target tissues after administration to a patient. In order to reduce this degradation, shorter neutron irradiation times must be used; however, this limits the total amount of radioactivity that can be produced to potentially sub-therapeutic levels.

Di Pasqua et al. explored the use of mesoporous silica nanoparticles (MSNs) as a carrier for neutron-activatable isotopes for intraperitoneal administration [9]. Because of our interest in using neutron-activated nanocarriers as a means to treat various types of cancers by systemic administration, high specific activities (mCi of ^{166}Ho mg^{-1} of nanocarrier) are required. This means that long neutron irradiation times are needed to produce these high specific activities. Therefore, the nanocarriers required for this application need to have relatively high adsorption capacities for stable holmium and also need to be resistant to degradation in the relatively harsh nuclear reactor environment. In addition, it is desirable to avoid high-density nanocarriers to prevent settling of the particles during administration through an indwelling catheter. MCNs appeared to be an excellence choice as a nanocarrier for this theranostic application due to their

desirable characteristics of lower toxicity than MSNs, heat resistance and high metal adsorption capacity [13-15]. Nanocarriers composed of mesoporous carbon were evaluated for their ability to serve as a suitable delivery vehicle for therapeutic radionuclides produced by neutron activation. Here we report that sufficient quantities of the stable isotope holmium (^{165}Ho) could be incorporated into MCNs using a wet impregnation technique, and that minimal leaching of the radionuclide produced by neutron activation (^{166}Ho) following irradiation in a nuclear reactor was observed. A novel nuclear magnetic resonance (NMR) method was used to characterize the pore size distribution of the prepared MCNs. In addition, an *in vitro* cell-based assay was used to confirm that these stable holmium-containing MCNs did not induce cellular toxicity and that MCNs containing radioactive holmium demonstrated a sufficient tumor-killing effect. Furthermore, the surfaces of the MCNs were modified by the addition of a polyethylene glycol (PEG) moiety to allow them to be dispersed in physiological solutions for intravenous administration and as a means of improving their biocompatibility.

3.3 Materials and Methods

3.3.1 Chemicals

Phenol, Pluronic® F127 (triblock copolymer consisting of poly(ethylene oxide)–poly(propylene oxide)–poly(ethylene oxide)), holmium (III) nitrate pentahydrate and holmium (III) oxide were purchased from Sigma-Aldrich (St. Louis, MO). Sodium hydroxide was obtained from Fisher Chemical (Fair Lawn, NJ). Formaldehyde (37%, ACS Reagent Grade) was received from Ricca Chemical (Arlington, TX). Holmium (III) acetylacetonate ($Ho(AcAc)_3$) was acquired from GFS Chemicals (Columbus, OH). 1,2-distearoyl-*sn*-glycero-3-phospho-ethanolamine-N-[methoxy (polyethylene glycol)-3000] (DSPE-PEG) was purchased from Avanti Polar Lipids Inc. (Alabaster, Alabama).

3.3.2 Synthesis of MCNs

MCNs were synthesized from phenol formaldehyde resin by adopting the soft-template method of Zhao et al [16]. Briefly, phenol (0.6 g) was added to a mixture of formalin solution (2.1 mL) and sodium hydroxide solution (15 mL, 0.1 M), and stirred at 70 ^{o}C for 30 min at 360 rpm. A solution containing 0.96 g of Pluronic® F127 in 15 mL of Milli-Q water) was added to the reaction and the temperature was lowered to 66 ^{o}C. After 2 h, the mixture was diluted with 50 mL of Milli-Q water and the reaction was stopped when a reddish solid precipitate appeared. After measuring the volume of the suspension, a 3.16-fold excess of Milli-Q water was added. A hydrothermal reaction was then conducted at 130 ^{o}C for 24 h. After multiple washings with Milli-Q water, carbonization was performed at 700 ^{o}C under argon gas for 3 h after which time the final product (MCNs) was collected [16].

3.3.3 Wet impregnation on MCNs (WI-MCNs)

A wet impregnation (WI) approach was employed to produce MCNs from which entrapped holmium was less likely to leak. WI was accomplished by adding holmium nitrate pentahydrate (100 mg) and MCNs (10 mg) to 20 mL of ethanol and stirring for 24 h at room temperature. The suspension was then centrifuged at 2000 x g for 15 min and the supernatant was decanted to remove unbound holmium. The solids were held under vacuum at room temperature overnight; the temperature was subsequently raised to 400 ^{o}C for an additional 4 h to form holmium oxide. Any holmium oxide formed outside of the MCNs was removed by centrifugal filtration (Ultracel®, 50K MWCO) [17]. For a control study, $Ho(AcAc)_3$ was loaded to MCNs by a physical adsorption method (MCNs-$Ho(AcAc)_3$). This was accomplished by

mixing 100 mg of $Ho(AcAc)_3$ and 10 mg of MCNs in ethanol for 24 h at room temperature. After removing unbound $Ho(AcAc)_3$, the mixture was dried in a vacuum oven overnight.

3.3.4 Surface modification of MCNs (MCNs-PEG)

The surfaces of these WI-MCNs were modified through non-covalent PEGylation by exploiting hydrophobic interactions between the MCNs and a phospholipid-based PEGylating agent. This was accomplished by adding DSPE-PEG to MCNs suspended in water and sonicating the suspension for 10 min.

3.3.5 Physicochemical characterization of MCNs

The hydrodynamic diameter and zeta potential of MCNs, WI-MCNs and WI-MCNs-PEG samples were measured using a Malvern Zetasizer Nano ZS. Scanning electron microscopy (SEM; Hitachi S-4700) was used to obtain images of the particles. Elemental composition of samples was determined by X-ray photoelectron spectroscopy (XPS; Kratos Axis Ultra DLD). As part of the sample preparation process, a powder form of the MCNs and WI-MCNs was pressed into an indium foil; interference from indium in the XPS analysis was normalized (**Table 3.1**). Powder X-ray powder diffraction (PXRD; Rigaku Multiflex X-ray diffractometer with Cu K_α radiation (λ= 1.5418 Å)) was used to assess the structure of impregnated holmium oxide in the MCNs.

3.3.6 Holmium loading on MCNs

The amount of holmium content was estimated by thermogravimetric analysis (TGA; TA Instruments Q50). A 5 mg sample of WI-MCNs or MCNs-$Ho(AcAc)_3$ was heated from 25

^{o}C to 1000 ^{o}C with a heating rate of 10 ^{o}C minute^{-1}. The holmium content of the MCNs was also determined by neutron-activation analysis utilizing the PULSTAR Reactor Facility at North Carolinas State University (reactor power = 1 MW; thermal neutron flux = 5.5 x 10^{12} neutrons cm^{-2} s). An ORTEC 42% high purity germanium detector system with a Canberra AFT research amplifier, multi-port II analog-to-digital converter and Genie 2000 MCA spectroscopy software were used to quantify the amount of ^{166}Ho produced which was then used to calculate the amount of holmium (^{165}Ho) in the sample.

3.3.7 Stability of MCNs following neutron irradiation

For assessing the stability and retention of holmium in the MCN formulations following neutron irradiation, samples were irradiated for 1, 5 and 10 h in the PULSTAR nuclear reactor, placed in centrifugal filter (Ultracel®, 50K MWCO) and centrifuged at 2500 x g for 20 minutes. The amount of radioactivity (^{166}Ho) in the filtrate was measured using a γ-counter (PerkinElmer 2470 Wizard γ-counter).

3.3.8 Calculation of pore size distribution by NMR

The nanopore size, pore size distribution and pore volume were characterized using the NMR-based method of Wu et. Al [18]. The NMR measurements were performed on a 400 MHz (^{1}H frequency) pulsed NMR system at room temperature. Approximately 20 mg of MCN and holmium-loaded MCN powder samples were loaded into a 4 mm spinner followed by addition of approximately 35 mg of deionized water. The spinner was then tightly sealed to prevent water loss due to evaporation. A magic angle spinning (MAS) spectrum was obtained at ~7 kHz spinning by recording the free induction decay after a single 90-degree pulse (~5 μs).

The last delay was set long enough (10 s, and T_1 ~ 1.5 s) to ensure that the signal was fully recovered after each scan.

3.3.9 Evaluation of *in vitro* leaching

An *in vitro* leaching study was performed with ^{166}Ho in which 200 μL of MCN-Ho(AcAc)$_3$-PEG and WI-MCN-PEG samples (0.1 mg/mL) were placed in a dialysis cup (Slide-A-Lyzer MINI dialysis®, 3500 MWCO) which was suspended in 20 mL of Phosphate Buffered Saline (PBS) at 37 ºC and shaken at 100 rpm (Thermo MAXQ 4450). A sample of the dialysate was collected at each time point (1, 2, 3, 6, 12, 24 and 36 h) and the holmium content was quantified in a γ-counter.

3.3.10 *In vitro* cytotoxicity and efficacy assessment of MCNs

The toxicity of each of the three MCN formulations was assessed in a human ovarian cancer cell line (A2780) using a CCK-8 assay kit (Dojindo Laboratories). The A2780 cells were cultured with RPMI-1640 medium with 10% FBS and 1% penicillin-streptomycin in 5% CO_2 at 37 ºC. The cells (5000 cells/well) were seeded in a 96-well plate and incubated for 24 h. Pre-determined amounts of the formulations were added to each well and cultured for 24, 48 and 72 h. After the formulations were removed and the wells were washed with PBS, the CCK-8 reagents (10 μL/well) were added. The cells were then incubated for 4 h and the absorbance at 450 nm was recorded with a plate reader (SpectraMax M5). To calculate the cell viability, the absorbance of each well was compared with an untreated group (control).

3.4 Results and Discussion

MCNs were successfully prepared using the soft template method [16]. Image analysis by SEM showed that MCNs were uniform and spherical in shape (**Fig. 3.2**a,b). The composition of MCNs was analyzed XPS and found to consist only of carbon (94.2%) and oxygen (5.8%) (**Table 3.1**). By dynamic light scattering (DLS) and zeta potential measurements, the MCNs were shown to have an average diameter of 154 nm, almost neutral in surface charge (zeta potential = -0.37 mV) and to be monodisperse (PDI = 0.152) (**Fig. 1**c). The Type IV isotherm curve obtained by nitrogen gas adsorption measurements was indicative of the mesoporous structure of the MCNs and, thus, were exhibited to have a large surface area (665.2 m^2 g^{-1}) as determined by Brunauer-Emmett-Teller (BET) (**Fig. 3.3**a).

Although the BET method has been widely used for characterization of porous carbon structures, the assumptions of BET theory have been questioned for micropores and mesopores because it tends to overestimate the specific surface area. Therefore, a newly developed NMR method, which is sensitive to pores less than ~3 nm, was used to characterize the pore size distribution of the MCNs [18, 19]. A typical NMR spectrum of a water/MCN mixture is shown in **Fig. 3.3**b. Intergranular water was used as the chemical shift reference (0 ppm) and the up-field peak at -1.5 ppm was from water inside the nanopores whose peak shape was used to derive the pore size distribution. The pore size was calculated from the nucleus-independent chemical shift (NICS) value by the following equation,

$$d = A_1 e^{\delta/0.53} + A_2 e^{\delta/3.7} + d_0$$

where A_1, A_2 and d_0 are empirical parameters depending on the carbon material synthesis condition. Because MCNs were carbonized at 700 ^oC, which led to a lesser degree of graphitization and a smaller NICS effect, these parameters were recalibrated (scaled by 0.75 from a previous report whose carbon was prepared at 900 ^oC) so that the average pore size

matched the value reported in the literature [16, 18, 20]. The nanopore volume per gram of carbon (excluding the intergranular pores) was calculated by the method of Xing et al.:

$$\frac{V_p}{m_{MCN}} = \frac{A_P}{A_{tot}} * m_w * \frac{1}{\rho_w * m_{MCN}}$$

where A_p is the peak area of water in the nanopores, A_{tot} is the total peak area, m_w is the total water mass in the spinner, $\rho_w = 0.9$ g cm^{-3} is the nanoconfined water density and m_{MCN} is the MCN mass in the spinner [18]. NMR analysis of water adsorption showed that the nanopore volume of MCNs was 0.69 cm^3 g^{-1}. The dominant pore size was 2.6 nm and the pore size distribution was narrow in that 95% of the pore sizes were between 2 and 4 nm (**Fig. 3.2**c). Intergranular pores were not considered because their contribution to the total surface area was negligible.

Initially, a hydrophobic form of holmium ($Ho(AcAc)_3$) was used to load ^{165}Ho into MCNs by physical adsorption. The amount of holmium loaded into MCNs was estimated by TGA, exploiting the fact that all of the carbon components were removed by pyrolysis between 400 ºC and 600 ºC, but holmium was retained even at 1,000 °C (**Fig. 3.5**). Holmium loading in the MCNs was determined to 6.96%. To maximize the loading of holmium as well as to prevent leaching, wet impregnation followed by a drying and calcination process was used to synthesize holmium oxide in the pores of the MCNs [17]. Although MCNs-$Ho(AcAc)_3$ were able to retain ^{166}Ho relatively well, intra-pore synthesis of holmium oxide by this technique was shown to essentially and completely prevent the leaching of radioactive holmium from these nanocarriers after they had been irradiated in the nuclear reactor for up to 10 h (**Fig. 3.6**). The particle size distribution and morphology of the WI-MCNs also did not change indicating that the structural integrity of the particles was not compromised by long irradiation times. The maximum loading of holmium by WI was determined to be approximately 14 w/w% by TGA and 18.2 w/w% by XPS (**Table 3.1**). The most accurate amount of holmium loading was

determined by neutron activation analysis (NAA). After ^{165}Ho was converted to ^{166}Ho in the nuclear reactor, the amount of holmium in the MCNs was calculated from the quantity of radioactivity (^{166}Ho) produced. NAA calculations determined that holmium loading in the MCNs was 5.34 w/w% and 16 w/w% by the physical adsorption method and WI, respectively. The PXRD pattern of WI-MCNs showed that holmium incorporation in MCNs resulted in significant reduction in signal intensity (**Fig. 3.4**). When it was contrasted with commercially purchased holmium oxide, several representative PXRD peaks of holmium oxide were absent in the WI-MCNs, which indicated crystalline structured holmium oxide was not formed outside of the mesoporous system. The total surface area of the MCNs was significantly reduced from 665.2 to 368.6 m^2 g^{-1} after the WI procedure. This is likely due to the holmium oxide particles occupying space in the pores of the MCNs (**Fig. 3.3**a). This was also evidenced by the NMR characterization. MCNs showed two ^{1}H peaks where the upfield peak (at -1.5 ppm) was from water in the nanopores. However, the nanoconfined water peak was absent in the NMR of the holmium impregnated MCNs, indicating occupation of the nanopores by holmium (**Fig. 3.3**b).

For enhancing their biocompatibility and *in vivo* stability, surface modification of the WI-MCNs was accomplished by PEGylation reactions; both covalent and non-covalent methods were evaluated. Non-covalent PEGylation with DSPE-PEG was selected because it could be accomplished quickly with minimum handing. The hydrophobic portion (DSPE) of this phospholipid PEGylating agent rapidly associated with the hydrophobic MCNs after sonication for 10 minutes. WI-MCNs-PEG were shown to increase in diameter by approximately 20 nm and the surface charge changed from neutral to a negative zeta potential (-24.9 mV) while retaining monodispersity (PDI = 0.126) (**Fig. 3.2**c). To assess if the non-covalent PEG surface coating was stable following exposure to the neutron irradiation process, DSPE-PEGylated MCNs were irradiated in the nuclear reactor for 1, 5 and 10 hours. After a 1 h irradiation, no sign of loss of surface coating was observed, and the MCNs were as readily

dispersed as they had been before neutron irradiation. However, when they were irradiated for 5 and 10 h in the nuclear reactor with the same neutron flux, the DSPE-PEG coating was apparently not stable as the particles could no longer be dispersed in aqueous media (**Fig. 3.7**a). The size and PDI of MCNs were not altered even after 10 h of irradiation (**Fig. 3.8**). If longer periods of irradiation are required to produce greater amounts of ^{166}Ho that result in desorption of the DSPE-PEG coating, then performing PEGylation after the neutron-activation process is a possibility because the non-covalent PEGylation reaction can be accomplished within minutes (**Fig. 3.9**). This strategy was shown to be effective for WI-MCNs that had been irradiated for 5 and 10 h (**Fig. 3.7**b). Post-irradiation PEGylation provides an added advantage in that it allows the attachment of protein or peptide ligands that target tumors to the surface of the PEGylated MCNs.

The cytotoxicity of MCNs was evaluated using a human ovarian cancer (A2780) cell line. The cells were exposed to three formulations (MCNs, WI-MCNs and DSPE-PEGylated WI-MCNs-PEG (WI-MCNs-PEG)), all containing the non-radioactive isotope of holmium (^{165}Ho), for 48 h. As shown in **Fig. 3.10**a, none of these formulations induced any cytotoxicity at concentrations up to 100 μg mL^{-1}. Thus, any tumor-killing activity by neutron-activated carbon nanoparticles would be due to the radiation and not be the result of chemical toxicity of the nanoparticle. After confirming the safety of non-radioactive MCNs, the efficacy of radioactive WI-MCNs-PEG that had been irradiated in a neutron flux for one hour using a longer incubation time (72 h) with the A2780 cells. While the non-radioactive (^{165}Ho) MCNs did not induce cytotoxicity after a 72 h incubation, the radioactive (^{166}Ho) MCNs showed a clear tumor-killing effect at the 24 h time point which significantly increased after longer incubation times (48 h and 72 h) (**Fig. 3.10**b). It has been well established that larger absorbed radiation doses induce a greater tumoricidal effect [21-24].

The amount of ^{166}Ho produced following irradiation of natural abundance holmium in a neutron flux was compared to the amount of other frequently employed therapeutic radionuclides (^{90}Y and ^{177}Lu) produced following neutron irradiation of yttrium and lutetium, respectively, under the same conditions. (**Fig. 3.11**) [25]. While both ^{165}Ho and ^{89}Y have an isotopic natural abundance of 100%, ^{165}Ho has much greater neutron capture cross-section than ^{89}Y (64 barns vs. 1.3 barns) and a shorter half-life (27 vs 64 h). While ^{176}Lu has an approximately 40-fold larger neutron cross-section than ^{165}Ho, its isotopic natural abundance is only 2.59% (Lu mostly exists as ^{175}Lu in nature) and the half-life of ^{177}Lu is also ~ 6-fold greater than ^{166}Ho. Thus, the maximum amount of ^{166}Ho that can be produced is much greater that the amount of ^{90}Y and ^{177}Lu, respectively, that can be produced when irradiating the same sample size under similar conditions.

3.5 Conclusion

In summary, MCNs were investigated as a carrier material for neutron-activatable holmium for use in systemic radiation therapy. When compared to other nanoparticle systems that deliver therapeutic radionuclides, the neutron activation approach allows for easy production and adjustment of the radiation dose by using a neutron source with a different flux density (e.g., a higher power nuclear reactor), changing the time of irradiation, or increasing the loading of the stable isotope in the nanoparticle. MCNs were synthesized as spherical monodisperse particles with a diameter of approximately 150 nm. Their surface charge was neutral and they possessed a large surface area. A novel NMR method was employed for estimating the pore size distribution of the MCNs and revealed that these particles had an average pore size of 2.6 nm in diameter with a narrow pore size distribution. The wet impregnation loading method increased the loading capacity of the MCNs for holmium and

resulted in no leaching of ^{166}Ho after irradiation for 10 h in a nuclear reactor. The surfaces of the MCNs were PEGylated in order to enhance their biocompatibility and to make them suitable for intravenous administration. A non-covalent PEGylation method was selected over a conventional covalent PEGylation approach because the latter requires oxidation of MCN surfaces with strong acids and multiple washing steps. This lengthy process would not be practical if it were applied to post-irradiation surface modification of the MCNs due to the relatively short half-life of ^{166}Ho. Finally, *in vitro* cytotoxicity studies employing a human ovarian cancer cell demonstrated that the non-radioactive MCNs were themselves not toxic, thus making them also suitable materials for non-radioactive therapeutic agents.

3.6 REFERENCES

[1] J. Ren, S. Shen, D. Wang, Z. Xi, L. Guo, Z. Pang, Y. Qian, X. Sun, X. Jiang, The targeted delivery of anticancer drugs to brain glioma by PEGylated oxidized multi-walled carbon nanotubes modified with angiopep-2, Biomaterials 33(11) (2012) 3324-3333.

[2] W. Zhang, Z. Guo, D. Huang, Z. Liu, X. Guo, H. Zhong, Synergistic effect of chemo-photothermal therapy using PEGylated graphene oxide, Biomaterials 32(33) (2011) 8555-8561.

[3] H. Zhang, L. Hou, X. Jiao, Y. Ji, X. Zhu, Z. Zhang, Transferrin-mediated fullerenes nanoparticles as Fe 2+-dependent drug vehicles for synergistic anti-tumor efficacy, Biomaterials 37 (2015) 353-366.

[4] A.B. Volnova, S.K. Gordeev, D.N. Lenkov, Targeted Delivery of 4-Aminopyridine Into the Rat Brain by Minicontainers from Carbon-Nanodiamonds Composite, Journal of Neuroscience and Neuroengineering 2(6) (2013) 569-573.

[5] J. Zhu, L. Liao, X. Bian, J. Kong, P. Yang, B. Liu, pH- Controlled Delivery of Doxorubicin to Cancer Cells, Based on Small Mesoporous Carbon Nanospheres, Small 8(17) (2012) 2715-2720.

[6] T. Ye, W. Xu, T. Shi, R. Yang, X. Yang, S. Wang, W. Pan, Targeted delivery of docetaxel to the metastatic lymph nodes: A comparison study between nanoliposomes and activated carbon nanoparticles, Asian Journal of Pharmaceutical Sciences 10(1) (2015) 64-72.

[7] X. Wu, Q. Lin, G. Chen, J. Lu, Y. Zeng, X. Chen, J. Yan, Sentinel Lymph Node Detection Using Carbon Nanoparticles in Patients with Early Breast Cancer, PloS one 10(8) (2015) e0135714.

[8] R.J. Mumper, U.Y. Ryo, M. Jay, Neutron-activated holmium-166-poly (L-lactic acid) microspheres: a potential agent for the internal radiation therapy of hepatic tumors, Journal of nuclear medicine: official publication, Society of Nuclear Medicine 32(11) (1991) 2139-2143.

[9] A.J. Di Pasqua, H. Yuan, Y. Chung, J.-K. Kim, J.E. Huckle, C. Li, M. Sadgrove, T.H. Tran, M. Jay, X. Lu, Neutron-activatable holmium-containing mesoporous silica nanoparticles as a potential radionuclide therapeutic agent for ovarian cancer, Journal of Nuclear Medicine 54(1) (2013) 111-116.

[10] J.K. Kim, K.-H. Han, J.T. Lee, Y.H. Paik, S.H. Ahn, J.D. Lee, K.S. Lee, C.Y. Chon, Y.M. Moon, Long-term clinical outcome of phase IIb clinical trial of percutaneous injection with holmium-166/chitosan complex (Milican) for the treatment of small hepatocellular carcinoma, Clinical cancer research 12(2) (2006) 543-548.

[11] S.Y. Lim, M. Suh, Intellectual Property Business Models Using Patent Acquisition: A Case Study of Royalty Pharma Inc, Journal of Commercial Biotechnology 22(2) (2016) 6-18.

[12] M.L. Smits, J.F. Nijsen, M.A. van den Bosch, M.G. Lam, M.A. Vente, W.P. Mali, A.D. van het Schip, B.A. Zonnenberg, Holmium-166 radioembolisation in patients with unresectable, chemorefractory liver metastases (HEPAR trial): a phase 1, dose-escalation study, The lancet oncology 13(10) (2012) 1025-1034.

[13] L. Wan, Q. Zhao, P. Zhao, B. He, T. Jiang, Q. Zhang, S. Wang, Versatile hybrid polyethyleneimine–mesoporous carbon nanoparticles for targeted delivery, Carbon 79 (2014) 123-134.

[14] C. Liang, Z. Li, S. Dai, Mesoporous carbon materials: synthesis and modification, Angewandte Chemie International Edition 47(20) (2008) 3696-3717.

[15] A. Yan, B.W. Lau, B.S. Weissman, I. Külaots, N.Y. Yang, A.B. Kane, R.H. Hurt, Biocompatible, hydrophilic, supramolecular carbon nanoparticles for cell delivery, Advanced Materials 18(18) (2006) 2373-2378.

[16] Y. Fang, D. Gu, Y. Zou, Z. Wu, F. Li, R. Che, Y. Deng, B. Tu, D. Zhao, A Low-Concentration Hydrothermal Synthesis of Biocompatible Ordered Mesoporous Carbon Nanospheres with Tunable and Uniform Size, Angewandte Chemie International Edition 49(43) (2010) 7987-7991.

[17] H. Huwe, M. Fröba, Synthesis and characterization of transition metal and metal oxide nanoparticles inside mesoporous carbon CMK-3, Carbon 45(2) (2007) 304-314.

[18] Y.-Z. Xing, Z.-X. Luo, A. Kleinhammes, Y. Wu, Probing carbon micropore size distribution by nucleus independent chemical shift, Carbon 77 (2014) 1132-1139.

[19] K. Kaneko, C. Ishii, M. Ruike, Origin of superhigh surface area and microcrystalline graphitic structures of activated carbons, Carbon 30(7) (1992) 1075-1088.

[20] A.C. Forse, J.M. Griffin, V. Presser, Y. Gogotsi, C.P. Grey, Ring current effects: factors affecting the NMR chemical shift of molecules adsorbed on porous carbons, The Journal of Physical Chemistry C 118(14) (2014) 7508-7514.

[21] J. Elgqvist, O.V. Timmermand, E. Larsson, S.-E. Strand, Radiosensitivity of Prostate Cancer Cell Lines for Irradiation from Beta Particle-emitting Radionuclide 177Lu Compared to Alpha Particles and Gamma Rays, Anticancer research 36(1) (2016) 103-109.

[22] A.I. Kassis, Therapeutic radionuclides: biophysical and radiobiologic principles, Seminars in nuclear medicine, Elsevier, 2008, pp. 358-366.

[23] Y. Zhou, L. Zhang, J. Fan, R. Jia, X. Song, X. Xu, L. Dai, A. Zhuang, S. Ge, X. Fan, Let-7b overexpression leads to increased radiosensitivity of uveal melanoma cells, Melanoma research 25(2) (2015) 119-126.

[24] A.E. Rossini, M.A. Dagrosa, A. Portu, G. Saint Martin, S. Thorp, M. Casal, A. Navarro, G.J. Juvenal, M.A. Pisarev, Assessment of biological effectiveness of boron neutron capture therapy in primary and metastatic melanoma cell lines, International journal of radiation biology 91(1) (2015) 81-89.

[25] J.M. Christensen, M. Ghannam, J.W. Ayres, Neutron activation of iron tablets to evaluate the effects of glycine on iron absorption, Journal of pharmaceutical sciences 73(11) (1984) 1529-1531.

[26] E.M. Baum, M.C. Ernesti, H.D. Knox, T.R. Miller, A.M. Watson, Nuclides and Isotopes :

Chart of the Nuclides, 17th ed., Knolls Atomic Power Laboratory. Inc. 2010.

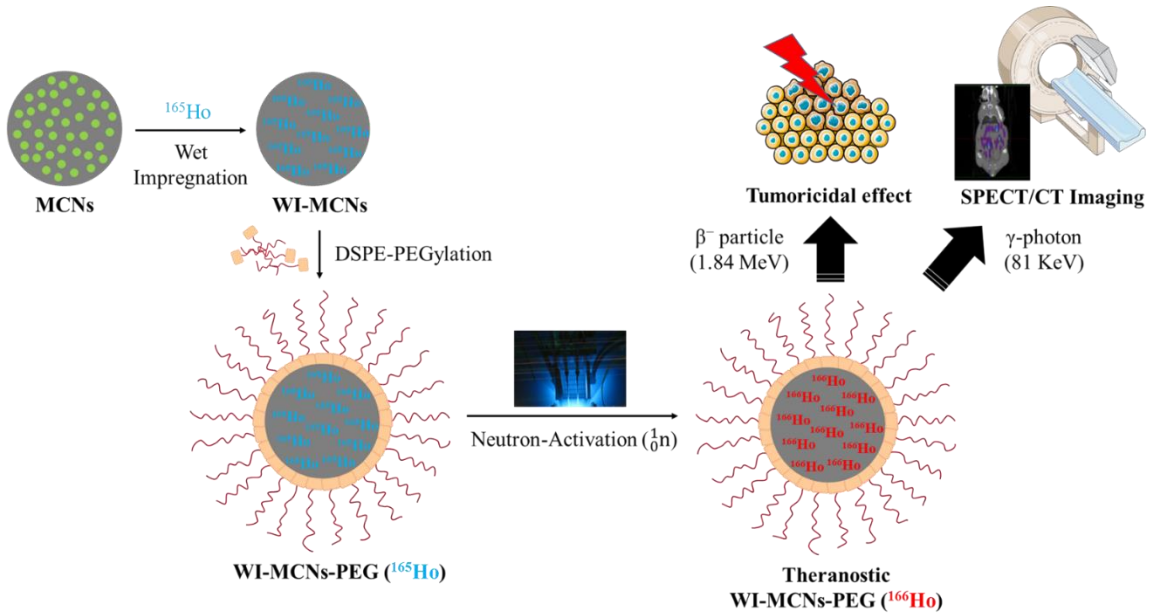

Figure 3.1 Theranostic application of mesoporous carbon nanoparticles **(**scheme produced using Servier Medical Art (www.servier.com))

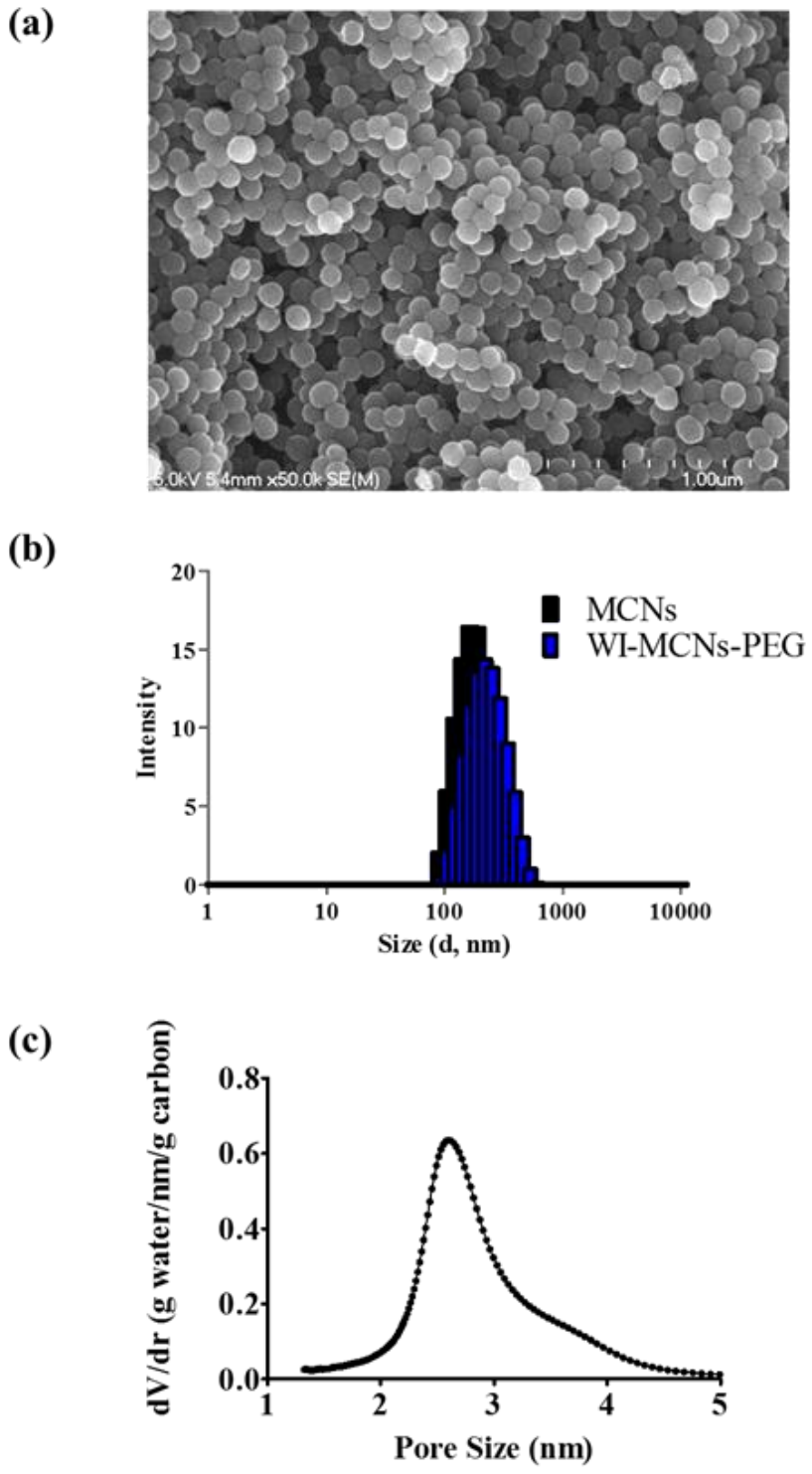

Figure 3.2 Characterization of MCNs. a) SEM image of MCNs. b) The average particle size of MCNs and PEGylated MCNs by DLS. c) Pore size distribution of MCNs by NMR.

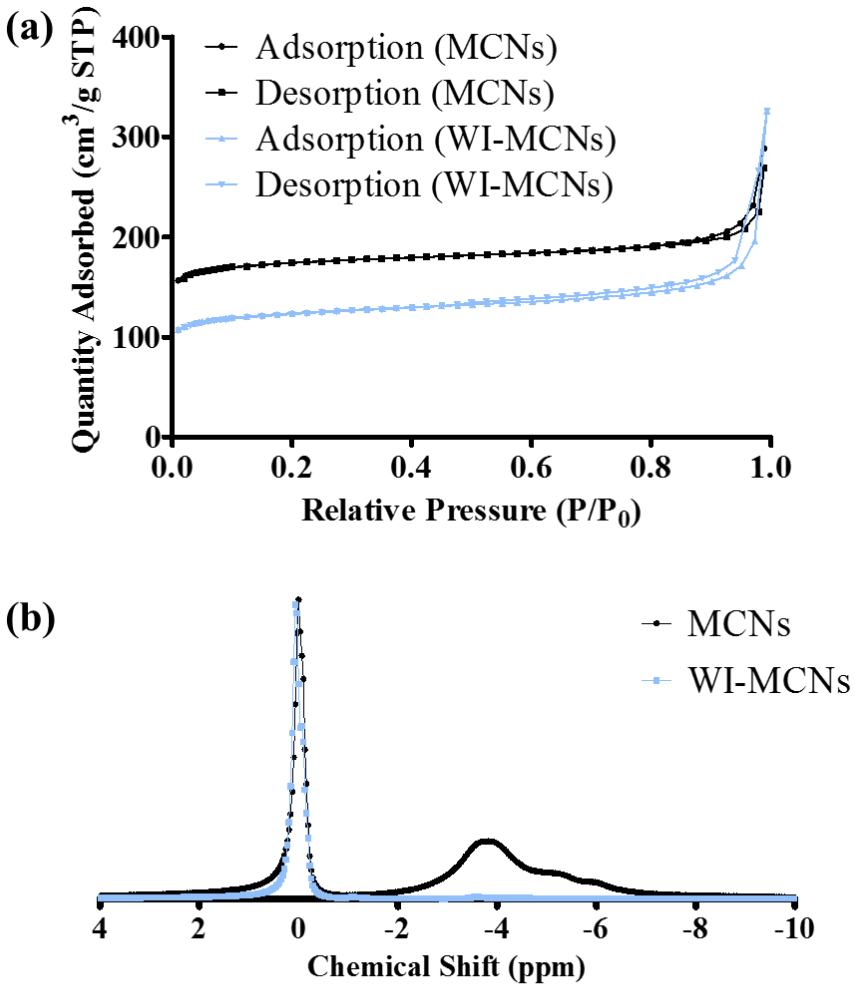

Figure 3.3 Change of physical characterization by WI a) N_2 adsorption-desorption isotherm of MCNs and WI-MCNs by BET. b) ^1H MAS spectrum of water in MCNs and WI-MCNs.

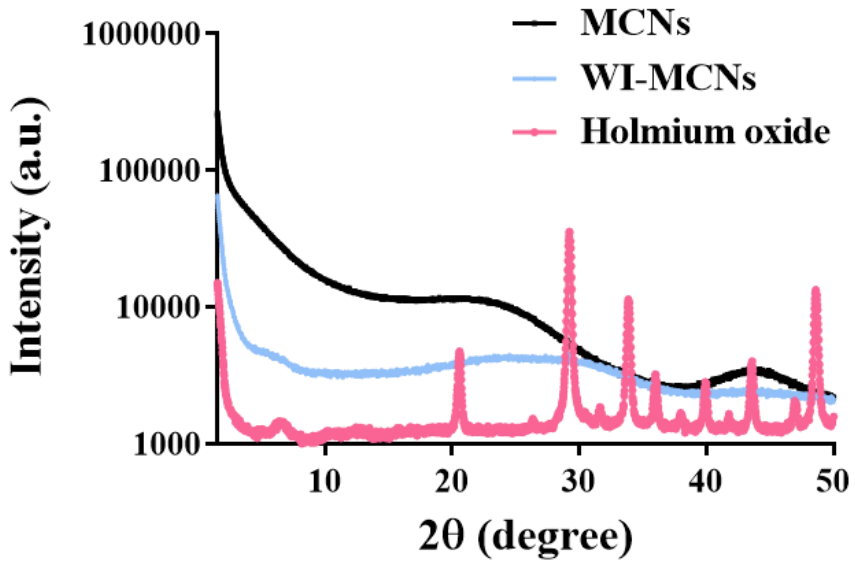

Figure 3.4 Powder X-ray powder diffraction Pattern of MCNs, WI-MCNs and holmium oxide.

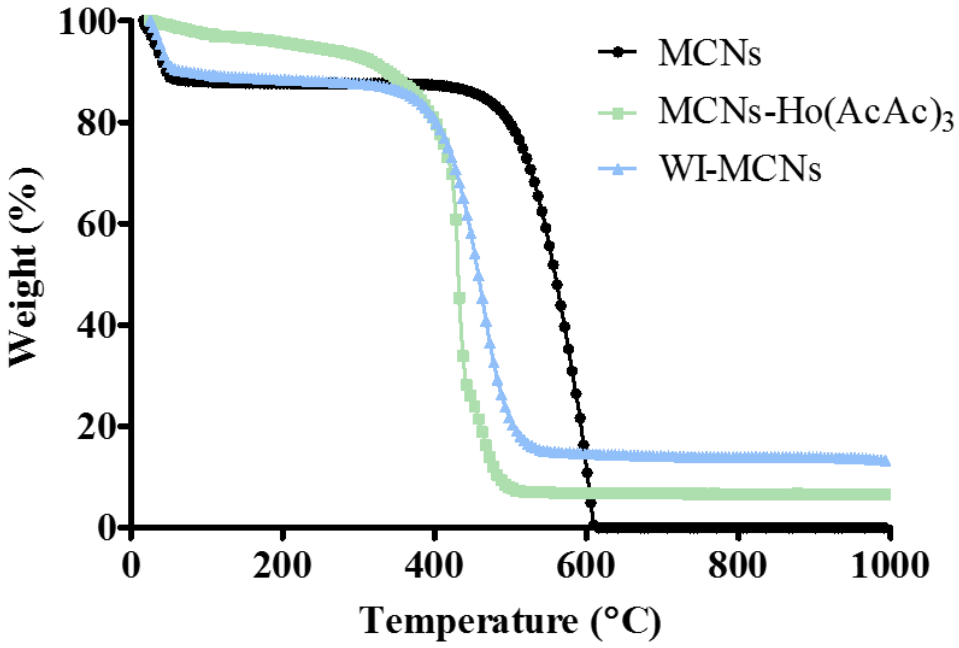

Figure 3.5 Estimation of holmium loading on MCNs, MCNs-Ho(AcAc)$_3$ and WI-MCNs by TGA.

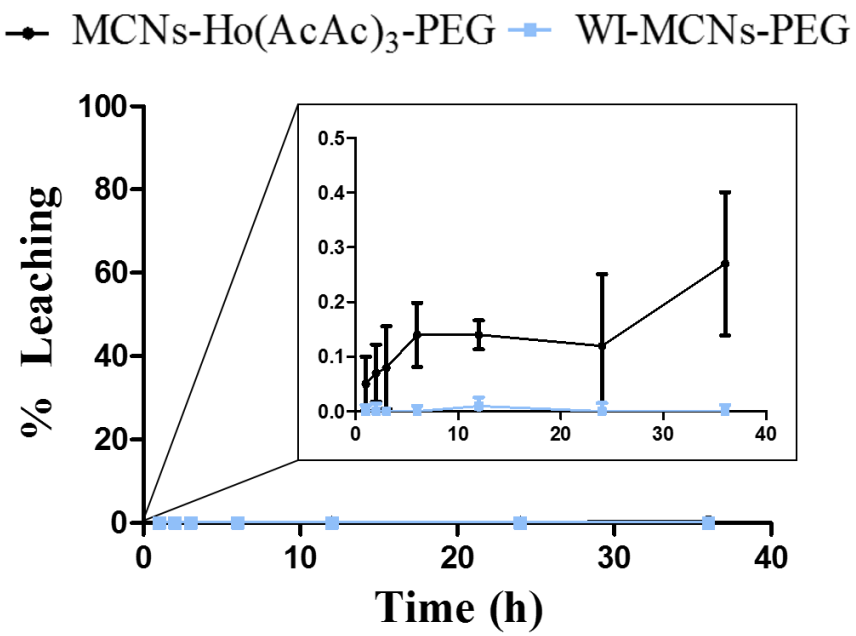

Figure 3.6 *In vitro* leaching study of MCNs-Ho(AcAc)$_3$-PEG and WI-MCNs-PEG.

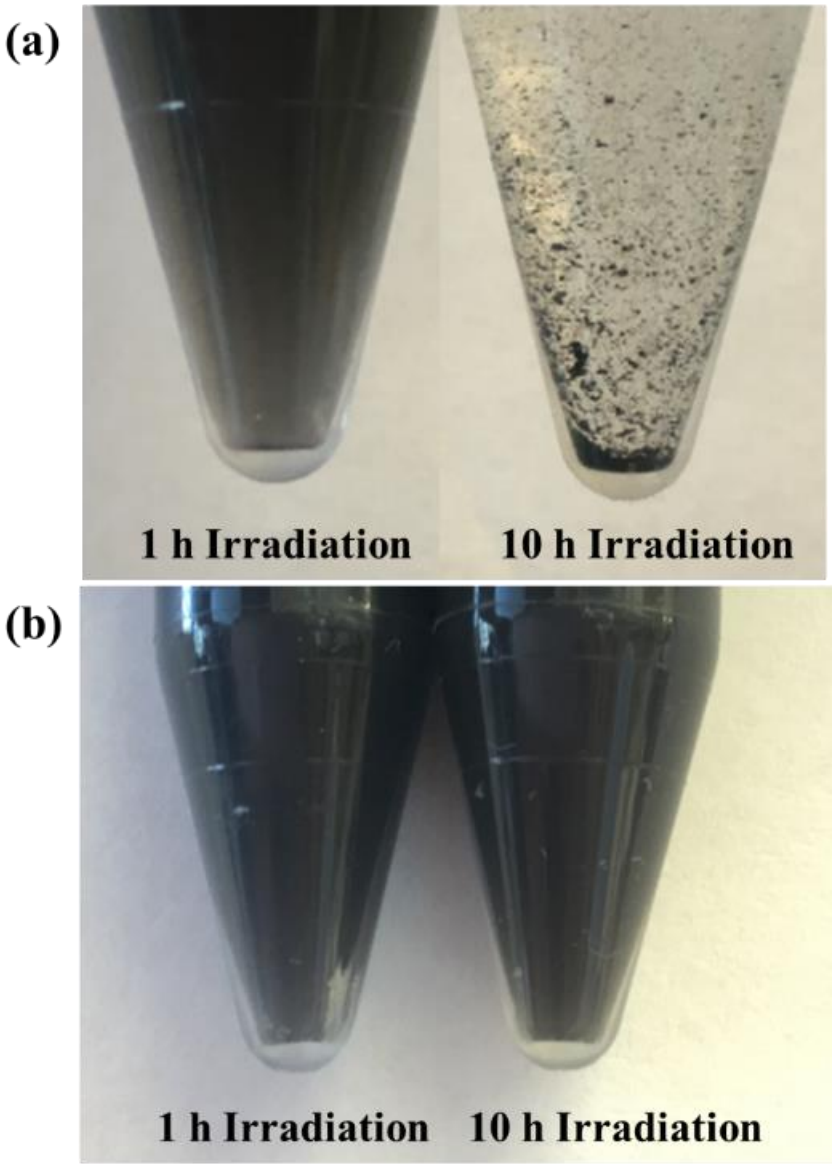

Figure 3.7 Stability of DSPE-PEGylation after Neutron-Activation (a) Pre-Irradiation PEGylation (b) Post-Irradiation PEGylation.

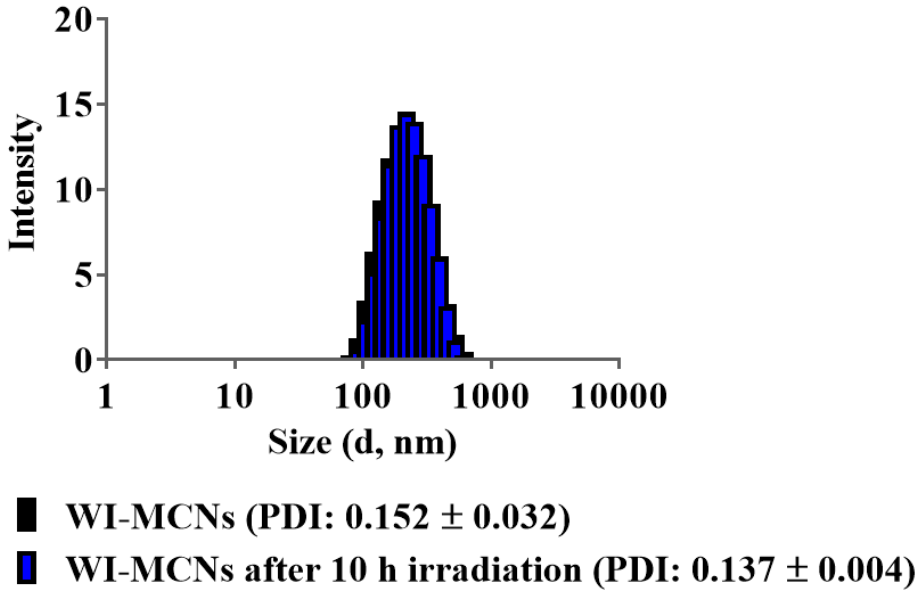

Figure 3.8 Particle size and PDI of MCNs and 10 h Irradiated MCNs by DLS.

.

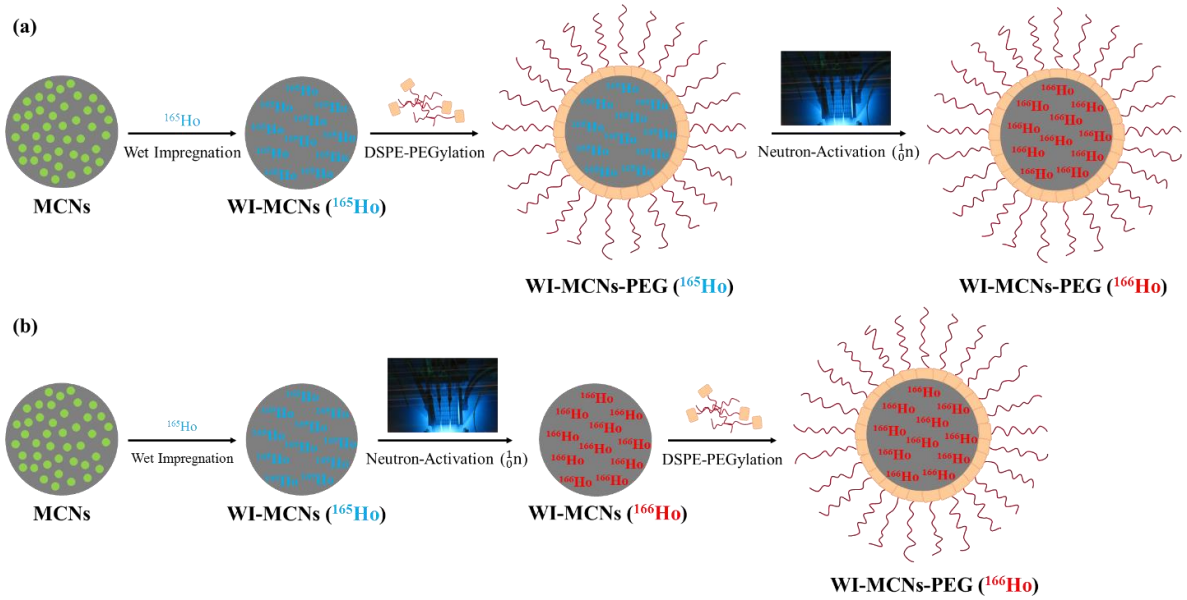

Figure 3.9 Illustration of (a) Pre-Irradiation PEGylation and (b) Post-irradiation PEGylation approaches.

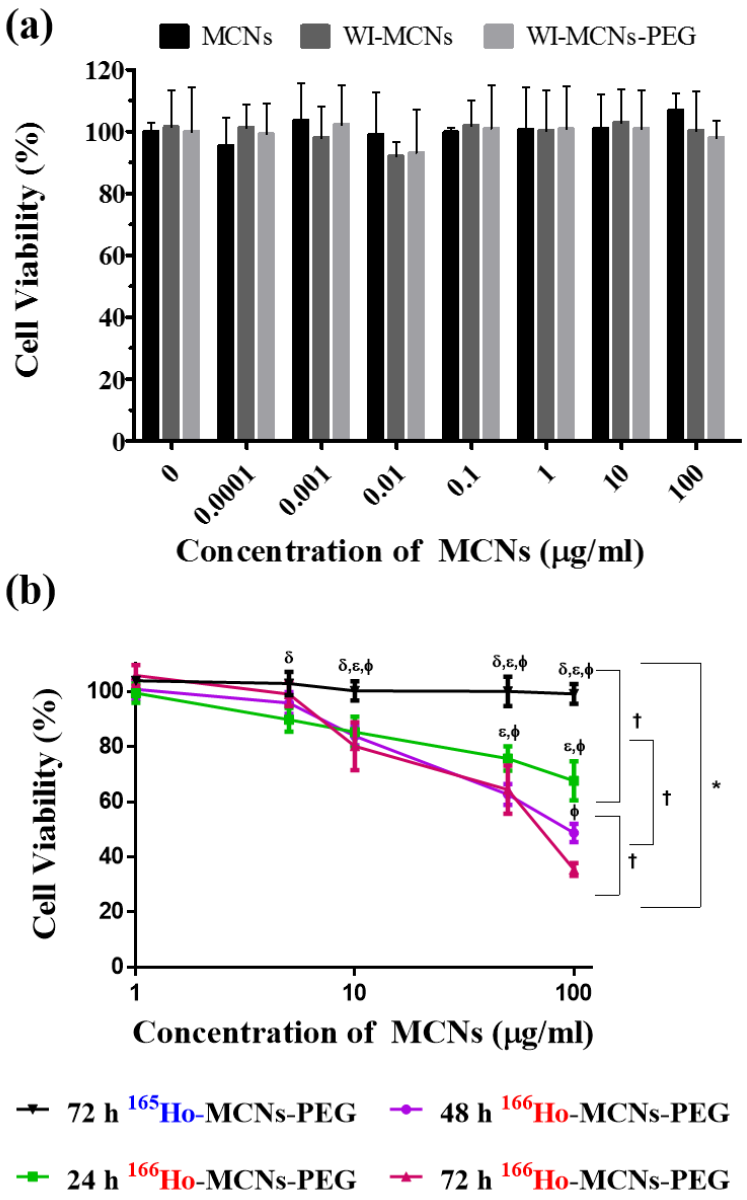

Figure 3.10 *In vitro* cell viability with formulations in a human ovarian cancer cell line (A2780). (a) Cytotoxicity of MCNs, WI-MCNs (^{165}Ho) and WI-MCNs-PEG (^{165}Ho). (b) *In vitro* efficacy of radioactive WI-MCNs-PEG (208 µCi at 100 µg MCNs/mL) vs. non-radioactive WI-MCNs-PEG. Groups were compared by two-way ANOVA (* for $p<0.05$ and † for Bonferroni-adjusted pairwise $p<0.05$ from Concentrations of MCNs) and each concentration was analyzed by independent t-test (δ for adjusted $p<0.05$ from ^{166}Ho-MCNs-PEG (24 h), ε for adjusted $p<0.05$ from ^{166}Ho-MCNs-PEG (48 h) and ϕ for adjusted $p<0.05$ from ^{166}Ho-MCNs-PEG (72 h)).

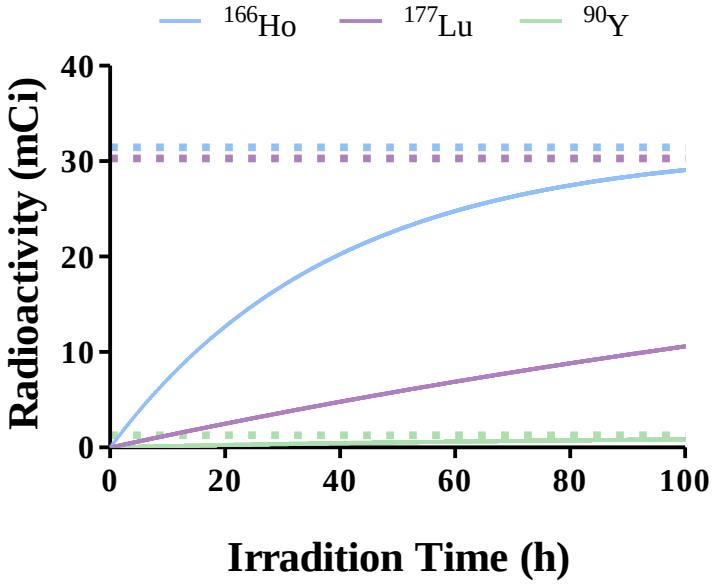

Figure 3.11 Calculated mCi of radionuclides produced following irradiation of 1 mg of natural abundance holmium, yttrium and lutetium in a thermal neutron flux of 5.5 x 10^{12} neutrons cm^{-2} s as a function of time. The dotted lines represent the maximum amount of the individual radionuclides that can be produced under these conditions (radionuclide decay after the end of irradiation is not displayed). The thermal neutron capture cross-sections and half-lives were obtained from the Chart of the Nuclides (Knoll Atomic Power Lab) [26].

Table 3.1 Elemental analysis of MCNs and WI-MCNs by XPS.

Element	MCNs		WI-MCNs	
	Atomic %	Weight %	Atomic %	Weight %
C	94.2	92.4	79.2	61.9
O	5.8	7.6	19.1	19.9
Ho	0	0	1.7	18.2

CHAPTER 4 NEUTRON-ACTIVATABLE NEEDLES FOR RADIONUCLIDE THERAPY OF SOLID TUMORS[3]

4.1 Overview

Various approaches have been undertaken to enhance the delivery of therapeutic agents, including tissue-killing radionuclides, into solid tumors. Here we describe the preparation of Ti and Mo conical needles coated with Ho and Re by pulsed laser deposition or chemical vapor deposition. These needles can readily yield radioactive isotopes following irradiation in a neutron flux. The radioactive needles, whose design were based on solid microneedle arrays used in transdermal drug delivery, can be produced with minimal handling of radioactivity and subsequently inserted into tumors as a means of internal radiation therapy. Ho and Re, were specifically chosen because of their large neutron capture cross-sections as well as the desirable radiotherapeutic properties of the resultant radionuclides. Neutron-absorbing shields were also developed to prevent the production of unwanted radionuclides after neutron irradiation of the needle base materials. Neutron activation calculations showed that therapeutically significant amounts of radionuclides can be produced for treating solid tumors and stability studies demonstrated that Re did not leach off the Mo needles. These coated neutron-activatable needles offer a new approach to internal radiation therapy of tumors that allows precise tailoring of the absorbed radiation dose delivered to the tumor by controlling the coating thickness and the irradiation time.

[3] Part of this chapter was submitted as an article to the Nulear Medicine and Biology as follows: J. Kim, R.J. Narayan, X. Lu, M. Jay "Neutron-Activatable Needles for Radionuclide Therapy of Solid Tumors.", *Journal of Biomedical Materials Research Part A* (under review).

4.2 Introduction

The treatment of solid tumors, which continue to account for a significant number of deaths worldwide, remains a challenge. In order to deliver therapeutic agents to solid tumors, approaches that have been successfully used in the transdermal drug delivery field that do not involve simple passive diffusion have been investigated for intra-tumoral delivery of drugs, proteins and other therapeutics. These approaches include the use of focused ultrasound, iontophoresis and electroporation [1-3]. One approach that has not been previously explored is the use of microneedle technology. Microneedles have been fabricated in solid form to allow transport of therapeutics across the stratum corneum, in hollow form to allow delivery of drugs through a small orifice in the tip of the needle, and in a form composed of dissolvable materials that permit extended release of therapeutics. The focus of the current work is to fabricate a needle that would deliver therapeutic doses of radiation to tumors after penetration of the needle into solid tumors. This approach involves making the needle itself radioactive by coating them with elements that are readily activated to therapeutic radionuclides following irradiation in a neutron flux. Because the thickness of most solid tumors is much greater than the thickness of the stratum corneum (~15 μm), our design involved needles of much greater length (300 μm - 1 cm) than seen with most microneedle assemblies.

The use of therapeutic (particle-emitting) radionuclides to treat solid tumors remains as a prominent therapeutic option. Internal radiation therapy with sealed radioactive sources (brachytherapy) involves the delivery of high doses of targeted radiation with minimal off-target effects by applying radioactive sources directly to or into the target tumors. Brachytherapy sources containing ^{192}Ir or ^{103}Pd are used in the treatment of prostate cancer, the second leading cause of cancer death in men in the United States, and cervical cancer, the second leading cause of cancer-related deaths in women in developing countries [4, 5]. In addition, ocular plaques containing ^{125}I and ^{106}Ru are used to treat tumors of the eye [6].

Neutron-activation is an attractive method of generating radioactivity while minimizing radioactive exposure during handling. Holmium (Ho) is a promising neutron-activatable element as it is 100% naturally abundant (^{165}Ho) and has a large neutron capture cross-section (59 barns; 1 barn = 10^{-24} cm^2) [7]. After irradiation in a neutron flux, ^{166}Ho is produced, which decays by the emission of high energy, tumor-killing β^- particles (E_{max} = 1.86 MeV, half-life = 26.8 h; maximum tissue penetration = 8.7 mm). This neutron-activation approach has been used to produce ^{166}Ho-nanoparticles composed of mesoporous silica, mesoporous carbon and graphene oxide. This method demonstrated the generation of sufficient radioactivity to induce tumoricidal effect as not handling any radioactivity during the formulation preparation steps [8, 9].

Radiotherapeutic rhenium (Re) radioisotopes can also be produced by neutron activation of naturally abundant Re. It is a refractory metal with a very high melting point (3180 °C) and is resistant to wear and corrosion even at low pH and high salt condition [10-12]. Among the refractory metals (niobium, molybdenum, tantalum and tungsten), Re element exhibits the greatest tensile and creep-rupture strength [10, 13]. In addition, Re does not form carbides, nor does it have a ductile-to-brittle transition temperature as it is ductile over a wide range of temperatures [12]. Thus, it has the capability to be utilized in various applications [11]. In nature, Re exists as two stable isotopes: 37.4% as ^{185}Re (neutron capture cross-section = 112 barns) and 62.6% as ^{187}Re (neutron cross-section = 73 barns) [7]. As such, neutron-activation generates ^{186}Re (E_{max}= 1.07 MeV, half-life = 89.2 h, maximum tissue penetration = 5 mm) and ^{188}Re (E_{max} = 2.12 MeV, half-life = 17.0 h, maximum tissue penetration = 11 mm) [14, 15]. The radioisotopes of Ho and Re produced by neutron activation also emit photons (γ-rays and x-rays). Any leaching of these elements from the microneedles after implantation in tumors can be monitored by obtaining images of their biodistribution using SPECT [14, 15]. Here we report on the production of custom-sized radiotherapeutic needles coated with neutron-

activatable elements (Ho and Re) with the goal of minimizing the handling of radioactive material and improving internal radiation therapy (**Fig. 1**).

4.3 Materials and Methods

4.3.1 Chemicals

Holmium foil (1 mm thick, 99.9% trace rare earth metal basis), methanol (HPLC grade) and acetone (HPLC grade) were purchased from Sigma-Aldrich (St. Louis, MO). Phosphate buffered saline (PBS pH 7.4) was obtained from Fisher Chemical (Fair Lawn, NJ). Acetate buffer (USP heavy metal testing grade, pH 3.5) was acquired from Ricca Chemical (Arlington, TX). Holmium ICP-MS standard (pure single-element standard, 1,000 µg/mL in 2% HNO_3) and rhenium ICP-MS standard (pure single-element standard, 1,000 µg/mL in 2% HNO_3) were received from PerkinElmer (Waltham, MA). Gadolinium sputtering target (76.2 mm diameter, 3.18 mm thick) was purchased from Alfa Aesar.

4.3.2 Pulsed laser deposition (PLD) of Ho on Titanium (Ti) needles

Ti needles were prepared by the North Carolina State University (NCSU) precision instrument machine shop. Prior to deposition of Ho, needles were placed in an ultrasonic bath for 10 minutes in acetone and 10 minutes in methanol to remove impurities. Substrates were then placed in the PLD chamber. Ho foil was utilized as the PLD target. A KrF Lambda Physik LPX 200 excimer laser was operated at a wavelength of 248 nm and an output energy of 450 mJ. A thin Ho film was deposited on the Ti needles using 10,000 shots, with a shot frequency of 20 Hz and a target frequency of 1 Hz.

4.3.3 Characterization of Ho-coated Ti needles

Scanning electron microscopy (SEM; Hitachi S-4700) was used for imaging of the micro-sized needles. Ho deposition was confirmed by energy-dispersive X-ray spectroscopy (EDS; Oxford instruments, INCA PentaFET). The thickness of Ho deposition was measured by atomic force microscopy (AFM, Asylum Research MFP3D Atomic Force Microscope).

4.3.4 Chemical vapor deposition (CVD) of Re on molybdenum (Mo) needles.

Three Re coatings of varying thickness (25, 75 and 125 μm) were uniformly deposited on Mo needles by CVD. During this process, a precursor vapor containing rhenium pentachloride was passed over a heated needle substrate. CVD deposits were formed on the substrate at the molecular level, and the process achieved purity levels in excess of 99.99%. In addition, the CVD coating process exhibited the greatest throwing power, i.e., the ability to uniformly deposit materials onto/into intricately shaped or textured substrates. An essentially 100% dense Re coating was deposited on Mo needles through the thermal decomposition of $ReCl_5$ at 1100ºC.

4.3.5 Gadolinium (Gd) neutron shield

A neutron shield made of pure Gd to prevent the formation of undesired Mo isotopes was produced by the NCSU precision instrument machine shop. The shield was designed to prevent exposure of the base material to the neutrons while allowing irradiation of the coated needle.

4.3.6 Stability assessment at different pH

Non-radioactive coated needles were incubated in 20 mL of PBS (pH 7.4) and in acetate buffer (pH 3.5) at 37 °C for up to 30 days. The leached amount of Ho and Re was quantified by inductively coupled plasma mass spectrometer (ICP-MS; Agilent 7500cx with Agilent 1260 Infinity Bioinert LC).

4.3.7 Leaching following by neutron-activation

Neutron-activatable radiation needles were irradiated for 10 minutes in the PULSTAR Reactor Facility at NCSU (reactor power = 1 MW; thermal neutron flux = 5.5 x 10^{12} neutrons cm^{-2} s). The irradiated samples were washed with 20 mL of Milli-Q water 3 times and the amount of radioactive Ho or Re in the washings was quantified with a γ-scintillation counter (PerkinElmer 2470 Wizard γ-counter).

4.4 Results and Discussion

In order to tailor the amount of radioactivity produced by neutron activation of the needle, the total amount of Ho loaded onto the needle can be varied by the deposition process. PLD is a widely-adopted method of adhering thin films to a substrate [16]. With this method, when Ho foil was ablated in a vacuum with an intense pulsed laser, it was transformed into a plasma plume that condensed on the needle [17]. Among many candidates, Ti was selected as a base material because of its relatively low material cost, low density, high strength, good biocompatibility, resistance against corrosion and, most importantly, the low amount of radioactive Ti isotopes produced following neutron irradiation [18, 19]. Two prototypes with different needle sizes (300 μm and 1 cm) were manufactured, and Ho was deposited by PLD.

Needles with varying dimensions can be prepared and customized to the size of the tumor to be treated (**Fig. 2**a). Successful deposition of Ho on the needle was confirmed by elemental analysis using EDS and by morphological changes observed by SEM (**Fig. 2**b). The thickness of Ho coating was estimated to be 1.19 μm by AFM. Coating thickness can be easily modified by changing PLD parameters such the number of shots or shortening the frequency to achieve desired amount of metal loading. A thicker Ho coating on the Ti needles would reduce the irradiation time necessary to produce therapeutic quantities of radioactivity (^{166}Ho).

A significant amount of heat is generated during the neutron activation process that could degrade the radiation delivery matrix leading to premature leaching of the radionuclide [20]. Therefore, it is important to assess how much radioactivity leaches from the matrix following neutron activation. In these studies, irradiation time was limited to 10 minutes in order to remain in compliance of our institution. The leaching studies showed that all of the Ho that had been deposited on the Ti needles by the PLD process remained on the needles following neutron irradiation and did not leach off when incubated and washed with water.

Since the neutron-activatable radiation needle was designed for use in solid tumors, a pH-stability study was conducted at physiological pH (7.4) as well as in a low pH environments that might be encountered with treating some solid tumors, e.g. cervical (pH 3.5) [21]. Ho deposition on the Ti needle was found to be stable at pH 7.4, but ultimately detached from the needle at pH 3.5. A change in color of the Ho coating, possibly due to oxidation, was also observed in acidic conditions. Thus, all subsequent efforts focused on the Re-coated Mo needles.

Mo is another refractory metal that is a reasonable choice for use as a needle base material due to its mechanical strength, resistance to corrosion, excellent machinability and biocompatibility [22]. We considered making entire needles of Re, but it is much more expensive than Mo and does not possess many of the desirable characteristic of Mo [12]. Mo-

Re allows are often formed to offer protection against oxidation, wear and corrosion. Different compositions of Re-Mo alloys have been extensively investigated and employed for various applications, including biomedical, e.g., artificial heart valves [23, 24].

Based on the capacity for Mo to alloy favorably with Re, a needle was made of Mo and coated with Re by CVD. The size of this needle was 4 mm which was selected specifically for use in tumor-bearing mice models (**Fig. 3**a). Like PLD, CVD is often utilized for preparing elemental films via chemical deposition of a vapor-phase target onto a heated substrate [25]. Due to a faster and more homogenous deposition at a lower cost, CVD is generally considered to be more suitable for large-scale commercial production versus PLD. Based on these factors as well as from previous publications that reported success with CVD methods, the current study used CVD for Re deposition onto a Mo substrate (**Fig. 3**b,c) [12, 17]. Stability testing indicated that the Re coating stayed intact without leaching from the Mo needle even after incubation in different pH buffers for up to 30 days (**Table 1**). Only minimal leaching of radioactive Re was observed following neutron irradiation of the Re-coated Mo needles.

Although the Re-coated Mo needle was readily machinable, scalable and did not exhibit leaching of Re under diverse conditions, a new issue arose in terms of the production of undesirable radioisotopes of Mo following neutron irradiation. Compared to a Ti needle base, the Mo base generates a number of detectable isotopes, some of which are produced in substantial amounts (**Table 2**). ^{101}Mo and ^{101}Tc resulting from irradiation of Mo are produced in the greatest amounts, measuring 13.8 and 11.5 mCi, respectively, under simulated conditions (1h irradiation in a flux of 5.5 x 10^{12} neutrons cm^{-2} s). However, these isotopes decay quickly and concentrations becomes negligible within few hours due to their short half-lives (14.6 minutes for ^{101}Mo, 14.2 minutes for ^{101}Tc). An additional isotope, ^{93}Mo, can also be produced during the irradiation process. Neutron activation calculations revealed that non-negligible amounts (48.6 pCi) of ^{93}Mo ($t_{½}$ = 3500 y) could be produced under the standard irradiation

conditions. Although this amount of radioactivity is not very great, it must be taken into consideration when calculating radiation dosimetry for patients. The most noteworthy isotope resulting from Mo irradiation is ^{99m}Tc, which is a commonly used radionuclide in nuclear medicine for SPECT imaging. Contrary to previously discussed radioisotopes, the radioactivity of ^{99m}Tc increases with time from the decay of ^{99}Mo until transient equilibrium is established (after ~24 h).

In order to avoid the production of these radioisotopes, a neutron shield was manufactured that would allow irradiation of the Re-coated needle, but not the Mo base. Gd was chosen as the shielding material because it has a very high neutron cross-section (49,700 barns), and thus could shield the base of the needle by absorbing neutrons before they reach the base [26, 27]. As shown in **Fig. 4**, the Gd neutron shield was customized to the size of Mo needle and was comprised of two separate compartments (top and bottom) for easy separation following irradiation. Since the Gd shield itself will become radioactive following neutron-activation, this facile shield removal method is desirable to minimize the handling time. Originally, only the needle itself was to be coated with the Re film, but during the process, some Re was unavoidably deposited on the base as well. (**Fig. 3**c). Therefore, the Gd shield was designed so that only the needle itself was exposed to neutrons.

Neutron-activation of Ho and Re was simulated and compared to yttrium (Y) (**Fig. 5**a), a therapeutic radionuclide used in commercial products (e.g., Zevalin®, TheraSphere®) due to the energetic beta particles (β_{max}= 2.28 MeV) it emits [7, 28]. In spite of the 100% natural abundance of ^{89}Y, its low neutron capture cross-section (1.28 barns) results in the production of small amounts of ^{90}Y compared to ^{166}Ho, ^{188}Re and ^{186}Re when neutron-activated under the same conditions. Although ^{185}Re and ^{187}Re both have larger neutron capture cross-sections than ^{165}Ho, the 100% natural abundance of ^{165}Ho results in significantly larger amounts of radioactivity that can be produced. The difference between ^{166}Ho and ^{188}Re in the amount of

radioactivity that can be produced by neutron activation is not very different for irradiation times up to 20 h; longer irradiation times yield a greater amount of ^{166}Ho that is produced.

Calculations were also performed to assess the time at which elements reached the maximum theoretical amount of radioactivity that could be produced under identical conditions (1 mg of natural abundance Ho, Re and Y irradiated in a thermal neutron flux of 5.5 x 10^{12} neutrons cm^{-2} s). The properties of the stable and radioactive isotopes of these elements are shown in **Table 3**. Radionuclides with relatively short half-lives, such as ^{166}Ho and ^{188}Re, reached 90% of their maximum theoretical amount after 100 h of irradiation whereas ^{186}Re and ^{90}Y reached only 54.0% and 66.1%, respectively. **Fig. 5**b depicts the amount of Ho, Re and Y radioisotopes produced under a protocol feasible for clinical utility, e.g., 10 h of neutron irradiation followed by a decay period of up to 2 days. It can be seen that similar amounts of ^{166}Ho and ^{188}Re are available at the end of irradiation, but ^{188}Re decays faster than ^{166}Ho. Although a much smaller amount of ^{186}Re is present at the end of irradiation, if a 48 h period is necessary to process and ship the neutron-activated needles, the amount ^{186}Re would be essentially equal to the amount of ^{188}Re after this time period due to the longer half-life of the former.

The amount of Re isotopes that can be produced from Re-coated Mo needles can be controlled by varying the amount of Re deposited on the needles. The different thicknesses of Re coating (25, 75, and 125 μm) correspond to depositions of 5.04, 15.6 and 26.9 mg of Re, respectively. **Fig. 5**c shows the calculated amounts of ^{186}Re and ^{188}Re produced after irradiation of needles coated with varying Re thickness for 10 h followed by an extended decay period. Interestingly, the 125 μm-coated ^{186}Re needle was able to be produced more radioactivity for a longer period of time compared to the 25 μm-coated ^{188}Re needle.

4.5 Conclusion

The use of neutron-activated materials that can be inserted into tumors offers the possibility of customizing internal radiation therapy by selecting needle geometries, coating thicknesses and irradiation times for solid tumors of specific sizes and shapes. Ti and Mo were selected as base materials for the needles because of their machinability, while Ho and Re were selected as the neutron-activatable materials to be coated on the needles because of their favorable nuclear properties (high neutron capture cross-sections, isotopic natural abundance, half-lives and decay properties of the resultant radionuclides). The ultimate dose of radiation produced by neutron activation of Ho or Re can be also easily controlled either by varying the thickness of the Ho/Re coating or selecting an appropriate neutron-irradiation time. The stability of the coatings, which was accomplished using PLD for Ho deposition on Ti needles and CVD for Re deposition on Mo needles, was assessed following irradiation in a nuclear reactor and incubation in solutions of varying pH, including those anticipated at tumor sites. The irradiation of the Ti base material produces very small amounts of short-lived Ti radioisotopes. However, when Mo is used as the base material, Mo radioisotopes and daughters (^{99m}Tc) can be produced by neutron activation. Thus, a neutron absorbing shield comprised of Gd was used during the irradiation of the Re-coated Mo needle to minimize the production of non-rhenium radioisotopes that could complicate the calculation of absorbed radiation does to the tumors and non-target other tissues. The implementation of a neutron-activatable needles would create new opportunities for tailoring the internal radiation of solid tumors. The next generation of this technology will involve the use of true microneedles that can deliver soluble radionuclides into tumor cells in a manner that transdermal microneedles deliver drugs across the skin through the stratum corneum layer.

4.6 REFERENCES

[1] N. Rapoport, A. Payne, C. Dillon, J. Shea, C. Scaife, R. Gupta, Focused ultrasound-mediated drug delivery to pancreatic cancer in a mouse model, Journal of therapeutic ultrasound 1(1) (2013) 11.

[2] J.D. Byrne, M.R. Jajja, A.N. Schorzman, A.W. Keeler, J.C. Luft, W.C. Zamboni, J.M. DeSimone, J.J. Yeh, Iontophoretic device delivery for the localized treatment of pancreatic ductal adenocarcinoma, Proceedings of the National Academy of Sciences 113(8) (2016) 2200-2205.

[3] D.P. Rabussay, G.S. Nanda, P.M. Goldfarb, Enhancing the effectiveness of drug-based cancer therapy by electroporation (electropermeabilization), Technology in cancer research & treatment 1(1) (2002) 71-82.

[4] F. Kamangar, G.M. Dores, W.F. Anderson, Patterns of cancer incidence, mortality, and prevalence across five continents: defining priorities to reduce cancer disparities in different geographic regions of the world, Journal of clinical oncology 24(14) (2006) 2137-2150.

[5] R.L. Siegel, K.D. Miller, A. Jemal, Cancer statistics, 2016, CA: a cancer journal for clinicians 66(1) (2016) 7-30.

[6] P.T. Finger, Radiation therapy for choroidal melanoma, Survey of ophthalmology 42(3) (1997) 215-232.

[7] E.M. Baum, M.C. Ernesti, H.D. Knox, T.R. Miller, A.M. Wastson, Nuclides and Isotopes: Chart of the Nuclides, 17th ed., Knolls Atomic Power Laboratory2010.

[8] A.J. Di Pasqua, H. Yuan, Y. Chung, J.-K. Kim, J.E. Huckle, C. Li, M. Sadgrove, T.H. Tran, M. Jay, X. Lu, Neutron-activatable holmium-containing mesoporous silica nanoparticles as a potential radionuclide therapeutic agent for ovarian cancer, Journal of Nuclear Medicine 54(1) (2013) 111-116.

[9] J. Kim, Z.-X. Luo, Y. Wu, X. Lu, M. Jay, In-situ formation of holmium oxide in pores of Mesoporous Carbon Nanoparticles as substrates for neutron-activatable radiotherapeutics, Carbon 117 (2017) 92-99.

[10] A.J. Sherman, R.H. Tuffias, R.B. Kaplan, The properties and applications of rhenium produced by CVD, JOM Journal of the Minerals, Metals and Materials Society 43(7) (1991) 20-23.

[11] J.-C. Carlen, B.D. Bryskin, Rhenium-a unique rare metal, MATERIAL AND MANUFACTURING PROCESS 9(6) (1994) 1087-1104.

[12] N. Eliaz, E. Gileadi, Induced codeposition of alloys of tungsten, molybdenum and rhenium with transition metals, Modern aspects of electrochemistry, Springer2008, pp. 191-301.

[13] J.W. Pugh, Refractory metals: tungsten, tantalum, columbium, and rhenium, J. Metals 10 (1958).

[14] M. Hamoudeh, M.A. Kamleh, R. Diab, H. Fessi, Radionuclides delivery systems for nuclear imaging and radiotherapy of cancer, Advanced drug delivery reviews 60(12) (2008) 1329-1346.

[15] J. Pinkert, J. Kropp, W. Lin, S. Wang, Rhenium radioisotopes for therapeutic radiopharmaceutical development, Therapeutic applications of radiopharmaceuticals (2001) 59.

[16] D.H. Lowndes, D. Geohegan, A. Puretzky, D. Norton, C. Rouleau, Synthesis of novel thin-film materials by pulsed laser deposition, Science 273(5277) (1996) 898.

[17] P. Willmott, J. Huber, Pulsed laser vaporization and deposition, Reviews of Modern Physics 72(1) (2000) 315.

[18] G. Lütjering, J.C. Williams, Titanium Based Intermetallics, Titanium (2007) 337-366.

[19] D.C. Hansen, Metal corrosion in the human body: the ultimate bio-corrosion scenario, The Electrochemical Society Interface 17(2) (2008) 31.

[20] J.F.W. Nijsen, B.A. Zonnenberg, J.R.W. Woittiez, D.W. Rook, I.A. Swildens-van Woudenberg, P.P. van Rijk, A.D. van het Schip, Holmium-166 poly lactic acid microspheres applicable for intra-arterial radionuclide therapy of hepatic malignancies: effects of preparation and neutron activation techniques, European Journal of Nuclear Medicine 26(7) (1999) 699-704.

[21] E. Amaral, A. Faúndes, L. Zaneveld, D. Waller, S. Garg, Study of the vaginal tolerance to Acidform, an acid-buffering, bioadhesive gel, Contraception 60(6) (1999) 361-366.

[22] A.M. Ribeiro, T.H. Flores-Sahagun, R.C. Paredes, A perspective on molybdenum biocompatibility and antimicrobial activity for applications in implants, Journal of materials science 51(6) (2016) 2806-2816.

[23] B.D. Ratner, A.S. Hoffman, F.J. Schoen, J.E. Lemons, Biomaterials science: an introduction to materials in medicine, Third Edition ed., Academic press2012.

[24] A. Krajnikov, F. Morito, M. Danylenko, Embrittlement of molybdenum–rhenium welds under low and high temperature neutron irradiation, Journal of Nuclear Materials 444(1) (2014) 404-415.

[25] H.O. Pierson, Handbook of chemical vapor deposition: principles, technology and applications, William Andrew1999.

[26] G. Leinweber, D. Barry, M. Trbovich, J. Burke, N. Drindak, H. Knox, R. Ballad, R. Block, Y. Danon, L. Severnyak, Neutron capture and total cross-section measurements and resonance parameters of gadolinium, Nuclear Science and Engineering 154(3) (2006) 261-279.

[27] V.F. Sears, Neutron scattering lengths and cross sections, Neutron news 3(3) (1992) 26-37.

[28] S.J. Goldsmith, Radioimmunotherapy of lymphoma: Bexxar and Zevalin, Seminars in nuclear medicine, Elsevier, 2010, pp. 122-135.

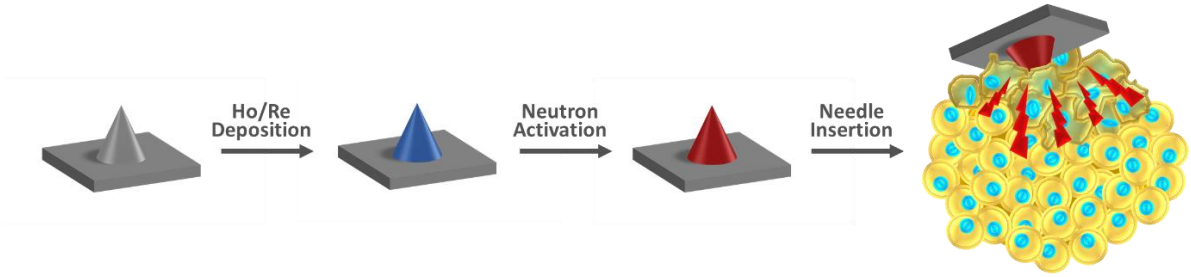

Figure 4.1 Illustration of neutron-activatable coated needles for internal radiation therapy.

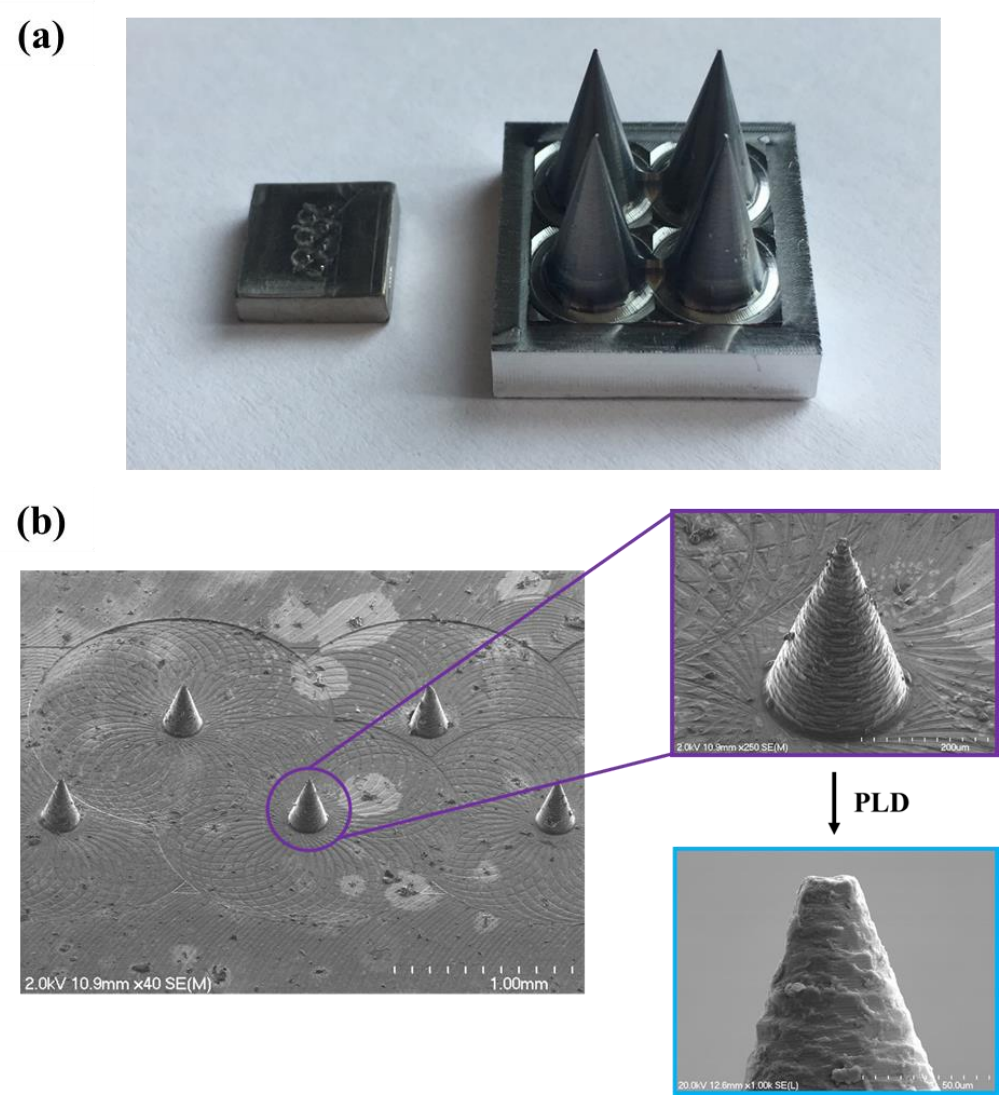

Figure 4.2 Ho deposition on Ti needles by PLD. a) Ho-coated Ti needles: 300 µm (left) and 1 cm (right). b) SEM image of 300 µm Ti needle showing surface morphology before and after Ho deposition.

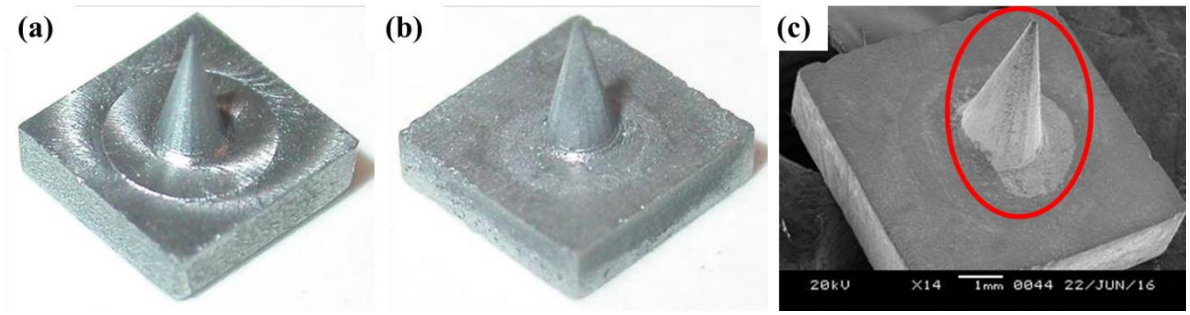

Figure 4.3 Mo needle coated with Re by CVD. a) Mo needle b) Re-coated Mo needle (25 µm coating). c) SEM image of Re-coated Mo needle (red mark indicates area of Re coating).

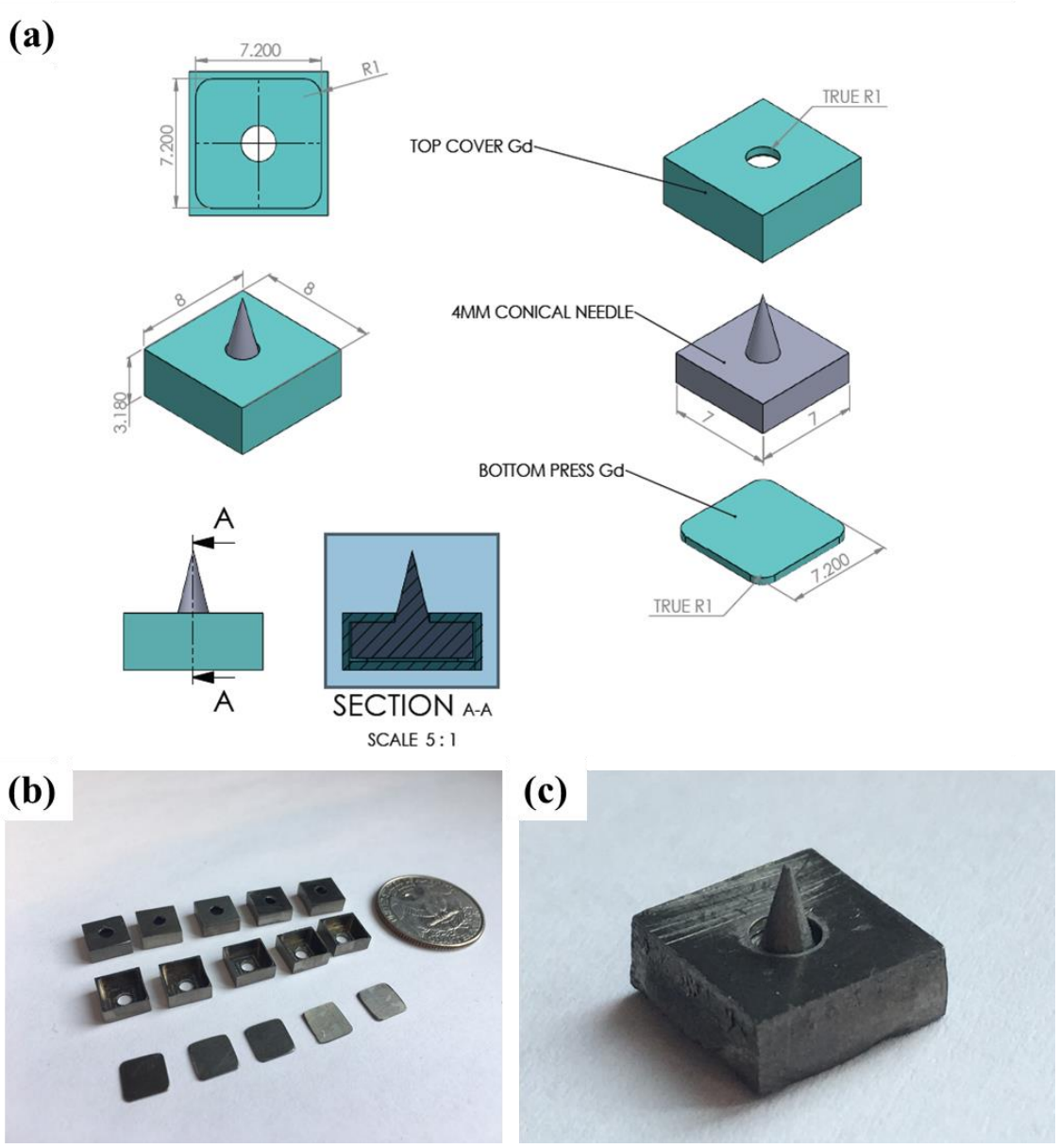

Figure 4.4 Gd neutron shield for Re-coated Mo needle. a) Schematic design of Gd neutron shield. b) Customized two-compartment Gd neutron shield (top and bottom). c) Re-coated Mo needle covered with the Gd neutron shield.

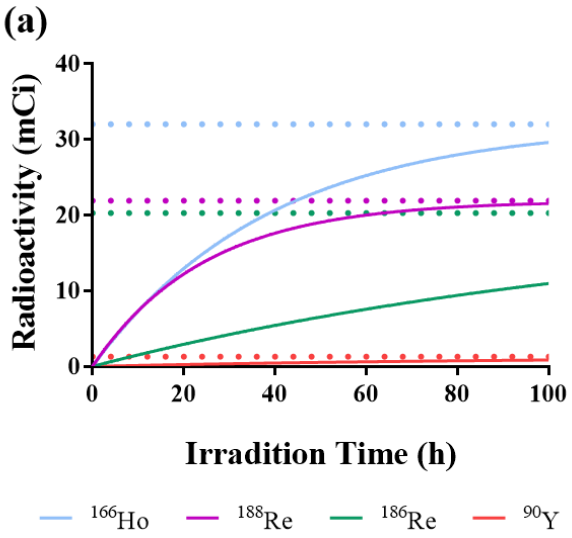
(a)
Radioactivity (mCi)
40
30
20
10
0
0
20
40
60
80
100
Irradition Time (h)
166Ho
188Re
186Re
90Y

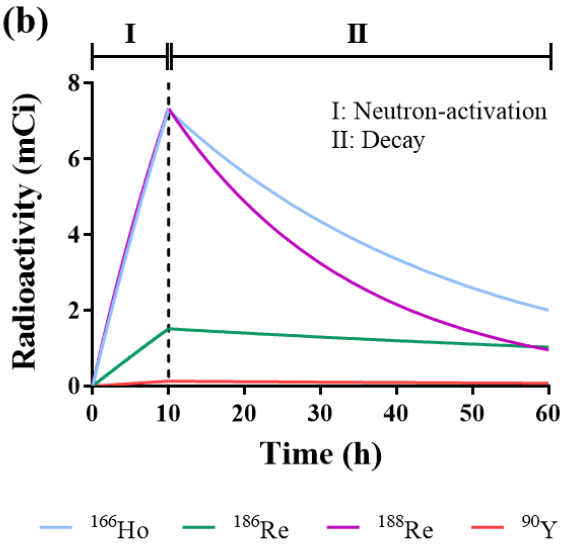
(b)
I
II
I: Neutron-activation
II: Decay
Radioactivity (mCi)
8
6
4
2
0
0
10
20
30
40
50
60
Time (h)
166Ho
186Re
188Re
90Y

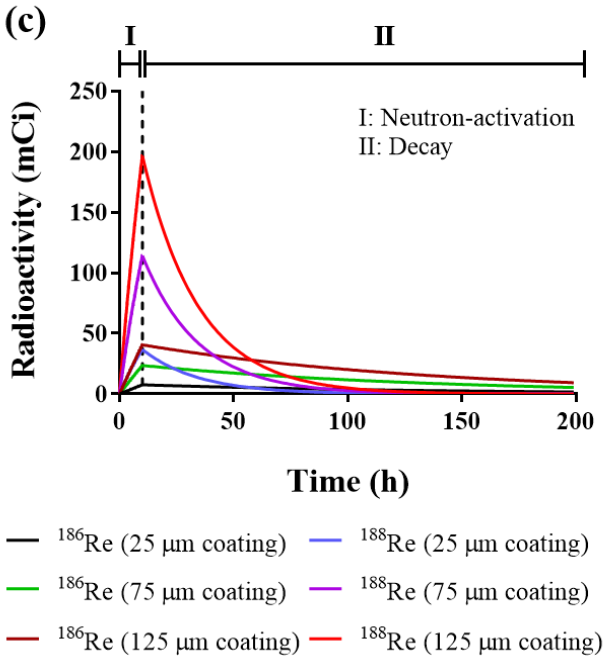
(c)
I
II
I: Neutron-activation
II: Decay
Radioactivity (mCi)
250
200
150
100
50
0
0
50
100
150
200
Time (h)
186Re (25 µm coating)
188Re (25 µm coating)
186Re (75 µm coating)
188Re (75 µm coating)
186Re (125 µm coating)
188Re (125 µm coating)

Figure 4.5 Calculated amounts of radioactivity produced in a thermal neutron flux of 5.5 x 10^{12} neutrons cm^{-2} s as a function of irradiation time [7]. (a) Irradiation of 1 mg of natural abundance Ho, Re and Y (the dotted lines denote the maximum theoretical amount of the individual radionuclides that can be produced under these conditions). (b) The amount of Ho, Re and Y radioisotopes produced by a 10 h neutron irradiation followed by a 48 h decay. (c) The amount of Re radioisotopes produced by a 10 h neutron irradiation of Re-coated needles of various Re-coating thickness followed by a lengthy decay period.

Table 4.1 Leaching of Re and Mo from Re-coated Mo needles when incubated in buffers of different pH values, and after neutron irradiation and three 20 mL washing with Milli-Q water.

Testing Condition		Mo leaching (%)	Re leaching (%)
Acetate Buffer (pH 3.5)	Day 1	0.006	0.001
	Day 2	0.006	0.000
	Day 3	0.007	0.000
	Day 30	0.133	0.001
PBS (pH 7.4)	Day 1	0.032	0.001
	Day 2	0.029	0.001
	Day 3	0.031	0.000
	Day 30	0.627	0.002
Neutron Irradiation	Wash 1	-	0.109
	Wash 2	-	0.009
	Wash 3	-	0.011

Table 4.2 Calculation of radioactivity generated by irradiation of 900 mg of natural abundance Mo for 1h in a thermal neutron flux = 5.5 x 10^{12} neutrons cm^{-2} s and allowing for decay for up to 240 hours after the end of irradiation [7].

		Radioactivity after x h Delay				
Radionuclides	Half-life	0 h	10 h	24 h	168 h	240 h
^{93}Mo	3500 y	48.6 pCi	48.6 pCi	48.6 pCi	48.6 pCi	48.6 pCi
^{99}Mo	65.9 h	264 µCi	237 µCi	205 µCi	45.1 µCi	21.2 µCi
^{99m}Tc	6.01 h	12.8 µCi	152 µCi	182 µCi	43.5 µCi	20.4 µCi
^{101}Mo	14.6 m	13.8 mCi	6.09E-15 Ci	0	0	0
^{101}Tc	14.2 m	11.5 mCi	1.23E-13 Ci	0	0	0

Table 4.3 Properties of stable neutron-activatable nuclides and resultant radionuclides following neutron irradiation [7].

Stable Isotope	Natural abundance (%)	Thermal Neutron-Capture Cross-Section (barn)	Radioactive Isotope	Half-life (h)
^{165}Ho	100	59	^{166}Ho	26.8
^{187}Re	62.6	73	^{188}Re	17.0
^{185}Re	37.4	112	^{186}Re	89.2
^{89}Y	100	1.28	^{90}Y	64.1

CHAPTER 5 SUMMARY AND FUTURE DIRECTIONS

In this dissertation, carbon nanomaterials and custom-sized needles were investigated as material matrices for the purpose of producing therapeutic radionuclides by neutron-activation. To examine radiation therapies practiced in the clinic, various types were reviewed and a neutron-activation strategy was chosen for development of some applications. Parameters involved in neutron-activation and several candidates for neutron-activatable radionuclides were also discussed to determine the ideal option to be loaded or coated on material matrices. Following a thorough selection process, holmium (Ho) was chosen for its 100% natural abundance, therapeutically applicable energy level, proper radioactive $t_{1/2}$ and capability of theragnostic application with SPECT imaging [1].

The use of nanocarriers was required for neutron-activatable radionuclides to target various cancers via the passive tumor-targeting effect [2]. Carbon-based nanocarriers were hypothesized to be an ideal candidate for this application due to desirable characteristics such as rigid structure, high metal loading capacity, low density, heat-resistance and ability to withstand the harsh environment during the neutron-activation process. Subsequent to reviewing carbon nanomaterials in biomedical applications, two different carbon nanocarriers - graphene oxide nanoplatelets (GONs) and mesoporous carbon nanoparticles (MCNs) - were selected as potential Ho delivery carriers.

GONs were successfully synthesized from a graphite and characterized by analytical techniques. By non-covalent PEGylation, their dispersity and Ho-loading capacity were significantly enhanced. Also, they did not leach Ho under 1 h of neutron-irradiation and condition mimicking physiological stress. On the other hand, they were able to steadily release

radioactive Ho in an *in vitro* model of the tumor microenvironment, which is expected to be beneficial for enhanced tumor penetration. Cytotoxicity evaluation of GONs with non-radioactive Ho confirmed their biocompatibility. In future studies, *in vivo* efficacy and pharmacokinetics of the formulation will be assessed in a tumor-bearing animal model. Moreover, Ho will be adhered to GONs via employing chelators, which will prevent the release of Ho in a mildly acidic condition, and they will be used as the control for demonstrating the advantage of selective Ho release from GONs. GONs will also be explored for the platform technology with other radionuclides which can offer varying merits.

In spite of the superior properties of GONs, there was some difficulty to produce GONs of uniform size and shape (critical factors in clinical translation) since large sized GONs were broken down to a nano-scale by strong mechanical energy. To compensate for these shortcomings, MCNs was synthesized from a phenol formaldehyde resin by a soft-template method. Their physical characteristics – morphology, size, pore size, and elemental composition – were assessed with imaging and analytical methods. In addition, surface modification on MCNs conferred dispersibility and biocompatibility. One of the main objectives of this project was achieving the complete prevention of Ho leaching. Therefore, holmium oxide particles were physically entrapped inside of MCNs by synthesis within the pores, and this resulted in complete prevention of holmium leaching even after prolonged irradiation period (10 h). *In vitro* cell-based assays confirmed that the inactive MCN-based formulation was not toxic and the same formulation following a 1 h irradiation demonstrated a sufficient tumoricidal effect.

The MCN formulation will be validated for efficacy with *in vivo* cancer models. For systemic radiation therapy application, xenograft tumor model with an ovarian cancer cell line was already developed. Upon intravenous injection of ^{166}Ho-incorporated MCNs to tumor-bearing mice, tumor shrinkage and survival will be evaluated in contrast to the non-radioactive

control. Furthermore, this formulation will be explored for brachytherapy application with an orthotopic glioblastoma (GBM) mouse model [3]. After removing the GBM by surgery, ^{166}Ho-MCNs will be directly placed in the resection cavity and survival function of this formulation will be analyzed. As discussed in Chapter 3, post-irradiation PEGylation is available for MCNs, which creates an opportunity to attach biological targeting ligands (peptides or proteins). By conjugating targeting ligands to the end of a PEG chain, an active targeting approach on MCNs can be pursed in the future.

A combination therapy of neutron-activatable radionuclide carriers with radiosensitizing chemotherapeutics is anticipated to maximize the therapeutic outcomes; GONs and MCNs have proven to be excellent chemo-drug carriers with a superb loading capacity [4, 5]. However, determining the stability of candidate chemotherapeutics in a nuclear reactor is prerequisite for the chemoradiation therapy.

The last application of neutron-activation technology was developing a radiation needle for solid tumors. To replace large-sized radiation applicators in current use, custom-sized needles were manufactured with titanium (Ti) and molybdenum (Mo). In the first generation of the needle, Ho was deposited to a Ti needle by pulsed laser deposition (PLD); however, Ho was leached under acidic environment by oxidation. Thus, a new version of the needle was prepared with another neutron-activatable radionuclide, rhenium (Re). Since Re-Mo alloys have been utilized for protection purposes against oxidation, wear and corrosion, Re was coated on a Mo needle by chemical vapor deposition (CVD) [6]. Though this needle improved upon the leaching issues of the first generation, undesirable radioisotopes of Mo were produced by neutron irradiation. A gadolinium (Gd) neutron shield was designed and customized to the size of the Mo needle as a solution of preventing Mo irradiation. In the future study, radioactive Re-coated Mo needles will be inserted in the xenograft tumor model to assess Re leaching

under *in vivo* condition. A successful *in vivo* stability test will lead the needle subsequent assessment of *in vivo* efficacy.

In conclusion, the successful outcome of these projects conducted in this dissertation is expected to yield a new paradigm for more convenient and less invasive treatment of cancer patients, potentially increasing not only objective outcomes of response rates and survival, but also subjective patient satisfaction and quality of life.

5.1 REFERENCES

[1] J. Kim, Z.-X. Luo, Y. Wu, X. Lu, M. Jay, In-situ formation of holmium oxide in pores of Mesoporous Carbon Nanoparticles as substrates for neutron-activatable radiotherapeutics, Carbon 117 (2017) 92-99.

[2] S. Hirsjarvi, C. Passirani, J.-P. Benoit, Passive and active tumour targeting with nanocarriers, Current drug discovery technologies 8(3) (2011) 188-196.

[3] J.R. Bagó, A. Alfonso-Pecchio, O. Okolie, R. Dumitru, A. Rinkenbaugh, A.S. Baldwin, C.R. Miller, S.T. Magness, S.D. Hingtgen, Therapeutically engineered induced neural stem cells are tumour-homing and inhibit progression of glioblastoma, Nature communications 7 (2016).

[4] X. Sun, Z. Liu, K. Welsher, J.T. Robinson, A. Goodwin, S. Zaric, H. Dai, Nano-graphene oxide for cellular imaging and drug delivery, Nano research 1(3) (2008) 203-212.

[5] G. Xu, S. Liu, H. Niu, W. Lv, R.a. Wu, Functionalized mesoporous carbon nanoparticles for targeted chemo-photothermal therapy of cancer cells under near-infrared irradiation, RSC Advances 4(64) (2014) 33986-33997.

[6] M.S. El-Genk, J.-M. Tournier, A review of refractory metal alloys and mechanically alloyed-oxide dispersion strengthened steels for space nuclear power systems, Journal of Nuclear materials 340(1) (2005) 93-112.